



**University of
Nottingham**

UK | CHINA | MALAYSIA

**An investigation of the Activity of α/β -Hydrolase
Domain-Containing 6 (ABHD6) in Rat Brain**

Abdullah Alatawi

**Thesis submitted to the University of
Nottingham for the degree of Master of
Research**

October 2024

Abstract

The endocannabinoid system plays a role in various physiological processes, with 2-arachidonoylglycerol (2-AG) and anandamide (AEA) as key signalling molecules. Within this system α/β -Hydrolase Domain-Containing 6 (ABHD6) and α/β -Hydrolase Domain-Containing 12 (ABHD12) regulate 2-AG hydrolysis while also metabolizing other endogenous lipid substrates. ABHD6 hydrolyzes multiple lipid classes, including lysophospholipids, bis(monoacylglycero)phosphate (BMP), and diacylglycerol (DAG), while ABHD12 plays a central role in the metabolism of lysophosphatidylserine (Lyso-PS). Given their involvement in diverse lipid signaling pathways, this thesis aims to investigate the activity of ABHD6 in rat brain tissue using a recently developed spectrophotometric assay based on 4-methylumbelliferylheptanoate (4-MUH) hydrolysis and to validate the selectivity and potency of ABHD6 and ABHD12 inhibitors through the Activity-Based Protein Profiling (ABPP) technique.

This study demonstrates that while the 4-MUH assay was effective in recombinant systems, complete inhibition of 4-MUH hydrolysis in rat brain tissue was not achieved, even with the selective ABHD6 inhibitor KT203. At the highest concentration tested (10 μ M), KT203 inhibited 4-MUH hydrolysis but failed to fully suppress enzyme activity, with over 50% of hydrolysis still remaining in both the soluble and particulate fractions. This suggests that other serine hydrolases contribute to 4-MUH hydrolysis in rat brain tissue, limiting the specificity of this assay for measuring ABHD6 activity. In contrast, the ABPP approach allowed for the simultaneous assessment of multiple enzymes, including ABHD6 and ABHD12. Using the probes MB064 and FP-rhodamine, analysis of ABPP gels identified ABHD6 activity and confirmed KT203's selectivity for ABHD6. Moreover, this method enabled the profiling of ABHD12 and confirmed DO264's selectivity as an ABHD12 inhibitor. These results suggest that while the 4-MUH assay can effectively measure ABHD6 in recombinant systems, ABPP offers greater reliability for profiling multiple enzymes in complex proteomes.

Acknowledgement

First and foremost, all thanks and praise be to Allah, the Lord of all worlds, for granting me the strength and guidance to complete this work.

I would like to extend my deepest gratitude to Dr. Stephen Alexander, my principal supervisor, for his invaluable guidance, support, and mentorship throughout the course of this study. His expertise and encouragement were fundamental to my progress.

I am also profoundly thankful to Dr. Richard Roberts, my second supervisor, for his consistent support and assistance during this journey.

I owe an immense debt of gratitude to my family for their unwavering support and patience, especially my mother, who has been my pillar of strength. My heartfelt thanks also go to my dear friends, Muteb Alsahli, Mohammed Almutairi, Qulayl Aldosswary, Masi Almalki, and Abdullah Alosaimi, for their constant encouragement and companionship throughout this study.

Lastly, I wish to express my sincere appreciation to everyone who contributed to the completion of this work in any capacity.

Table of Contents

AN INVESTIGATION OF THE ACTIVITY OF A/B-HYDROLASE DOMAIN-CONTAINING 6 (ABHD6) IN RAT BRAIN I

ABSTRACT..... II

LIST OF ABBREVIATIONS X

CHAPTER 1: INTRODUCTION.....1

1.1 THE ENDOCANNABINOID SYSTEM1

1.2 ABHD6.....4

1.2.1 ROLE OF ABHD6 IN PATHO/PHYSIOLOGICAL CONDITIONS5

1.2.2 SUBSTRATES OF ABHD68

1.2.3 PHARMACOLOGY OF ABHD6 INHIBITORS10

1.2.4 ASSAYS TO MEASURE ABHD6 ACTIVITY13

1.3 ABHD1214

1.3.1 ROLE OF ABHD12 IN PATHO/PHYSIOLOGICAL CONDITIONS14

1.3.2 ABHD12 INHIBITORS16

1.4 NAGLY.....17

1.5 OBJECTIVES OF THE THESIS18

CHAPTER 2: MATERIALS AND METHODS19

2.1 TISSUE PREPARATION (CONDUCTED BY SPH ALEXANDER)19

2.2 PROTEIN DETERMINATION.....20

2.3 THE 4-MUH BASED ASSAY20

2.3.1 DATA ANALYSIS.....22

2.4 ACTIVITY-BASED PROTEIN PROFILING (ABPP)22

2.4.1 CONDUCTING ABPP23

2.4.2 DATA ANALYSIS.....29

CHAPTER 3: SPECTROPHOTOMETER-BASED ASSAY OF ABHD6 ACTIVITY IN RAT BRAIN PREPARATIONS31

3.1 OBJECTIVE31

3.2 RESULTS31

3.2.1 MAFP33

3.2.2 KT20335

3.2.3 WWL7038

3.2.4 JJKK04840

3.2.5 COMBINING KT203 AND JJKK04842

3.3 DISCUSSION.....44

3.3.1 MAFP44

3.3.2 KT203.....46

3.3.3 WWL70.....48

3.3.4 JJKK04849

3.3.5 COMBINING JKK048 AND KT203 51

CHAPTER 4: ACTIVITY-BASED PROTEIN PROFILING 53

4.1 OBJECTIVE 53

4.2 RESULTS 53

4.2.1 ENZYME ACTIVITIES IN RAT BRAIN FRACTIONS MEASURED USING FP-RHODAMINE 53

4.2.2 ENZYME ACTIVITIES IN RAT BRAIN FRACTIONS MEASURED USING MB064 62

4.3 DISCUSSION 67

4.3.1 DETECTION OF ABHD6 AND ABHD12 IN RAT BRAIN FRACTIONS 68

4.3.2 SELECTIVITY OF ABHD6 AND ABHD12 INHIBITOR 71

4.3.3 ADDITIONAL ENZYME ACTIVITIES DETECTED WITH FPR AND MB064 IN RAT BRAIN FRACTIONS 73

CHAPTER 5: GENERAL DISCUSSION 77

5.1 FUTURE PERSPECTIVES 80

LIST OF REFERENCES 82

List of Figures

FIGURE 1.1 COMPREHENSIVE OVERVIEW OF THE ENDOCANNABINOID SYSTEM, HIGHLIGHTING ITS THREE PRIMARY METABOLIC PHASES: SYNTHESIS, HYDROLYSIS, AND TRANSFORMATION. THE BIOSYNTHESIS OF ENDOCANNABINOIDS INVOLVES TWO PRIMARY ENZYMES: DAGL, WHICH PRODUCES 2-AG, AND NAPE-PLD, RESPONSIBLE FOR SYNTHESIZING ANANDAMIDE (AEA). THE DEGRADATION OF THESE ENDOCANNABINOIDS OCCURS THROUGH DISTINCT HYDROLYTIC ENZYMES. 2-AG IS PRIMARILY HYDROLYZED BY MAGL, ABHD6, AND ABHD12, WHILE AEA IS HYDROLYSED BY FAAH, FAAH2, AND NAAA. BOTH 2-AG AND AEA CAN ALSO UNDERGO TRANSFORMATION INTO BIOLOGICALLY ACTIVE METABOLITES THROUGH PATHWAYS INVOLVING LIPOXYGENASE (LOX), EPOXYGENASE/CYTOCHROME P450 (EPOX/CYP), AND CYCLOOXYGENASE-2 (COX-2). ADAPTED FROM (HOURANI & ALEXANDER, 2018).	3
FIGURE 1.2 SUBCELLULAR LOCALIZATION OF MAGL, ABHD6 AND ABHD12 (DENG & LI, 2020).	4
FIGURE 1.3 SUBSTRATE SPECIFICITY OF ABHD6. ABHD6 EXHIBITS MONOACYLGLYCEROL (MAG) HYDROLASE ACTIVITY, CATALYZING THE HYDROLYSIS OF 2-MONOACYLGLYCEROL (2-MAG) AND SN-1(3)-MONOACYLGLYCEROL (SN-1(3)-MAG) TO GENERATE GLYCEROL AND A FREE FATTY ACID. ADDITIONALLY, ABHD6 CONTRIBUTES TO THE METABOLISM BMP BY HYDROLYZING IT INTO LYSO-PG AND A FATTY ACID. LYSO-PG UNDERGOES FURTHER DEGRADATION BY ABHD6, PRODUCING GLYCEROPHOSPHOGLYCEROL AND AN ADDITIONAL FATTY ACID. THE HYDROLYSIS SITES ARE INDICATED BY RED STARS, WHILE “R” REPRESENTS THE VARIABLE ACYL CHAIN. ADAPTED FROM (PUSCH ET AL., 2022).	9
FIGURE 1.4 ABHD6 INHIBITORS.	10
FIGURE 2.1 SCHEMATIC CLARIFY THE CHEMICAL REACTION OF 4-MUH HYDROLYSIS.	20
FIGURE 2.2 4-MUH HYDROLYSIS IN RECOMBINANT ENZYME-HEK293 MEMBRANE PREPARATIONS (PCDNA, MAGL1, MAGL2, ABHD6, AND ABHD12). RECOMBINANT ABHD6 SELECTIVELY HYDROLYZES 4-MUH COMPARED TO OTHER ESTERASES. REPRODUCED FROM DR. NADA MAHMOOD’S THESIS (2018).	21
FIGURE 2.3 HYDROLYSIS OF 4-MUH BY ABHD6-HEK293 MEMBRANE PREPARATIONS TREATED WITH 1 μ M CONCENTRATIONS OF ELEVEN DISTINCT INHIBITORS. DATA REPRESENT MEAN \pm SEM FROM SEVEN SEPARATE PREPARATIONS PERFORMED IN DUPLICATE. REPRODUCED FROM DR. NADA MAHMOOD’S THESIS (2018).	22
FIGURE 2.4 CHEMICAL STRUCTURE OF FP-RHODAMINE.	25
FIGURE 2.5 CHEMICAL STRUCTURE OF MB064.	25
FIGURE 2.6 PRESENTS A SCHEMATIC REPRESENTATION OF THE ABPP ASSAY USED TO ANALYZE ENZYME ACTIVITY IN THE SOLUBLE AND PARTICULATE FRACTIONS OF RAT BRAIN TISSUE. THE WORKFLOW OUTLINES THE KEY EXPERIMENTAL STEPS, INCLUDING SAMPLE PREPARATION, INHIBITOR INCUBATION, ACTIVITY PROBE LABELING, REACTION TERMINATION, PROTEIN DENATURATION, SDS-PAGE ELECTROPHORESIS, AND GEL IMAGING.	27
FIGURE 2.7 ILLUSTRATES THE GEL LANE ORGANIZATION USED DURING ELECTROPHORESIS TO FACILITATE LANE TRACKING, ANALYSIS, AND TO IMPROVE THE PRECISION OF MOLECULAR WEIGHT ESTIMATION. IN THE FIGURE, BLUE CIRCLES REPRESENT SAMPLE LANES IN THE FIRST GEL LAYOUT, WHILE ORANGE CIRCLES INDICATE SAMPLE LANES IN THE SECOND LAYOUT. GREEN SQUARES DENOTE MOLECULAR WEIGHT MARKERS IN THE FIRST LAYOUT, WHEREAS PURPLE SQUARES REPRESENT MOLECULAR WEIGHT MARKERS IN THE SECOND LAYOUT.	28
FIGURE 2.8 NON-LINEAR REGRESSION ANALYSIS OF MOLECULAR WEIGHT (MW) VERSUS RELATIVE Rf VALUE FOR CY3- AND CY5-SCANNED GELS. THE STANDARD CURVE WAS GENERATED USING MOLECULAR WEIGHT MARKERS DETECTED VIA CY3 AND CY5 CHANNELS, PROVIDING A REFERENCE FOR ESTIMATING MOLECULAR WEIGHTS OF UNIDENTIFIED PROTEIN BANDS. THE CLOSE ALIGNMENT OF Rf VALUES BETWEEN CY3 AND CY5 MARKERS VALIDATES THE COOMASSIE-BASED MOLECULAR WEIGHT ESTIMATION APPROACH IN CASES WHERE FLUORESCENT CY3 DETECTION IS LIMITED.	30
FIGURE 3.1 THE HYDROLYSIS RATES OF 4-MUH WERE MEASURED FOR BOTH SOLUBLE (S1, S2) AND PARTICULATE (P1, P2) FRACTIONS OF RAT BRAIN AT VARIOUS DILUTIONS. DATA REPRESENT MEAN \pm SEM OF A SINGLE EXPERIMENT PERFORMED IN TRIPLICATE, REPRESENTATIVE OF FOUR SEPARATE PREPARATIONS.	32
FIGURE 3.2 CONCENTRATION INHIBITION CURVES OF MAFP FOR 4-MUH HYDROLYSIS IN SOLUBLE AND PARTICULATE FRACTIONS OF RAT BRAIN. THE BLUE LINE REPRESENTS THE SOLUBLE FRACTION, WHILE THE RED LINE CORRESPONDS TO THE PARTICULATE FRACTION, ALLOWING FOR A COMPARATIVE ANALYSIS OF MAFP INHIBITION IN EACH FRACTION. DATA WERE ANALYZED USING A NONLINEAR REGRESSION MODEL, COMPARING BOTH ONE-SITE (FOUR-PARAMETER LOGISTIC, 4PL) AND TWO-SITE BINDING MODELS TO DETERMINE THE BEST FIT FOR INHIBITION DYNAMICS. DATA ARE MEANS \pm SEM OF FIVE INDEPENDENT PREPARATIONS, EACH CONDUCTED IN TRIPLICATE.	34
FIGURE 3.3 CONCENTRATION INHIBITION CURVES OF KT203 FOR 4-MUH HYDROLYSIS IN SOLUBLE AND PARTICULATE FRACTIONS OF RAT BRAIN. THE BLUE LINE REPRESENTS THE SOLUBLE FRACTION, WHILE THE RED LINE CORRESPONDS TO THE PARTICULATE FRACTION, ALLOWING FOR A COMPARATIVE ANALYSIS OF	

MAFP INHIBITION IN EACH FRACTION. DATA WERE ANALYZED USING A NONLINEAR REGRESSION MODEL, COMPARING BOTH ONE-SITE (FOUR-PARAMETER LOGISTIC, 4PL) AND TWO-SITE BINDING MODELS TO DETERMINE THE BEST FIT FOR INHIBITION DYNAMICS. DATA ARE MEANS \pm SEM OF FIVE INDEPENDENT PREPARATIONS, EACH CONDUCTED IN TRIPLICATE.	36
FIGURE 3.4 CONCENTRATION INHIBITION CURVES OF WWL70 FOR 4-MUH HYDROLYSIS IN SOLUBLE AND PARTICULATE FRACTIONS OF RAT BRAIN. THE BLUE LINE REPRESENTS THE SOLUBLE FRACTION, WHILE THE RED LINE CORRESPONDS TO THE PARTICULATE FRACTION, ALLOWING FOR A COMPARATIVE ANALYSIS OF MAFP INHIBITION IN EACH FRACTION. DATA WERE ANALYZED USING A NONLINEAR REGRESSION MODEL, COMPARING BOTH ONE-SITE (FOUR-PARAMETER LOGISTIC, 4PL) AND TWO-SITE BINDING MODELS TO DETERMINE THE BEST FIT FOR INHIBITION DYNAMICS. DATA ARE MEANS \pm SEM OF FIVE INDEPENDENT PREPARATIONS, EACH CONDUCTED IN TRIPLICATE.	39
FIGURE 3.5 ILLUSTRATES THE CONCENTRATION-DEPENDENT INHIBITION OF 4-MUH HYDROLYSIS BY JKK048 IN THE SOLUBLE AND PARTICULATE FRACTIONS OF RAT BRAIN TISSUE. THE BLUE LINE REPRESENTS THE SOLUBLE FRACTION, WHILE THE RED LINE CORRESPONDS TO THE PARTICULATE FRACTION, ALLOWING FOR A COMPARATIVE ANALYSIS OF MAFP INHIBITION IN EACH FRACTION. DATA WERE ANALYZED USING A NONLINEAR REGRESSION MODEL, COMPARING BOTH ONE-SITE (FOUR-PARAMETER LOGISTIC, 4PL) AND TWO-SITE BINDING MODELS TO DETERMINE THE BEST FIT FOR INHIBITION DYNAMICS. DATA ARE MEANS \pm SEM OF FIVE DIFFERENT PREPARATIONS, EACH CONDUCTED IN TRIPLICATE.....	41
FIGURE 3.6 4-MUH HYDROLYSIS IN SOLUBLE AND PARTICULATE FRACTIONS OF RAT BRAIN IN THE PRESENCE OF SERIAL DILUTIONS OF KT203 AND A SINGLE CONCENTRATION (100 nM) OF JKK048. THE FIGURE COMPARES THE INHIBITORY EFFECTS OF KT203 ALONE, JKK048 ALONE, AND THEIR COMBINATION. DATA REPRESENT MEAN \pm SEM FROM SIX INDEPENDENT PREPARATIONS, EACH CONDUCTED IN TRIPLICATE. A ONE-WAY ANOVA FOLLOWED BY ŠÍDÁK'S MULTIPLE COMPARISONS TEST WAS PERFORMED TO ASSESS INHIBITION IN BOTH FRACTIONS.	43
FIGURE 4.1 REPRESENTATIVE GEL SCANS OF A RAT BRAIN PARTICULATE (A) AND SOLUBLE (B) FRACTION MEASURED USING THE ACTIVITY-BASED PROBE FP-RHODAMINE (500 nM) IN THE ABSENCE AND PRESENCE OF VARIOUS INHIBITORS. SAMPLES WERE PRE-INCUBATED WITH KT203 (100 μ M, 10 μ M, AND 1 μ M), DO264 (100 μ M, 10 μ M, AND 1 μ M), AND NAGLY (1000 μ M) TO EVALUATE THEIR EFFECTS ON TARGET ENZYME ACTIVITY. THE LEFT-HAND LANE IN THE PARTICULATE FRACTION (A) DISPLAYS MOLECULAR WEIGHT MARKERS CORRESPONDING TO THE PARTICULATE FRACTION, WHILE THE RIGHT-HAND LANE IN THE SOLUBLE FRACTION (B) CONTAINS MOLECULAR WEIGHT MARKERS FOR THE SOLUBLE FRACTION. PROTEIN BANDS DETECTED AND QUANTIFIED ARE INDICATED NUMERICALLY (RED ARROWS), WITH NOTABLE BANDS MAGL AND ABHD6 LABELLED FOR REFERENCE. THE GEL CONTAINED SAMPLES FROM A SINGLE ANIMAL; TISSUES FROM FIVE OTHER ANIMALS WERE PROCESSED IN AN IDENTICAL MANNER.....	55
FIGURE 4.2 COMPARISON OF ENZYME ACTIVITY IN THE PARTICULATE (A) AND SOLUBLE (B) FRACTIONS OF RAT BRAIN USING ABPP WITH FP-RHODAMINE. DATA ARE PRESENTED AS MEAN \pm SEM OF ADJUSTED VOLUMES, EXPRESSED AS A PERCENTAGE OF BAND 13 (MAGL) FOR THE PARTICULATE FRACTION (A) AND BAND 10 (MAGL) FOR THE SOLUBLE FRACTION (B). DATA WERE OBTAINED FROM SIX INDEPENDENT PREPARATIONS. THE VERTICAL DASHED LINE MARKS THE HIGHER MOLECULAR WEIGHT (MW) BAND OF MAGL IN BOTH FRACTIONS, PROVIDING A REFERENCE FOR MIGRATION PATTERNS AND RELATIVE ENZYME ACTIVITY ACROSS THE FRACTIONS.	57
FIGURE 4.3 THE EFFECTS OF SELECTIVE INHIBITORS ON BAND DENSITIES FROM ABPP GEL SCANS OF RAT BRAIN PREPARATIONS. SAMPLES WERE PRE-INCUBATED WITH KT203 (100 μ M, 10 μ M, AND 1 μ M) OR DO264 (100 μ M, 10 μ M, AND 1 μ M). ACTIVITY WAS MEASURED USING FP-RHODAMINE (500 nM).	59
FIGURE 4.4 REPRESENTATIVE GEL SCANS OF THE PARTICULATE (A) AND SOLUBLE (B) FRACTIONS OF RAT BRAINS MEASURED USING THE ACTIVITY-BASED PROBE MB064 (500 nM) IN THE ABSENCE AND PRESENCE OF VARIOUS INHIBITORS. SAMPLES WERE PRE-INCUBATED WITH KT203 (100 μ M, 10 μ M, AND 1 μ M), DO264 (100 μ M, 10 μ M, AND 1 μ M), AND NAGLY (1000 μ M) TO EVALUATE THEIR EFFECTS ON TARGET ENZYME ACTIVITY. THE LEFT-HAND LANE IN THE PARTICULATE FRACTION (A) DISPLAYS MOLECULAR WEIGHT MARKERS CORRESPONDING TO THE PARTICULATE FRACTION, WHILE THE RIGHT-HAND LANE IN THE SOLUBLE FRACTION (B) CONTAINS MOLECULAR WEIGHT MARKERS FOR THE SOLUBLE FRACTION. PROTEIN BANDS DETECTED AND QUANTIFIED ARE INDICATED NUMERICALLY (RED ARROWS), WITH NOTABLE BANDS ABHD12 AND ABHD6 LABELLED FOR REFERENCE. THE GEL CONTAINED SAMPLES FROM A SINGLE ANIMAL; TISSUES FROM FIVE OTHER ANIMALS WERE PROCESSED IN AN IDENTICAL MANNER.....	63
FIGURE 4.5 THE EFFECTS OF SELECTIVE INHIBITORS ON BAND DENSITIES FROM ABPP GEL SCANS OF RAT BRAIN PREPARATIONS. SAMPLES WERE PRE-INCUBATED WITH KT203 (100 μ M, 10 μ M, AND 1 μ M) OR DO264 (100 μ M, 10 μ M, AND 1 μ M). ACTIVITY WAS MEASURED USING MB064 (500 nM).....	65
FIGURE 4.6 THE EXPRESSION OF RECOMBINANT MOUSE BRAIN SERINE HYDROLASES WAS ANALYZED IN COS-7 CELLS TRANSIENTLY TRANSFECTED WITH cDNAs ENCODING THESE ENZYMES. FOLLOWING TRANSFECTION, CELLS WERE INCUBATED WITH FP-RHODAMINE (2 mM) FOR 1 HOUR. PROTEINS WERE THEN SEPARATED VIA	

SDS-PAGE AND ANALYZED USING IN-GEL FLUORESCENCE SCANNING FOR VISUALIZATION, CONFIRMATION OF ENZYME EXPRESSION, AND QUANTIFICATION OF BAND INTENSITIES CORRESPONDING TO ACTIVE ENZYMES. FOR CLARITY, ENZYME NAMES HAVE BEEN LABELED IN RED NEXT TO THEIR CORRESPONDING BANDS TO ENHANCE READABILITY AND FACILITATE IDENTIFICATION. ADAPTED FROM BLANKMAN ET AL. (2007).69

FIGURE 4.7 MOUSE BRAIN MEMBRANE PROTEOME LABELED WITH MB064 PROBE PERFORMED USING LEI104 (10 mM) (A SELECTIVE INHIBITOR OF DAGL-A), LEI105 (10 mM) (A REVERSIBLE DUAL DAGL-A/DAGL-B INHIBITOR), OMDM188 (1 mM) (A DAGL INHIBITOR), AND THL (10 mM) AS INHIBITORS. PROTEINS WERE LABELED WITH MB064 (250 nM) AND SUBSEQUENTLY SEPARATED VIA SDS-PAGE, FOLLOWED BY IN-GEL FLUORESCENCE SCANNING TO ASSESS THE INHIBITION OF TARGET ENZYMES. THE DETECTED PROTEIN BANDS CORRESPOND TO ACTIVE SERINE HYDROLASES, INCLUDING DAGL-A, DDHD2, ABHD16A, ABHD12, AND ABHD6, WHICH WERE DIFFERENTIALLY INHIBITED BY THE TESTED COMPOUNDS. THE RESULTING FLUORESCENT GEL IMAGE IS DISPLAYED IN GRAYSCALE. ADAPTED FROM (BAGGELAAR ET AL.,2015)74

List of Tables

TABLE 2.1 REAGENTS AND SOURCES.....	19
TABLE 2.2 PRESENTS COMPONENTS REQUIRED TO PREPARE A SINGLE 10% ACRYLAMIDE GEL.	23
TABLE 3.1 A COMPARISON OF ONE-SITE VS TWO-SITE MODELS FOR MAFP INHIBITION OF 4-MUH HYDROLYSIS IN RAT BRAIN SOLUBLE FRACTIONS.	34
TABLE 3.2 A COMPARISON OF ONE-SITE VS. TWO-SITE MODELS FOR MAFP INHIBITION OF 4-MUH HYDROLYSIS IN RAT BRAIN PARTICULATE FRACTIONS.....	35
TABLE 3.3 A COMPARISON OF ONE-SITE VS TWO-SITE MODELS FOR KT203 INHIBITION OF 4-MUH HYDROLYSIS IN RAT BRAIN SOLUBLE FRACTIONS.	37
TABLE 3.4 A COMPARISON OF ONE-SITE VS TWO-SITE MODELS FOR KT203 INHIBITION OF 4-MUH HYDROLYSIS IN RAT BRAIN PARTICULATE FRACTIONS.....	37
TABLE 3.5 A COMPARISON OF ONE-SITE VS TWO-SITE MODELS FOR WWL70 INHIBITION OF 4-MUH HYDROLYSIS IN RAT BRAIN SOLUBLE FRACTIONS.	39
TABLE 3.6 A COMPARISON OF ONE-SITE VS. TWO-SITE MODELS FOR WWL70 INHIBITION OF 4-MUH HYDROLYSIS IN RAT BRAIN PARTICULATE FRACTIONS.....	40
TABLE 3.7 A COMPARISON OF ONE-SITE VS TWO-SITE MODELS FOR JJKK048 INHIBITION OF 4-MUH HYDROLYSIS IN RAT BRAIN SOLUBLE FRACTIONS.	42
TABLE 3.8 A COMPARISON OF ONE-SITE VS. TWO-SITE MODELS FOR JJKK048 INHIBITION OF 4-MUH HYDROLYSIS IN RAT BRAIN PARTICULATE FRACTIONS.....	42
TABLE 4.1 THE EFFECTS OF SELECTED INHIBITORS ON ENZYME ACTIVITY IN RAT BRAIN PARTICULATE FRACTIONS LABELLED WITH FP-RHODAMINE.	60
TABLE 4.2 THE EFFECTS OF SELECTED INHIBITORS ON ENZYME ACTIVITY IN RAT BRAIN SOLUBLE LABELLED WITH FP-RHODAMINE.	61
TABLE 4.3 THE EFFECTS OF SELECTED INHIBITORS ON ENZYME ACTIVITY IN RAT BRAIN PARTICULATE FRACTION LABELLED WITH MB064.	66
TABLE 4.4 THE EFFECTS OF SELECTED INHIBITORS ON ENZYME ACTIVITY IN RAT BRAIN SOLUBLE FRACTION LABELLED WITH MB064.	66

List Of Abbreviations

2-AG	2-arachidonoylglycerol
ABHD6	α/β -hydrolase domain containing 6
ABHD12	α/β -hydrolase domain containing 12
ABPP	Activity-based protein profiling
AEA	Anandamide
BBB	Blood brain barrier
BSA	Bovine serum albumin
CB	Cannabinoid receptor
CB1	Cannabinoid receptor 1
CB2	Cannabinoid receptor 2
CNS	Central nervous system
DAG	Diacylglycerol
DAGL α	Diacylglycerol lipase alpha
DAGL β	Diacylglycerol lipase beta
FAAH	Fatty acid amide hydrolase
MAFP	Methyl arachidonyl fluorophosphonate
MAGL	Monoacylglycerol lipase
MUH	4-methylumbelliferylheptanoate
NAPE	N-arachidonoyl phosphatidylethanolamine
SDS	Sodium dodecyl sulphate
SDS-PAGE	SDS-polyacrylamide gel electrophoresis
TEMED	(N, N, N',N'-tetramethylethylenediamine)

Chapter 1: Introduction

1.1 The endocannabinoid system

The endocannabinoid system is composed of endogenous ligands, known as endocannabinoids, as well as the cannabinoid receptors and the enzymes involved in their production and breakdown. The key endocannabinoids include 2-arachidonoylglycerol (2-AG) (Sugiura et al., 1995) and anandamide (AEA) (Devane et al., 1992).

Cannabinoid receptors CB1 and CB2 belong to the rhodopsin-like subfamily of G protein-coupled receptors (GPCRs), which are characterised by a ligand-binding domain formed within their seven transmembrane-spanning regions embedded in the plasma membrane (Pertwee et al., 2010). Unlike most rhodopsin-like GPCRs, structural studies have identified four distinct crystal structures of CB1, revealing that its extracellular surface also plays a role in ligand binding (Shao et al., 2016; Hua et al., 2016).

Both CB1 and CB2 primarily couple to inhibitory G proteins (G_i/o), leading to the suppression of adenylyl cyclase activity and voltage-sensitive calcium channels, while stimulating the activation of mitogen-activated protein kinases (MAPKs) and inwardly rectifying potassium channels (GIRKs) (Howlett et al., 2002). These receptors also contribute to beta-arrestin recruitment and other downstream cellular signalling pathways. The signalling diversity of CB1 receptors is further augmented by their propensity to form heterodimers with other GPCRs, including opioid, D2 dopamine, and hypocretin receptors (Wootten et al., 2018). A key distinction between CB1 and CB2 receptors lies in their distribution patterns. Initially, CB1 receptors were identified as highly expressed in the central nervous system (CNS) (Devane et al., 1988), leading to their classification as the “central cannabinoid receptor”. Meanwhile, CB2 receptors were initially identified in immune cells of myeloid lineage and the spleen, leading to their classification as “peripheral cannabinoid receptors.” However, these distinctions have since been deemed inaccurate, as CB1 receptors are also present in peripheral tissues, while CB2 receptors have been detected in the CNS. This revised understanding has prompted the development of CB1-selective agonists with restricted peripheral activity to minimise CNS side effects (Yu et al., 2010). CB1 receptors are predominantly expressed in various regions of the brain, including the cerebellum, hippocampus, and cerebral cortex (Pertwee et al., 2010). Beyond the CNS, CB1 receptors are expressed in various peripheral tissues, such as the liver, heart, adipose tissue, and gastrointestinal tract (Kurz et al., 2008). In contrast, CB2 receptors exhibit low levels of

expression in the CNS but are more prominently associated with immune cells, such as peripheral macrophages (Cabral et al., 2008). 2-AG is a principal endocannabinoid that functions as a full agonist at both CB1 and CB2 receptors, leading to maximum activation of their associated intracellular signalling pathways. In contrast, AEA acts as a partial agonist at these receptors, producing a more limited receptor activation and downstream signalling response (Mechoulam et al., 1995; Sugiura et al., 1995).

AEA is synthesised from N-acyl phosphatidylethanolamine (NAPE), a phospholipid precursor formed through the transacylation of membrane phosphatidylethanolamine by a calcium-dependent N-acyltransferase enzyme (Fowler et al., 2017). NAPE is subsequently broken down into AEA by the enzyme N-acylphosphatidylethanolamine phospholipase D (NAPE-PLD) (Liu et al., 2006). The synthesis of 2-AG is primarily initiated through the enzymatic cleavage of membrane phospholipids by phospholipase, resulting in the production of diacylglycerol (DAG). Diacylglycerol then acts as a substrate for two isoforms of diacylglycerol lipases, DAGL α and DAGL β , which catalyse its conversion to 2-AG. This process represents the principal pathway for 2-AG biosynthesis in many cell types (Bisogno et al., 2005; Bisogno et al., 2003).

The breakdown of 2-AG and AEA occurs through distinct pathways. The enzyme primarily responsible for the degradation of 2-AG is monoacylglycerol lipase (MAGL). AEA is mainly metabolized by fatty acid amide hydrolase (FAAH). However, FAAH is not the sole enzyme involved in AEA degradation; other enzymes such as FAAH2 and N-acylethanolamine acid amidase (NAAA) also contribute to the degradation of AEA into arachidonic acid and ethanolamine in different species and different tissues (Figure 1.1) (Ahn et al., 2008; Kaczocha et al., 2010). The degradation of 2-AG is primarily controlled by MAGL, which accounts for approximately 85% of its hydrolysis. MAGL is a soluble enzyme that associates peripherally with membranes, primarily at presynaptic terminals, where it hydrolyses excess 2-AG into arachidonic acid (AA) and glycerol, effectively terminating endocannabinoid signaling and preventing overstimulation of cannabinoid receptors. The remaining 2-AG hydrolysis is mediated by α/β -hydrolase domain-containing 6 (ABHD6) and α/β -hydrolase domain-containing 12 (ABHD12), which collectively contribute to about 13% of 2-AG breakdown in mouse brain membranes (Figure 1.1) (Blankman et al., 2007). ABHD6 is an integral membrane protein localized to the postsynaptic neuronal membrane, where it degrades newly synthesized 2-AG, facilitating localized regulation of endocannabinoid signaling. In contrast, ABHD12 acts as an ectohydrolase, with its active site oriented toward

the extracellular or luminal space, where it regulates extracellular 2-AG levels (Figure 1.2) (Blankman et al., 2007; Savinainen et al., 2012).

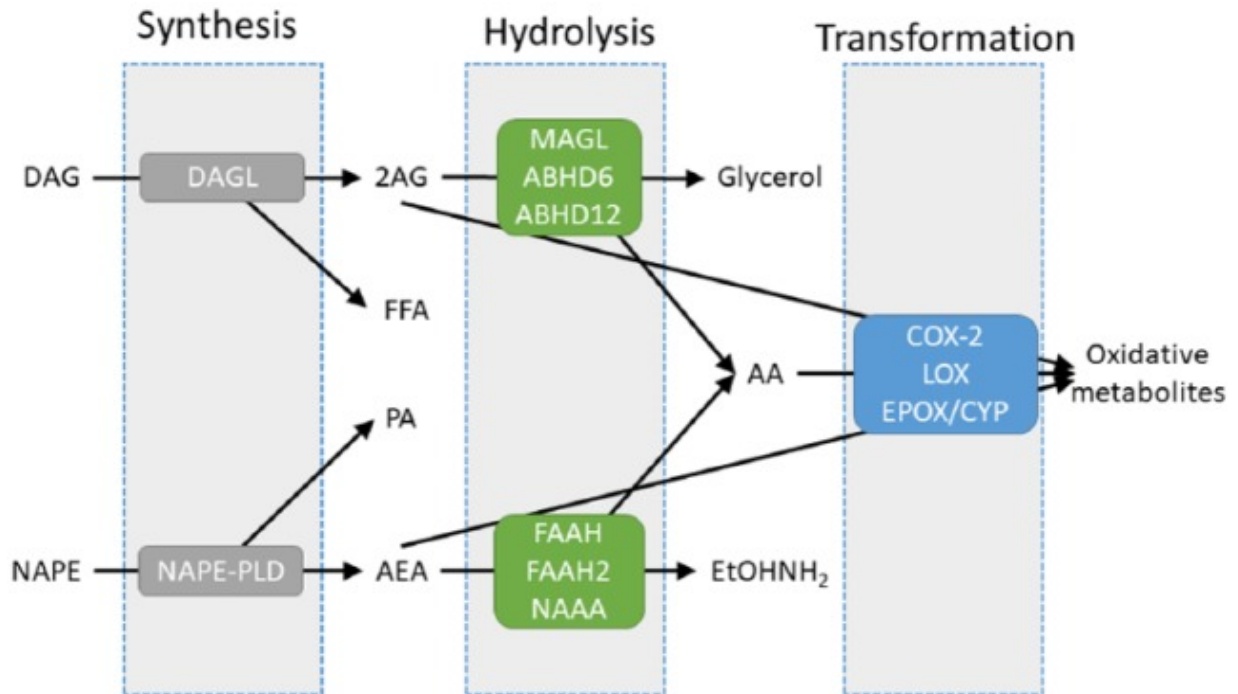


Figure 1.1 Comprehensive overview of the endocannabinoid system, highlighting its three primary metabolic phases: synthesis, hydrolysis, and transformation. The biosynthesis of endocannabinoids involves two primary enzymes: DAGL, which produces 2-AG, and NAPE-PLD, responsible for synthesizing AEA. The degradation of these endocannabinoids occurs through distinct hydrolytic enzymes. 2-AG is primarily hydrolyzed by MAGL, ABHD6, and ABHD12, while AEA is hydrolysed by FAAH, FAAH2, and NAAA. Both 2-AG and AEA can also undergo transformation into biologically active metabolites through pathways involving lipoxygenase (LOX), epoxygenase/cytochrome P450 (EPOX/CYP), and cyclooxygenase-2 (COX-2). Adapted from (Hourani & Alexander, 2018).

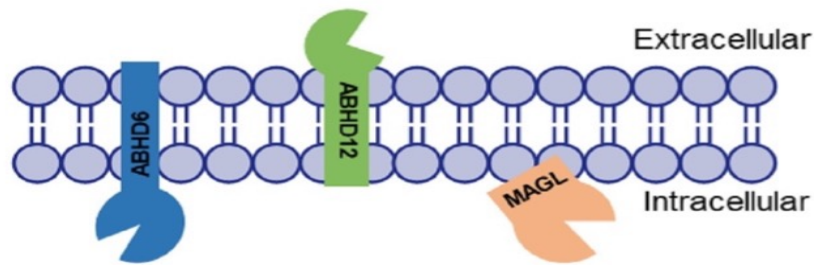


Figure 1.2 Subcellular localization of MAGL, ABHD6 and ABHD12.

Adapted from (Deng & Li, 2020).

1.2 ABHD6

ABHD6 is a transmembrane serine hydrolase that is found in peripheral and central tissues. It belongs to the large family of α/β hydrolase enzymes (Labar et al., 2010a). It is involved in the degradation of monoacylglycerol lipids, particularly 2-AG to generate glycerol and AA. The first evidence suggesting other enzymes were involved in 2-AG hydrolysis came from studies on the BV2 microglial cell line, which lacks MAGL expression but still exhibits 2-AG hydrolysis activity (Muccioli et al., 2007). Using the ABPP technique (see below) on mouse brain membranes, ABHD6 and ABHD12 were identified as enzymes involved in the breakdown of 2-AG (Blankman et al., 2007). Prolonged inhibition or genetic deletion of MAGL lead to increased 2-AG levels in neurons and was found to result in desensitization of CB1 receptors (Schlosburg et al., 2010). In contrast, ABHD6-deficient mice did not exhibit changes in CB1 receptor signalling (Grabner et al., 2019), indicating that ABHD6 plays a less critical role in the termination of 2-AG signalling.

Marrs et al. (2011) presented additional evidence supporting the involvement of ABHD6 in the degradation of 2-AG. Their findings showed that the inhibitor UCM710, which targets both ABHD6 and FAAH, led to an increase in 2-AG levels, even when MAGL remained active. ABHD6 is expressed in a variety of tissues, with particularly high levels found in the brown adipose tissue, brain and intestines (Lord et al., 2013). In the brain, ABHD6 is primarily located postsynaptically, where it likely plays a role in inhibiting the synthesis of 2-AG at postsynaptic terminals. In contrast, MAGL is localized presynaptically alongside CB1 receptors, where it functions to terminate 2-AG signalling (Marrs et al., 2011; Blankman et al., 2007). The different subcellular localizations and tissue distributions of MAGL, ABHD6, and ABHD12 suggest their involvement in the differential regulation of 2-AG signaling duration within the nervous system (Figure 1.2).

1.2.1 Role of ABHD6 in patho/physiological conditions

ABHD6 is implicated in various physiological processes and pathological conditions, positioning it as a promising target for therapeutic interventions, where inhibiting its activity has demonstrated potential therapeutic benefits. Three pharmacological tools have been used to help elucidate the role/s of ABHD6: WWL123, WWL70 and KT203.

The selective ABHD6 inhibitor WWL123 (Bachovchin et al., 2010) demonstrated seizure-suppressing effects in mouse models, reducing the severity of pentylenetetrazole (PTZ)-induced seizures (Naydenov et al., 2014). The anticonvulsant effects were mediated through GABAA receptors, as they were abolished by the GABAA receptor antagonist picrotoxin and were independent of CB1 and CB2 receptor activation. Similarly, Westenbroek et al. (2023) reported that deletion of ABHD6, as well as its pharmacological inhibition using KT-182 significantly attenuated the duration of thermally induced seizures in a Dravet syndrome mouse model. This effect was linked to the potentiation of extrasynaptic GABAA receptor currents. These findings suggest the therapeutic potential of ABHD6 inhibitors in epilepsy via modulation of GABAergic transmission.

Pharmacological inhibition of ABHD6 using WWL70 (Li et al., 2007) resulted in increased 2-AG levels within the cerebral cortex, diminished infiltration of macrophages and T lymphocytes, and suppressed pro-inflammatory cytokine secretion in a murine model of multiple sclerosis. Some of these therapeutic effects could be attributed to the activation of endocannabinoid receptors. Similarly, ABHD6 knockout (KO) in murine peritoneal macrophages and blocking ABHD6 activity with KT203 in human THP1 macrophages led to a reduction in pro-inflammatory markers and an increase in the expression of lipid metabolism-related genes (Poursharifi et al., 2023).

Furthermore, alterations in ABHD6 expression and enzymatic activity were observed in a murine model of paracetamol-induced liver injury. By regulating the hydrolysis of 2-AG, ABHD6 likely influences both pro-inflammatory and protective pathways in the liver.

Increased ABHD6 expression in the liver was associated with decreased levels of acylglycerols, including 2-AG (Rivera et al., 2020). As an endogenous lipid mediator, 2-AG exerts anti-inflammatory effects, serving as an intrinsic defense mechanism against excessive immune activation and inflammatory damage (Turcotte et al., 2015). This reduction in 2-AG levels coincided with elevated expression of pro-inflammatory cytokines such as *Mcp1*, *Tnfa*, and *Il6*, as well as fibrogenic markers α Sma and Col3a1 (Rivera et al., 2020), suggesting that

ABHD6 may regulate lipid mediators to influence inflammation and fibrotic responses. In a mouse model of cortical spreading depression (CSD)-induced periorbital allodynia, the induction of CSD elicited a progressive neuroinflammatory cascade within the PAG, characterized by astroglial and microglial reactivity alongside a gradual elevation in PGE2 synthesis, which became evident following the reduction in 2-AG levels. This increase in PGE2 concentration aligns with the expected consequences of heightened 2-AG hydrolysis, further implicating ABHD6 activity in the regulation of neuroinflammatory pathways. Pharmacological inhibition of ABHD6 with KT182 effectively reversed and prevented CSD-induced allodynia (Liktor-Busa et al., 2023). These findings suggest that ABHD6 inhibition may mitigate CSD-induced neuroinflammation and pain hypersensitivity, making it a promising target for headache-related pain management. However, WWL70 significantly alleviated heat-induced hypersensitivity and mechanical pain hypersensitivity in mice. Additionally, the treatment led to a reduction in pro-inflammatory cytokine levels, decreased astrocyte and microglial activation, and diminished macrophage infiltration. As the effects were independent of cannabinoid receptors, the authors suggested that these effects were primarily driven by the reduction in PGE2 production, rather than through the inhibition of 2-AG hydrolysis (Wen et al., 2018).

A correlation has been established between heightened ABHD6 expression and the onset of Systemic Lupus Erythematosus (SLE), a complex autoimmune disorder (Oparina et al., 2015). Notably, this correlation is particularly evident in individuals of European descent. Moreover, a specific single nucleotide polymorphism (SNP) variant associated with lower ABHD6 expression has been found to provide protective effects against the disease (Poursharifi et al., 2017).

In a study involving pancreatic islets isolated from male Wistar rats and humans, insulin secretion in isolated islets and the INS82/13 rat insulin-secreting cell line was assessed. ABHD6 and MAGL were either overexpressed or knocked down using RNAi silencing, with subsequent assays for High-Performance Liquid Chromatography (HPLC), insulin secretion and western blot analysis. During glucose metabolism, 1-MAG, a signalling molecule, was produced near β -cell membranes to enhance insulin secretion. ABHD6 was responsible for hydrolysing 1-MAG, and its knockdown led to increased glucose-stimulated insulin secretion (GSIS) and elevated monoacylglycerol levels, both *ex vivo* and *in vivo* (Zhao et al., 2014; Zhao et al., 2015). In contrast, inhibiting MAGL via pharmacological or siRNA approaches did not affect GSIS. Additionally, administering WWL70, an ABHD6 inhibitor, improved

glucose tolerance and restored normal GSIS in a diabetic animal model induced by low dose streptozotocin (Zhao et al., 2014).

A study by Thomas et al. (2013) explored the role of ABHD6 in peripheral tissues, revealing its involvement in metabolic disorders. In the experiment, male mice were placed on either a standard or high-fat diet and treated with ABHD6 antisense oligonucleotides (ASO) to knock down ABHD6 expression, excluding the brain. The results showed that ABHD6 mRNA was elevated in the liver and small intestine in response to a high-fat diet. Notably, ABHD6 knockdown protected the mice from diet-induced weight gain after four weeks, along with reductions in hepatic triacylglycerol, hyperglycaemia, hyperinsulinemia, and improvements in glucose and insulin tolerance. The knockdown also protected against hepatic steatosis without affecting endocannabinoid levels or CB1 desensitization (Thomas et al., 2013). These findings suggest ABHD6 plays a role in lysophospholipid metabolism and may help protect against obesity.

Further research by the same group confirmed these results, showing that ABHD6 knockout mice were protected from obesity, hyperinsulinemia, and liver steatosis, with enhanced energy expenditure, partially due to browning of white adipose tissue and increased thermogenic activity within brown adipose tissue (Zhao et al., 2016).

Building on these findings, Lau et al. (2024) investigated the central role of ABHD6 in the mesoaccumbens circuitry, demonstrating its distinct functions in the nucleus accumbens (NAc) and ventral tegmental area (VTA). ABHD6 deletion in NAc neurons prevented diet-induced obesity, increased physical activity, and reduced food- and drug-seeking behaviors, linked to reduced inhibitory synaptic transmission onto medium spiny neurons (MSNs). In contrast, VTA ABHD6 deletion exhibited region-specific effects; the ablation of ABHD6 across all neuronal populations resulted in a significant reduction in spontaneous locomotor activity when exposed to a high-fat diet, whereas dopamine neuron-specific deletion heightened food-seeking behavior during fasting. Further supporting the therapeutic potential of ABHD6 inhibition, the selective ABHD6 inhibitor WWL70 was used to pharmacologically target central ABHD6. Administered via intracerebroventricular (ICV) infusion, WWL70 produced outcomes similar to those observed with NAc-specific ABHD6 deletion, leading to a reduced risk of diet-induced obesity, an upregulation of metabolic energy expenditure, and a marked decrease in overall food consumption. These findings suggest that central ABHD6 inhibition through pharmacological agents like WWL70 could serve as a promising therapeutic strategy for obesity and metabolic disorders (Lau et al., 2024). In addition to its involvement in metabolic and neurological conditions, ABHD6 has

been implicated in addiction-related behaviours through its regulation of endocannabinoid signalling. Repeated intraperitoneal administration of morphine to male Sprague Dawley rats at a dose of 10 mg/kg per day for five consecutive days led to a significant reduction in ABHD6 expression within the ventral tegmental area (VTA), a critical brain region associated with reward and motivation (Zhang et al., 2021). This alteration in ABHD6 levels disrupts the homeostasis of the endocannabinoid system, which is intricately linked to the opioid system in modulating reward-related behaviours. Previous evidence suggests that ABHD6 is critical for regulating long-term synaptic depression (LTD) in the CNS via two distinct mechanisms: one involving the 2-AG/CB1 receptor pathway and another that is independent of endocannabinoid signaling, which operate through AMPA receptor regulation (Wei et al., 2016; Cao et al., 2019). Sustained morphine exposure leading to ABHD6 downregulation may contribute to opioid-induced alterations in synaptic plasticity, reinforcing neuroadaptive changes that underlie addiction-related behaviors (Zhang et al., 2021). These findings highlight the potential role of ABHD6 in opioid addiction and its associated neurochemical adaptations, suggesting that targeting ABHD6 could influence reward processing and offer therapeutic benefits in treating addiction.

Beyond its role in neurological and metabolic disorders, ABHD6 has also been implicated in cancer biology, with altered expression in various malignancies. ABHD6 expression is elevated in specific tumour types, yet its knockdown does not significantly influence abnormal cell proliferation, as demonstrated in studies on Ewing Family Tumours (EFT) (Navia-Paldanius et al., 2012; Max et al., 2009). Additionally, ABHD6 has been recognized as a target of Epstein-Barr virus nuclear antigen 2 (EBNA2), which is associated with numerous Epstein-Barr virus (EBV)-related malignancies, showing high expression in bone, prostate, and leukocyte cancers (Maier et al., 2006; Li et al., 2009). In pancreatic ductal adenocarcinoma (PDAC), inhibiting ABHD6 reduced tumour proliferation and metastasis in both in vitro and in vivo models, highlighting its potential as a therapeutic target (Gruner et al., 2016). RNA sequencing data suggest ABHD6 might serve as an anti-oncogene marker in advanced hepatocellular carcinoma, where its expression is reduced (Yu et al., 2016). These reports identify the potential for ABHD6 as a drug target associated with multiple diseases or disorders.

1.2.2 Substrates of ABHD6

ABHD6 hydrolyzes at least four groups of endogenous lipid substrates, as illustrated in Figure 1.3. These include the following:

1. Monoacylglycerols (MAGs) (Navia-Paldanius et al., 2012).
2. Lysophospholipids (Pribasniig et al., 2015).
3. Bis(monoacylglycero)phosphate (BMP) (Pribasniig et al., 2015)
4. Diacylglycerol (DAG) (van Esbroeck et al., 2019).

Additionally, ABHD6 has been shown to hydrolyse the synthetic substrate 4-methylumbelliferyl-heptanoate (4-MUH) using recombinant human ABHD6 (Nada Mahmood., 2018). Previously, 4-MUH was considered a suitable substrate for measuring lipase activity, as it is more resistant to hydrolysis by non-lipolytic esterases (Gilham et al., 2005).

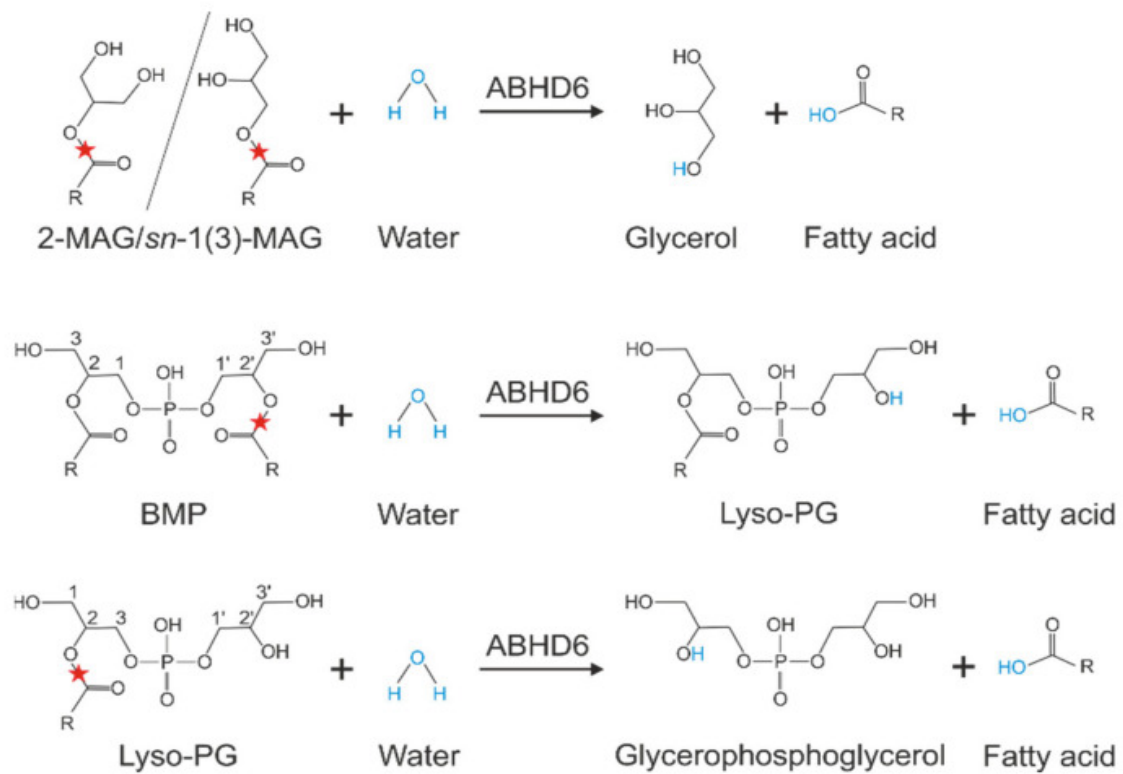
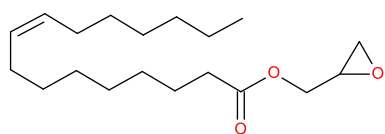


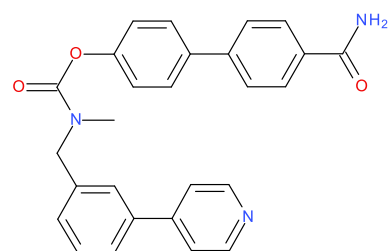
Figure 1.3 Substrate specificity of ABHD6. ABHD6 exhibits monoacylglycerol (MAG) hydrolase activity, catalyzing the hydrolysis of 2-monoacylglycerol (2-MAG) and sn-1(3)-monoacylglycerol (sn-1(3)-MAG) to generate glycerol and a free fatty acid. Additionally, ABHD6 contributes to the metabolism BMP by hydrolyzing it into Lyso-PG and a fatty acid. Lyso-PG undergoes further degradation by ABHD6, producing glycerophosphoglycerol and an additional fatty acid. The hydrolysis sites are indicated by red stars, while “R” represents the variable acyl chain. Adapted from (Pusch et al., 2022).

1.2.3 Pharmacology of ABHD6 inhibitors

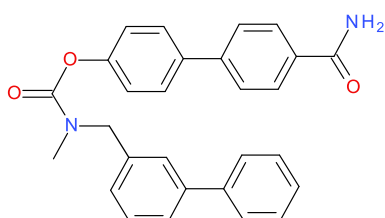
A range of ABHD6 inhibitors has been developed with different chemical structures, such as fatty acid-derived, carbamate-based, urea-containing, and glycine sulfonamide-based structures.



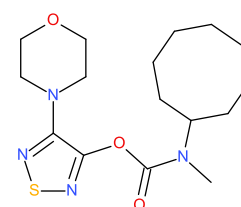
UCM710



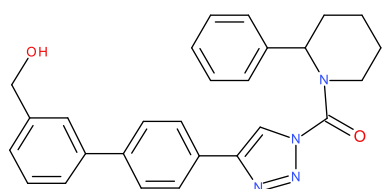
WWL70



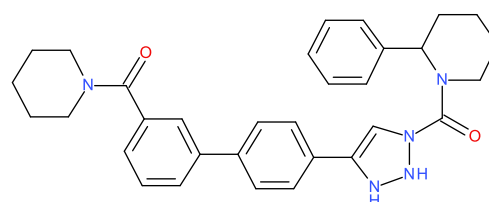
WWL123



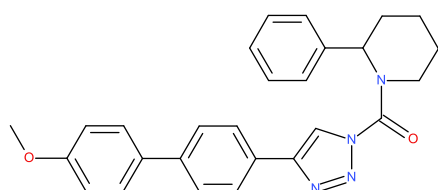
JZP430



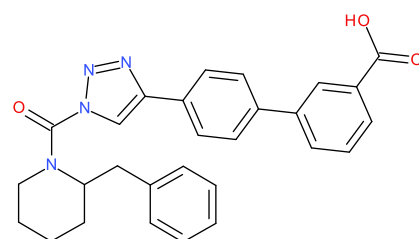
KT182



KT185



KT195



KT203

Figure 1.4 ABHD6 inhibitors

1.2.3.1 Fatty acid-based inhibitors

In a study by Marrs et al. (2011), a group of esters derived from 2-AG were synthesized with the goal of inhibiting endocannabinoid hydrolysis. Among these, UCM710 emerged as a potent inhibitor, targeting both FAAH and ABHD6 (Figure 1.4). UCM710 effectively inhibited the activity of both FAAH and ABHD6 in neuronal homogenates and COS-7 cell lysates without significantly affecting MAGL activity. Specifically, UCM710 showed concentration-dependent inhibition of both AEA hydrolysis by FAAH ($IC_{50} = 4.0 \mu\text{M}$) and 2-AG hydrolysis by ABHD6 ($IC_{50} = 2.4 \mu\text{M}$). However, UCM710's limited selectivity for ABHD6 restricts its application in functional studies (Deng & Li, 2020).

1.2.3.2 Carbamate-based inhibitors

Carbamate-based inhibitors have emerged as significant candidates for ABHD6 inhibition. Through ABPP in recombinant human ABHD6, Li et al. (2007) identified several carbamate molecules that reduced fluorescent probe labelling of ABHD6, suggesting their inhibitory potential. Biphenyl-4-yl methyl(3-(pyridin-4-yl)benzyl) carbamate was one of the most potent and selective inhibitor scaffolds identified. Further optimization of this molecule led to the development of WWL70, which exhibited an IC_{50} of 70 nM using ABPP and is considered a highly potent inhibitor of ABHD6 (Figure 1.4) (Li et al., 2007).

WWL123, another carbamate-based inhibitor identified by Bachovchin et al. (2010), demonstrated selectivity for ABHD6 both *in vitro* and *in vivo*, with an IC_{50} of 0.43 μM (Figure 1.4). This compound retained selectivity when administered to mice through intraperitoneal injection, providing a strong basis for its use in further studies.

Another carbamate-based compound, JZP430, exhibited an IC_{50} of 44 nM against ABHD6, showing irreversible inhibition as demonstrated by ABPP in complex proteome (Figure 1.4) (Patel et al., 2015). MJN193, identified through screening a library of carbamates, demonstrated potency and selectivity for ABHD6, despite its limited reactivity (Cognetta et al., 2015).

1.2.3.3 Urea-based inhibitors

Triazole urea derivatives have also been explored as potent inhibitors of ABHD6. KT195, initially developed by Hsu et al. (2012) as a DAGL β inhibitor, was later discovered to exhibit potent ABHD6 inhibition with an IC_{50} of 10 nM. Subsequent modifications of KT195 led to the development of KT182, KT185, and KT203, each with improved efficacy (Figure 1.4).

KT182, for instance, inhibits ABHD6 activity in liver and brain, while KT203 selectively inhibits peripheral ABHD6 without crossing blood-brain barrier (Hsu et al., 2013).

A group of chiral hydroxylated 2-benzylpiperidines, derived from triazole urea structures, were identified as inhibitors of DAGL and ABHD6. Three compounds of the library demonstrated significant inhibition of ABHD6 while exhibiting reduced activity towards DAGL α . This selectivity makes them promising candidates for the development of selective ABHD6 inhibitors (Deng et al., 2017).

1.2.3.4 Tetrahydroisoquinoline-based inhibitor

A new class of tetrahydroisoquinoline carbamate inhibitors has been identified as highly potent and selective for ABHD6. Among them, 1,1,1,3,3,3-Hexafluoropropan-2-yl 5-(2-morpholinoethoxy) isoindoline-2-carboxylate demonstrated high activity with an IC₅₀ value of 8 ± 0.6 nM. Notably, this compound was highly selective for ABHD6, showing minimal activity against other serine hydrolases, including FAAH and MAGL. Further studies revealed that 1,1,1,3,3,3-Hexafluoropropan-2-yl 5-(2-morpholinoethoxy) isoindoline-2-carboxylate was the most stable compound in human and rodent plasma, making it a promising candidate for therapeutic applications. Additionally, it displayed excellent brain permeability, allowing for central nervous system targeting. Functionally, 1,1,1,3,3,3-Hexafluoropropan-2-yl 5-(2-morpholinoethoxy) isoindoline-2-carboxylate demonstrated neuroprotective effects in retinal models by mitigating AMPA-induced excitotoxicity and reducing glial activation (Malamas et al., 2023). These findings suggest that this compound has therapeutic potential for treating retinal diseases.

1.2.3.5 Other ABHD6 Inhibitors

Orlistat (tetrahydrolipstatin, THL) a known inhibitor of pancreatic lipases used in the treatment of obesity, demonstrated high potency against ABHD6. Initially recognized for its potent inhibition of DAGL, THL was subsequently adapted as a scaffold for the development of serine hydrolase inhibitors such as MAGL. Subsequent studies demonstrated that THL exhibits significant inhibitory activity against ABHD6 (Navia-Paldanius et al., 2012).

Methylarachidonoyl fluorophosphonate (MAFP) acts as a broad-spectrum serine hydrolase inhibitor and is widely utilized as a reference compound in enzyme activity assays (Deutsch et al., 1997). Another inhibitor, LEI-106, a glycine sulfonamide derivative, inhibits both ABHD6 and DAGL α . However, it also showed cross-reactivity with other serine hydrolases,

as demonstrated in mouse brain proteomic assays (Janssen et al., 2014). Finally, ZP-169, with an IC_{50} of 216 nM for ABHD6 exhibits cross-reactivity with other serine hydrolases at higher concentrations (Patel et al., 2015).

1.2.4 Assays to Measure ABHD6 Activity

Several techniques have been applied in the literature to assess the activity of endocannabinoid enzymes like ABHD6. Among these methods, the radiometric assay is commonly regarded as the 'gold standard' due to its accuracy, though alternative methods are increasingly popular due to their efficiency.

- **Conventional Enzyme Activity Assays**

Conventional enzyme assays primarily use liquid chromatography/mass spectrometry (LC/MS) or radiolabelled substrate-based methods. While these techniques are effective for analysing enzyme activity, they are typically associated with high costs, require significant time, and are generally confined to evaluating the activity of a single enzyme at any given time (Bisogno et al., 2003).

- **Natural MAG Substrate [1(3)-AG] with Enzyme-Coupled Detection of Glycerol**

This method measures ABHD6's hydrolytic activity by measuring the glycerol generated from the hydrolysis of the natural monoacylglycerol substrate [1(3)-AG]. The resulting glycerol is then subjected to a cascade of enzyme reactions, ultimately producing a fluorescent compound, resorufin, which facilitates highly sensitive measurement (Savinainen et al., 2016). An advantage of this assay is the use of an endogenous substrate, although it is one that is hydrolysed through multiple routes.

- **High-Throughput Fluorescence Assay**

This high-throughput fluorescence assay utilizes 4-MUH as a synthetic substrate for ABHD6. The hydrolysis of 4-MUH by ABHD6 results in the release of a fluorescent product, enabling rapid and efficient measurement of enzyme activity (Nada Mahmood, 2018). This allows ready quantification of recombinant enzyme activity with plate readers, although the ability of the substrate to detect ABHD6 in complex proteomes is less clear.

- **Activity-Based Protein Profiling (ABPP).**

ABPP is a chemoproteomic approach frequently applied in drug discovery and development. It allows for the simultaneous measurement of multiple enzyme activities in complex biological preparations, eliminating the requirement for natural

substrates. ABPP overcomes the limitations of conventional substrate-based assays by using chemical probes that form covalent bonds with the active sites of target enzymes. These probes, equipped with a reporter tag, enable the detection and measurement of enzymatic activity (Liu et al., 1999). Two examples of ABPs used in profiling ABHD6 activity are fluorophosphonate (FP)-rhodamine and MB064. Whereas FP-rhodamine labels a wide range of serine hydrolases (Cravatt et al., 2008), MB064 is relatively selective for ABHD6 (Baggelaar et al., 2015).

1.3 ABHD12

1.3.1 Role of ABHD12 in patho/physiological conditions

ABHD12 is an integral membrane enzyme critically involved in the hydrolysis of 2-AG. It accounts for approximately 9% of 2-AG degradation in brain membranes, complementing the roles of MAGL and ABHD6 in maintaining the balance of endocannabinoid signaling (Blankman et al., 2007). Unlike MAGL and ABHD6, which predominantly regulate intracellular 2-AG pools, ABHD12 functions as an ectohydrolase, with its active site oriented toward the extracellular or luminal space. This localization enables ABHD12 to regulate the degradation of extracellular 2-AG (Blankman et al., 2007; Savinainen et al., 2011). However, the functional significance of ABHD12 extends beyond its role in 2-AG metabolism.

In addition to degrading 2-AG, ABHD12 plays a crucial role in the metabolism of lysophosphatidylserine (Lyso-PS), a hormone-like signaling lysophospholipid. Lyso-PS is highly abundant in the CNS, particularly in the brain, as well as in immune cells. It regulates diverse physiological and immune functions, including mast cell granule exocytosis (Iwashita et al., 2009), efferocytic clearance of apoptotic cells and macrophage activation (Frasch et al., 2013), as well as the regulation of glucose homeostasis in the CNS and skeletal musculature (Yea et al., 2009). ABHD12 knockout mice have been utilized as a model for PHARC (Polyneuropathy, Hearing loss, Ataxia, Retinitis pigmentosa, Cataract), a rare autosomal recessive disorder resulting from null mutations in the ABHD12 gene. Behavioural assessments of these mice revealed progressive impairments in motor coordination, auditory function, and vision that closely resembling the clinical manifestations observed in human PHARC patients. Notably, lipidomic profiling showed that the absence of ABHD12 did not lead to significant alterations in brain 2-AG concentrations (Blankman et al., 2013), thereby challenging the initial hypothesis that PHARC pathology is associated with impaired endocannabinoid metabolism (Fiskerstrand et al., 2010). To further elucidate the biological

pathways influenced by ABHD12, mass spectrometry-based lipidomic analysis was conducted on brain tissue from both wild-type and ABHD12-deficient mice. The analysis revealed a substantial accumulation of lyso-PS in the brain following ABHD12 deletion. Subsequent biochemical assays confirmed that ABHD12 functions as a crucial lyso-PS hydrolase, highlighting its essential role in lipid metabolism (Blankman et al., 2013). These findings support a mechanistic hypothesis in which the absence of ABHD12 leads to a sustained increase in lyso-PS within the CNS. Over time, this dysregulated lipid accumulation is proposed to interfere with normal signaling pathways, triggering persistent neuroinflammation. This chronic inflammatory state is believed to be a key contributor to the progressive neurobehavioral impairments, including motor and auditory dysfunction, observed in ABHD12-null mice (Blankman et al., 2013).

ABHD12 has been implicated in cancer biology, as a clinical omics analysis of colorectal cancer (CRC) revealed elevated expression in tumour tissues, particularly in recurrent cases (Yoshida et al., 2010). Elevated ABHD12 levels may promote tumour progression and metastasis, suggesting a potential oncogenic role for this enzyme. Beyond CRC, recent studies have highlighted the potential oncogenic role of ABHD12 in breast cancer progression. Immunohistochemical analysis and mRNA profiling showed that ABHD12 expression is significantly upregulated in breast cancer tissues and cell lines compared to normal tissues. Functional experiments demonstrated that knockdown of ABHD12 in breast cancer cell lines (MCF7 and MDA-MB-231) suppressed cell proliferation, migration, and invasion, suggesting that ABHD12 contributes to the aggressive phenotype of breast cancer (Jun et al., 2020).

The oncogenic role of ABHD12 extends to liver hepatocellular carcinoma (LIHC), where its upregulation has been associated with poor prognosis and resistance to sorafenib, a chemotherapeutic agent known to induce ferroptosis (Lu et al., 2022; Cai et al., 2023). Ferroptosis is a distinct form of regulated cell death, characterized by its dependence on iron-mediated lipid peroxidation. Unlike apoptosis, necrosis, and autophagy, this process operates through a distinct mechanism involving oxidative stress-induced lipid damage, which compromises cellular membrane integrity and ultimately triggers cell death (Dixon et al., 2012; Chen et al., 2021). ABHD12 promotes tumour progression by facilitating cell proliferation, migration, and sorafenib resistance, primarily through its influence on the antioxidant enzyme GPX4 and lipid peroxidation (Cai et al., 2023). Knockout or pharmacological inhibition of ABHD12 with the selective inhibitor DO264 sensitized liver cancer cells to sorafenib and ferroptosis, suggesting its potential as a therapeutic target for

improving treatment outcomes. These findings highlight ABHD12 as a promising biomarker and therapeutic target in LIHC management.

1.3.2 ABHD12 Inhibitors

1.3.2.1 Triterpenoid-Based Inhibitors

Parkkari et al. (2014) identified triterpenoid-based compounds as selective, reversible inhibitors of ABHD12. Among them, Maslinic acid ($IC_{50} = 1.3 \mu M$) was identified as a potent inhibitor. Structural optimization, particularly the substitution of the two hydroxyl groups in Maslinic Acid with a fused indole heterocycle at the central core, led to the development of a more potent derivative, which demonstrated a nearly 30% increase in inhibitory potency. These compounds act as reversible inhibitors, as demonstrated through dilution assays that examined the dissociation kinetics of the inhibitor-bound enzyme system. Additionally, target selectivity was assessed using ABPP in lysates derived from HEK293 cells and membrane fractions isolated from mouse brain homogenates, confirming their preferential inhibition of ABHD12 over other serine hydrolases, including ABHD6, MAGL, and FAAH.

1.3.2.2 Cycloartane-type triterpenes derivative

A cycloartane-type triterpene derivative, specifically cycloartenyl-2'E,4'E-decadienoate, isolated from *Euphorbia pterococca*, was identified as a moderate inhibitor of ABHD12 with an IC_{50} value of $11.6 \pm 1.9 \mu M$. Notably, among the tested derivatives, only this compound exhibited selective inhibitory activity toward ABHD12, while showing no activity against other enzymes, including ABHD6, MAGL, and FAAH (Benabdelaziz et al., 2018)

1.3.2.3 Thiourea-based inhibitor

Cravatt's research group introduced DO264, a thiourea-based derivative as a potent and selective inhibitor of ABHD12, both in vitro and in vivo. DO264 was shown to inhibit ABHD12 in a competitive and reversible manner, achieving an IC_{50} of 11 nM in ABPP assays. Despite its thiourea core structure, DO264 exhibits reversible inhibition of ABHD12. DO264 exhibited strong inhibitory effects on lyso-PS hydrolysis catalyzed by recombinant ABHD12 from both mouse and human sources. In transfected HEK293T cell lysates, the compound displayed inhibitory potency with IC_{50} values of approximately 30 nM for mouse

ABHD12 and 90 nM for its human counterpart. DO264 also exhibited strong enzymatic inhibition of lyso-PS hydrolysis in membrane fractions isolated from mouse brain and human THP-1 monocytes, with IC₅₀ values of 2.8 nM and 8.6 nM, respectively.

In C57BL/6 mice, administration of DO264 via intraperitoneal or oral routes resulted in effective inhibition of ABHD12 activity. This pharmacological blockade led to a significant accumulation of lyso-PS in the brain, closely mirroring the lipidomic alterations observed in ABHD12 knockout models. Notably, despite these biochemical changes, DO264-treated mice did not develop the auditory deficits typically associated with PHARC (Ogasawara et al., 2018).

DO264 has also been identified as a potent enhancer of ferroptotic cell death in various cancer models, as previously discussed, making it a promising pharmacological agent. Studies have demonstrated that DO264 treatment amplifies ferroptosis-mediated cell death in multiple cancer types, including fibrosarcoma and hepatocellular carcinoma (Kathman et al., 2020; Cai et al., 2023). Notably, in hepatocellular carcinoma models, co-administration of DO264 with sorafenib not only significantly suppressed tumor progression but also effectively reversed sorafenib resistance, highlighting its potential as an adjunct therapy (Cai et al., 2023). These therapeutic effects closely mirrored those observed in genetic models of ABHD12 deficiency (Kathman et al., 2020; Cai et al., 2023).

1.4 NAGLy

N-Arachidonoyl glycine (NAGLy) is an endogenous lipid metabolite derived from the enzymatic breakdown of the endocannabinoid anandamide (Huang et al., 2001). NAGLy has been identified as an agonist of the G-protein-coupled receptor GPR18, with no detectable affinity for cannabinoid receptor CB1 or the transient receptor potential vanilloid 1 (TRPV1) (Huang et al., 2001; Parmar & Ho, 2010). GPR18, a seven-transmembrane receptor consisting of 331 amino acids, is expressed in various cell types, including peripheral blood cells, lymphoid tissues, macrophages, and the brain. GPR18 expression varies among immune cells, with distinct patterns observed between cytotoxic and reparative cell populations (Kohno et al., 2006). Experimental studies in rat models of inflammatory pain have demonstrated the analgesic potential of NAGLy, where it effectively attenuated mechanical allodynia and thermal hyperalgesia through mechanisms independent of CB1 and CB2 receptor activity (Succar et al., 2007). The high expression of GPR18 in immune system components has prompted research into the immunomodulatory effects of NAGLy. Oral

administration of NAGly has been shown to reduce the migration of pro-inflammatory leukocytes, such as monocytes and neutrophils, into inflamed tissues in a dose-dependent manner. Furthermore, NAGly promotes the production of anti-inflammatory eicosanoids, including 15-deoxy-delta-13, 14-prostaglandin (PGJ2) and lipoxin A4 (LXA4). These mediators play crucial roles in resolving inflammation by modulating immune responses, promoting inflammatory cell apoptosis, and facilitating tissue repair (Burstein et al., 2011). These findings highlight the therapeutic potential of NAGly in modulating immune responses and resolving inflammatory conditions

1.5 Objectives of the Thesis

1. To evaluate the suitability of 4-MUH as a substrate for measuring ABHD6 activity in rat brain tissue, and to determine whether it selectively measures ABHD6 without interference from other serine hydrolases. Previous study (Nada Mahmood, 2018) demonstrated that ABHD6 hydrolyzes 4-MUH in recombinant systems, whereas MAGL and ABHD12 do not. This study extends these findings to rat brain homogenates to assess whether 4-MUH-based assays can reliably measure ABHD6 activity in complex proteome.
2. To utilize ABPP in rat brain tissues to evaluate the selectivity and potency of inhibitors targeting ABHD6 and ABHD12. While previous ABPP studies have predominantly focused on mouse models, the enzymatic activity and pharmacological regulation of these enzymes in rats remain less well-characterized. Since rats exhibit more complex behaviors than mice and are widely used in behavioral studies related to cognition, emotion, and reward processing, understanding their enzymatic profiles is important for translational research. This study investigates ABHD6 and ABHD12 in rat brain using FP-rhodamine and MB064 probes, alongside their selective inhibitors KT203 and DO264, to characterize ABHD6 and ABHD12 activity and inhibition profiles. By comparing these findings with previously reported data from mice, this study examines potential species-specific differences in enzyme function and inhibitor sensitivity. Furthermore, the results may help assess the pharmacological relevance of KT203 and DO264 and their potential for future pharmacological investigations.

Chapter 2: Materials and methods

Table 2.1 Reagents and sources.

Compound	Supplier	Catalogue Number	Comment
Acrylamide/bis-acrylamide	Sigma-Aldrich	Acrylamide/Bis-acrylamide solution 30%	Gel matrix
Ammonium persulfate	Sigma-Aldrich	Ammonium persulfate for molecular biology	Polymerisation initiator
DO264	Cayman Chemical	DO264	ABHD12 inhibitor
FP-rhodamine	Thermo Fisher	ActivX™ TAMRA-FP Serine Hydrolase Probe	Broad spectrum probe for serine hydrolases
JJKK048	Tocris Bioscience	JJKK048 (CAS 1515855-97-6)	High potency MAGL inhibitor
KT203	Cayman Chemical	KT203	ABHD6 inhibitor
MAFP	Sigma-Aldrich	Methyl arachidonyl fluorophosphonate (>98%)	Broad spectrum serine hydrolase inhibitor
MB064	Leiden University	MB064	Probe for limited serine hydrolase activities
MW markers	Sigma-Aldrich	ECL Plex™ Fluorescent Rainbow™ Markers	Provides a range from 225-12 kDa
4-MUH	Sigma-Aldrich	4-Methylumbelliferyl heptanoate (>95% GC)	ABHD6 synthetic substrate
NAGly	Tocris Bioscience	N-Arachidonylglycine (CAS 179113-91-8)	Endogenous metabolite (now withdrawn from sale)
TEMED	Sigma-Aldrich	N,N,N',N'-Tetramethylethylenediamine (>99%)	Polymerisation catalyst
WWL70	Tocris Bioscience	WWL70 (CAS 947669-91-2)	ABHD6 inhibitor

2.1 Tissue preparation (conducted by SPH Alexander)

Rat (male Sprague-Dawley, 150-250 g) brains were obtained after Schedule 1 killing and stored at -80 °C. The whole brain was thawed and homogenised in 8 volumes of 10 mM Tris:0.2 mM EDTA, pH 7.4 buffer using a glass: Teflon homogeniser. The suspension was then centrifuged at 20000 g for 30 min at 4 °C. The supernatant layer was removed and stored. The pellet was homogenised again in the same volume of buffer using the glass: Teflon homogeniser and the centrifugation step was repeated. The supernatant layer was removed and mixed with the previous supernatant and then stored as aliquots at -80 °C. The pellet was re-suspended in 6 volumes of the same buffer and then stored as aliquots at -80 °C.

2.2 Protein Determination

Protein concentrations in the biological samples were measured using the Lowry assay, which is based on the reaction between proteins and the Folin-Ciocalteu reagent in the presence of alkaline copper (Lowry et al., 1951). A standard curve was generated using Bovine serum albumin (BSA) with concentrations ranging from 0.05 to 0.40 $\mu\text{g}/\mu\text{L}$. After incubating both samples and standards at room temperature for 10 minutes, 1 mL of Lowry reagent mixture (composed of 0.2% SDS, 2% Na_2CO_3 in 1 M NaOH, 1% potassium sodium tartrate, and 0.5% $\text{CuSO}_4 \cdot \text{H}_2\text{O}$) was added and briefly vortexed. The samples were then incubated for 45 minutes at room temperature before 100 μL of diluted Folin-Ciocalteu reagent (1:1 in purified water) was added. Samples and standards were loaded into 96-well assay plates, and absorbance was measured using a 96-well plate reader (Dynex spectrophotometer). The sample concentrations were then calculated by interpolating the absorbance values from the BSA standard curve, using linear regression analysis in GraphPad Prism 10.

2.3 The 4-MUH based assay

A spectrophotometric assay was used to measure ABHD6 activity with 4-MUH as the substrate. During the reaction, 4-MUH was hydrolysed, producing the fluorescent compound 4-MU (Figure 2.1). The spectrophotometer detected the fluorescence of 4-MU, which allowed for the measurement of ABHD6 activity based on the intensity of the fluorescent signal produced during the reaction.

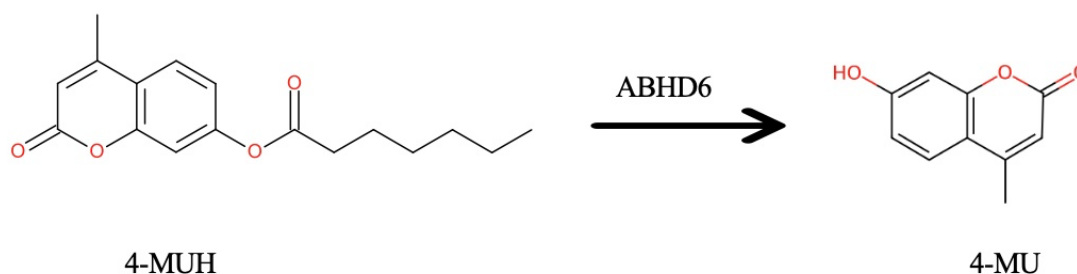


Figure 2.1 Schematic clarify the chemical reaction of 4-MUH hydrolysis.

For measuring ABHD6 activity in rat brain tissues, the 4-MUH hydrolysis assay was selected based on findings from a previous project using human recombinant ABHD6 (Nada Mahmood, 2018). This study demonstrated that ABHD6 but not splice variants of MAGL (MAGL1 and MAGL2) or ABHD12, was able to hydrolyse 4-MUH in a recombinant system, suggesting that it could be used in a mixed proteome to measure ABHD6 activity (Figure 2.2). The assay showed low background activity, indicating substrate stability, with a clear signal difference between ABHD6 and other transfects, including mock controls. MAGL exists as two splice variants, MAGL1 and MAGL2, which differ in their subcellular localization and pharmacological properties. MAGL1 is more abundant in the soluble fraction, whereas MAGL2 is primarily membrane-associated (Nada Mahmood, 2018). While both isoforms exhibit similar enzymatic activity, differences in their pIC₅₀ values and inhibition slopes suggest distinct biochemical properties. However, neither variant hydrolyzed 4-MUH, further reinforcing the specificity of this assay for ABHD6. To further validate the use of 4-MUH in ABHD6 screening, recombinant ABHD6 was tested in the presence of several inhibitors at a final concentration of 1 μ M. Nada Mahmood screened 11 inhibitors to assess their effect on 4-MUH hydrolysis. Among these, MAFP, JKKK048, and WWL70 significantly inhibited ABHD6 activity, while other inhibitors showed no notable effect (Figure 2.3). These findings provided evidence for 4-MUH acting as an appropriate substrate for measuring ABHD6 activity in the current study with rat brain tissues.

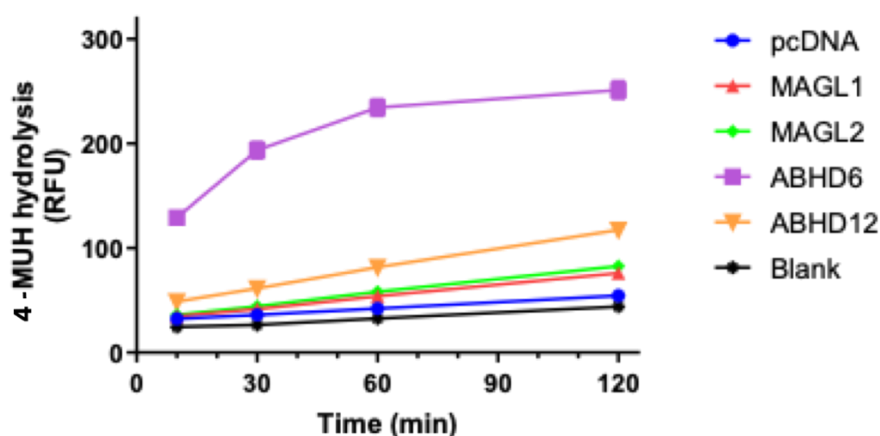


Figure 2.2 4-MUH hydrolysis in recombinant enzyme-HEK293 membrane preparations (pcDNA, MAGL1, MAGL2, ABHD6, and ABHD12). Recombinant ABHD6 selectively hydrolyzes 4-MUH compared to other esterases. Reproduced from Dr. Nada Mahmood's thesis (2018).

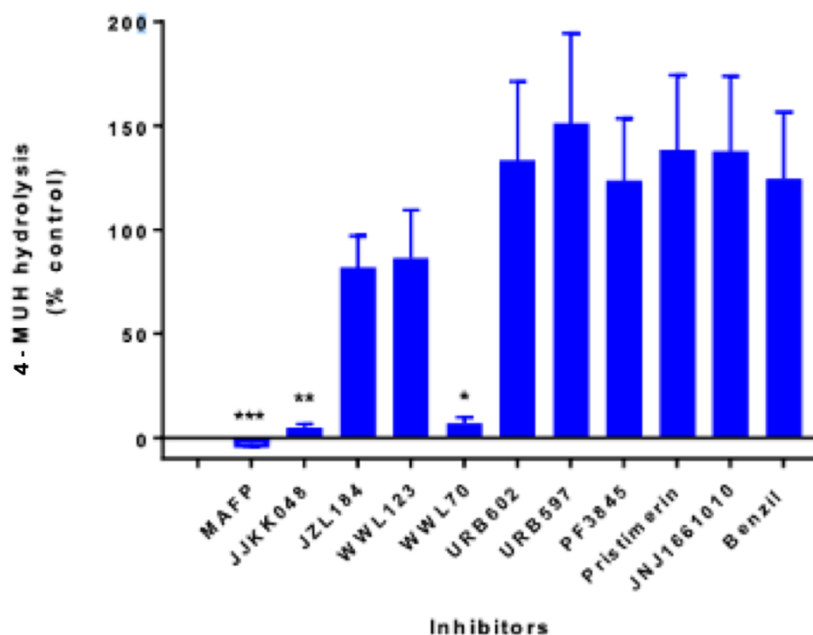


Figure 2.3 Hydrolysis of 4-MUH by ABHD6-HEK293 membrane preparations treated with 1 μ M concentrations of eleven distinct inhibitors. Data represent mean \pm SEM from seven separate preparations performed in duplicate.

Reproduced from Dr. Nada Mahmood's thesis (2018).

2.3.1 Data analysis

Linear regression analysis of the time course for 4-MUH hydrolysis was conducted to estimate rates of enzyme activity using GraphPad Prism 10 software.

For inhibitor concentration-response data, non-linear regression analysis was performed using the four-parameter logistic model. Both one-site and two-site binding models were compared to determine the best fit for the data using GraphPad Prism 10 software. The top value was constrained to 100%, representing enzyme activity in the absence of an inhibitor. LogIC₅₀ values and residual activities were calculated for each model to assess inhibitor potency and remaining enzyme activity.

2.4 Activity-Based Protein Profiling (ABPP)

ABPP is a chemoproteomic technique widely used in drug discovery and development to assess enzyme activities within complex biological systems in a single experiment, without relying on natural substrates. Instead of conventional substrate-based assays, ABPP employs

activity-based probes that covalently bind to the active site of target enzymes. These probes are designed with a reporter tag, enabling the detection of enzymatic activity (Liu et al., 1999). This approach has been particularly useful in characterizing the roles of ABHD6 and ABHD12 in 2-AG hydrolysis (Blankman et al., 2007) and allows for the simultaneous screening of multiple enzymes within the same protein family. However, due to their broad reactivity, ABPP probes often lack specificity, which can limit their ability to differentiate individual enzyme activities across various tissues.

2.4.1 Conducting ABPP

2.4.1.1 Gel Electrophoresis

The experiments used 10% acrylamide, gels measuring 20 cm by 20 cm (as outlined in Table 2.2). The gel was composed of a stacking gel, which made up about one-third of the total volume, and a resolving gel that occupied the remaining two-thirds. A constant current of 15 milliamperes was applied until the dye front passed through the stacking gel. Afterward, the current was increased to 30 milliamperes and run for 9-10 hours until the dye front reached the bottom of the gel.

Table 2.2 Presents components required to prepare a single 10% acrylamide gel.

Addition	Resolving gel	Stacking gel
Distilled water	14.35 mL	21.35 mL
Tris buffer	8.75 mL (1.5 M, pH 8.8)	8.75 mL (0.5 M, pH 6.8)
10% SDS solution	0.35 mL	0.35 mL
30% acrylamide	11.55 mL	4.55 mL
TEMED (tetramethyl ethylenediamine)	17.5 μ L	35 μ L
APS (ammonium persulfate) 10% (w/v)	175 μ L	175 μ L
Total	35 mL	35 mL

2.4.1.2 Preparation of the resolving gel

14.35 mL of deionized water was mixed with 8.75 mL of 1.5 M Tris buffer (pH 8.8), 0.35 mL of 10% SDS solution, 11.55 mL of 30% acrylamide solution, 17.5 μ L of TEMED, and 175 μ L of freshly prepared 10% ammonium persulfate (APS) solution. The mixture was gently Shaken to prevent the formation of air bubbles. Before pouring the solution into in the instrument, deionized water was used to check for leakage. The water was then discarded to ensure there were no leaks. Then, about 35 mL of the resolving gel solution was poured

between the glass plates, leaving enough space for the stacking gel (approximately one-third of the total gel height). Next, small volume of 1:1 butanol/deionized water solution was added on top of the resolving gel to create a flat interface and eliminate any air bubbles. The gel was allowed to polymerize for 45 to 60 minutes. After the polymerization of the gel, filter paper was used to remove butanol/deionized water solution.

2.4.1.3 Preparation of the stacking gel

21.35 mL of deionized water was mixed with 8.75 mL of 0.5 M Tris buffer (pH 6.8), 0.35 mL of 10% SDS solution, 4.55 mL of 30% acrylamide solution, 35 μ L of TEMED, and 175 μ L of freshly prepared 10% APS solution. The mixture was gently Shaked to ensure thorough dissolution. This stacking gel solution was then poured into the instrument between the glass plates, filling the remaining space above the already polymerized resolving gel. A gel comb was carefully inserted to form wells for loading protein samples, and the stacking gel was left to polymerize for approximately one hour before use.

2.4.1.4 Activity-based Probes

ABPs are typically designed to react with the active site of enzymes, forming irreversible covalent bonds. This tagging method enables the labelling of the active site in a specific enzyme or group of related enzymes. The broad-spectrum probe FP-rhodamine was ineffective in detecting DAGL activity (Figure 2.4) (Liu et al., 1999), leading to the development of a more selective probe, MB064 (Figure 2.5). This new probe successfully labelled DAGL, ABHD6, and ABHD12 (Baggelaar et al., 2013).

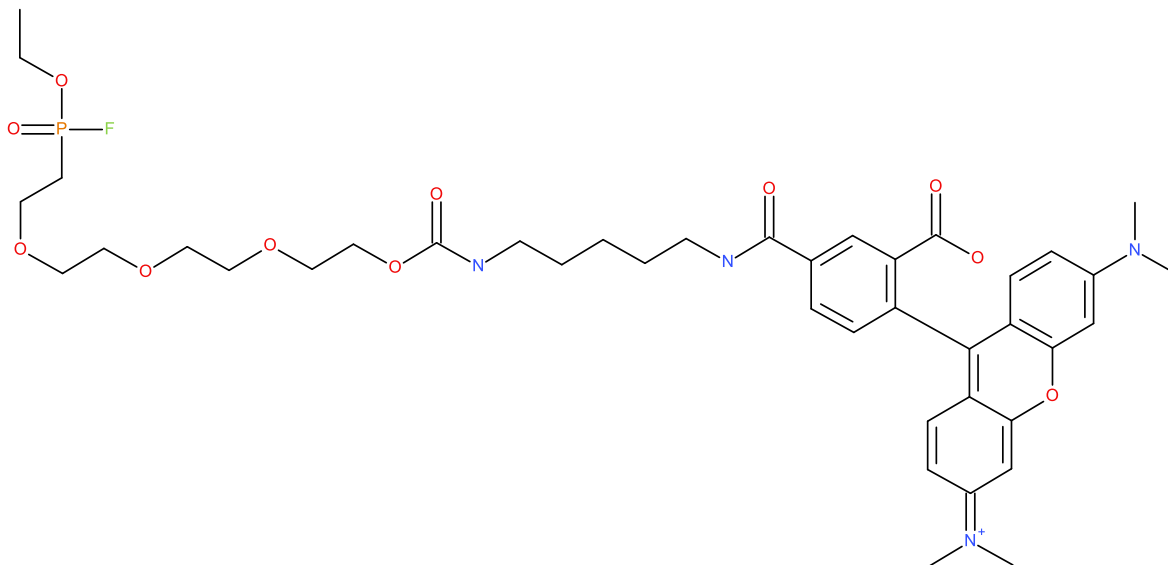


Figure 2.4 Chemical structure of FP-rhodamine.

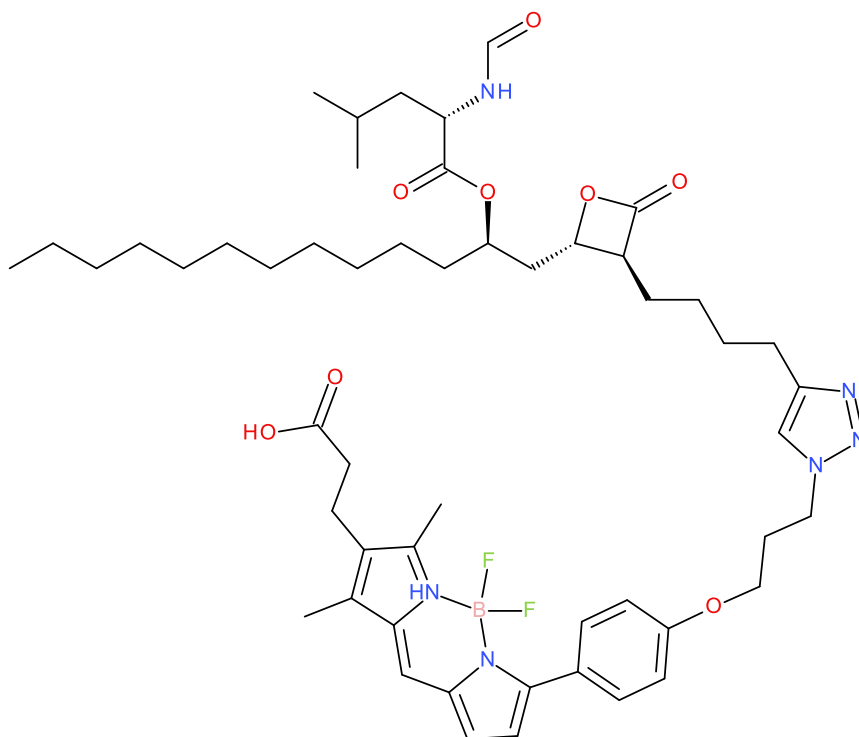


Figure 2.5 Chemical structure of MB064.

2.4.1.5 Reaction with the activity probes

The assay was conducted using rat brain tissues (soluble and particulate fractions). Tissues were prepared at a concentration of 3-4 mg/mL protein and incubated at 37 °C for 15 minutes. This pre-incubation step was aimed at reducing levels of endogenous substrates. After the initial incubation, 2 µL of inhibitors at varying concentrations (100 µM, 10 µM, 0.1 µM) or vehicle (DMSO) controls were added to 16 µL of tissue samples in mini-Eppendorf tubes. The tubes were vortexed briefly to ensure thorough mixing. Following a 15-minute pre-incubation at 37 °C in a shaking dry heater, 2 µL of either FP-rhodamine (500 nM final concentration) or MB064 (500 nM final concentration) was added. The tubes were vortexed again and incubated for an additional 30 minutes (for FP-rhodamine) or 45 minutes (for MB064) at 37 °C. The reactions were stopped by adding 4 µL of 6x Laemmli buffer to each tube, yielding a final reaction volume of 24 µL, and the samples were placed on ice to ensure complete termination. The samples were either used immediately or stored at 4 °C or -20 °C for subsequent analysis. Before electrophoresis, all samples were heated at 95 °C for 3-5 minutes to ensure complete denaturation, particularly for membrane-bound proteins. A volume of 20 µL of each sample was then loaded onto 10% SDS-PAGE gels and subjected to electrophoretic separation (Figure 2.6).

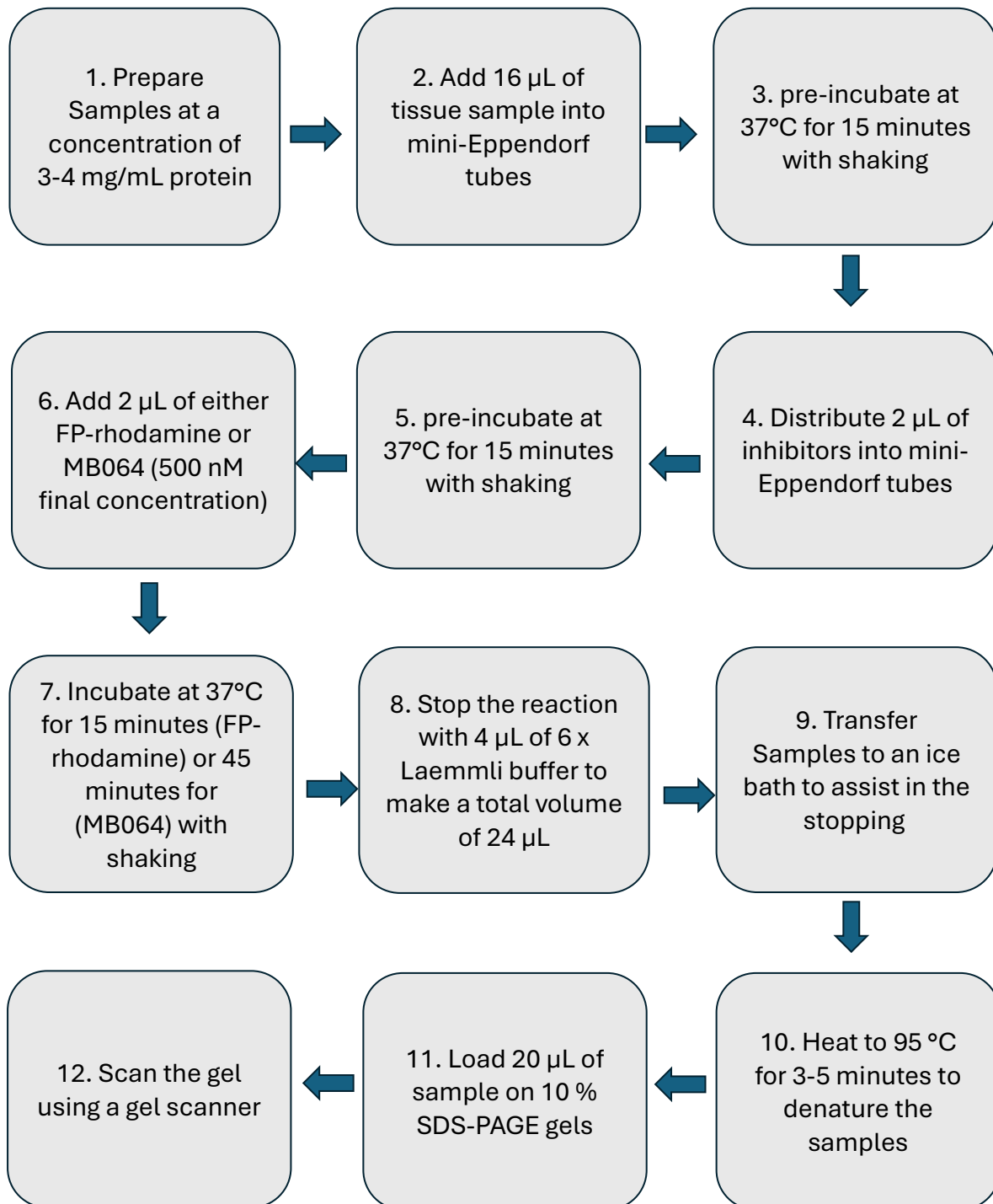


Figure 2.6 Presents a schematic representation of the ABPP assay used to analyze enzyme activity in the soluble and particulate fractions of rat brain tissue. The workflow outlines the key experimental steps, including sample preparation, inhibitor incubation, activity probe labeling, reaction termination, protein denaturation, SDS-PAGE electrophoresis, and gel imaging.

2.4.1.6 Gel Organization and Sample Loading

For efficient identification and organization, two asymmetric gel layouts were used during electrophoresis to simplify lane tracking and analysis. In the first layout, the molecular weight ladder (Rainbow, Amersham RPN500E) was loaded into lanes 1, 11, and 32, with samples loaded in lanes 2-10 and 12-31. In the second layout, the molecular weight ladder was loaded into lanes 1, 12, and 33, while samples were loaded in lanes 2-11 and 13-32 (Figure 2.7). This arrangement distributed molecular weight markers across the gel, allowing for accurate band identification and comparison in sample lanes.

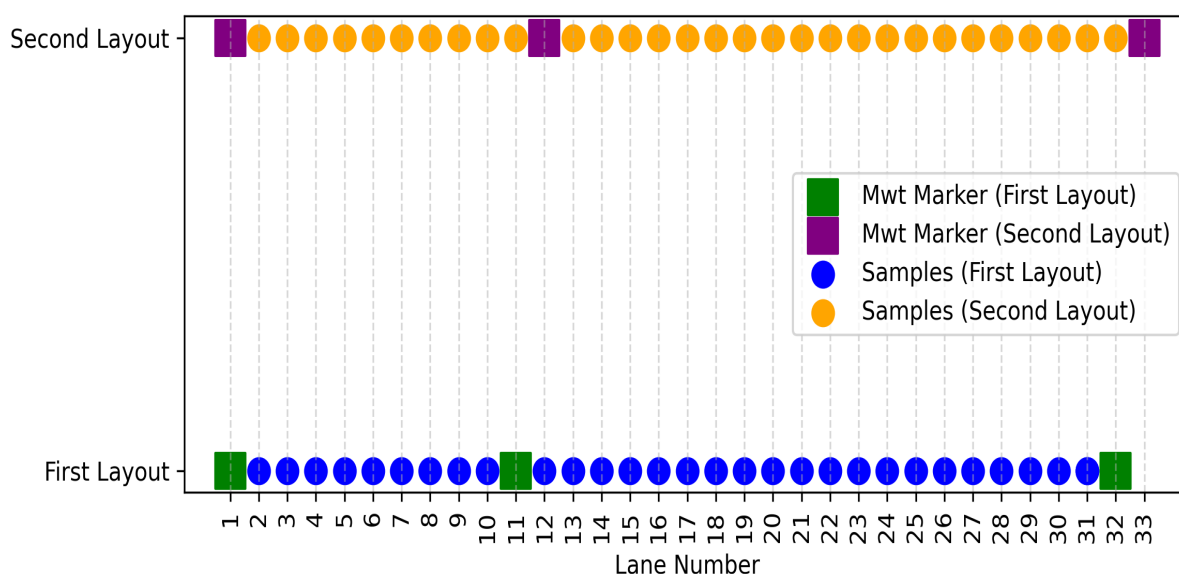


Figure 2.7 Illustrates the gel lane organization used during electrophoresis to facilitate lane tracking, analysis, and to improve the precision of molecular weight estimation. In the figure, blue circles represent sample lanes in the first gel layout, while orange circles indicate sample lanes in the second layout. Green squares denote molecular weight markers in the first layout, whereas purple squares represent molecular weight markers in the second layout.

2.4.1.7 Gel scanning and band quantification

Before imaging, the glass plates between which the gel was positioned during electrophoresis were gently dried using tissue paper. The gel was then placed on the Amersham Typhoon scanner for imaging, with the scanner set to the Cy3 filter (532 nm excitation, 580 nm emission). The scanned image was saved as a TIFF file. Following the scan, the gel was stained with Coomassie blue, which served as a protein loading control.

2.4.2 Data analysis

2.4.2.1 Gel Image Analysis

Gel images were analyzed using the Image Lab software (Bio-Rad). After scanning, the TIFF file of the gel was imported into the software. The molecular weight (MW) ladder was included in the analysis to estimate the molecular weight of the detected bands.

To enhance the clarity of the bands, brightness and contrast adjustments were applied. The gel image was then rotated and cropped, if necessary, to ensure proper alignment.

Lane Detection: Lanes were manually defined using the *Lane Tools* to ensure accurate alignment with the loaded samples. This manual adjustment ensured that each lane fully covered the appropriate area, improving the accuracy of subsequent analyses.

Band Detection: Bands were manually detected for all lanes to ensure consistency. This approach was particularly important for fainter bands that may have been missed by automatic detection.

Background Subtraction: Background signals were subtracted to reduce noise and enhance the precision of the intensity measurements. This step was critical for accurately quantifying the protein bands of interest.

Lane Profile Adjustment: The lane profile was adjusted to align the detected peaks with the actual bands, ensuring accurate quantification of band intensities. Data, including the molecular weight and band intensity measurements, were exported from Image Lab in tabular format for subsequent statistical analysis.

GraphPad Prism software 10 was used for further analysis to compare the adjusted volumes of the protein bands before and after inhibitor treatment. A two-way repeated measures ANOVA with Dunnett's multiple comparisons test was conducted to assess whether enzyme activity was significantly reduced in the presence of selective inhibitors.

The band intensities were measured under blinded conditions, where the identities of the samples were concealed until after the quantification was complete. Samples were coded (SPH Alexander) to maintain randomization and blinding throughout the entire process, from preparation to analysis.

2.4.2.2 Molecular weight estimation

Although the molecular weight standards included 10 different sizes, only four (150, 76, 52, and 31 kDa) were detectable at the wavelengths used by the fluorescent scanner (Cy3

channel). Image Lab was able to calculate the denatured molecular weight for bands within the range of 150 to 31 kDa.

To overcome the limitation in detecting molecular weights, a Coomassie Blue-stained gel was scanned with the Cy5 filter on the Amersham Typhoon scanner. The Coomassie-stained gel was analysed using the same process as the Cy3-scanned gel, utilizing the Image Lab software. With the Coomassie stain, Image Lab was able to detect seven molecular markers: 225, 150, 102, 76, 52, 38, and 31 kDa. The retardation factor (Rf values) for those denatured molecular markers were measured using the Image Lab software.

The Rf values of the protein bands from the Cy3-scanned gels were then imported into GraphPad Prism 10 for further analysis. A standard curve was created by plotting the denatured MW of the markers from the Cy5-scanned and the Cy3-scanned gel against their corresponding Rf values. This non-linear regression analysis allowed for the calculation of denatured MW for protein bands that fell outside the 150–31 kDa range detected by the Cy3 filter (Figure 2.8).

	Cy5	Cy3
Sigmoidal, 4PL, X is concentration		
Best-fit values		
Bottom	0.05449	0.06097
Top	1.254	1.127
IC50	40.21	43.40
HillSlope	-1.929	-2.177
logIC50	1.604	1.637
Span	1.199	1.066
Goodness of Fit		
Degrees of Freedom	17	8
R squared	0.9989	0.9993
Sum of Squares	0.001463	0.0004689
Sy.x	0.009277	0.007655
Number of points		
# of X values	63	63
# Y values analyzed	21	12

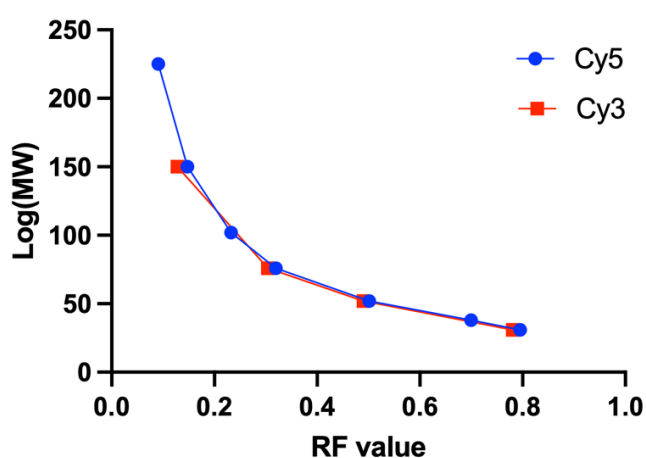


Figure 2.8 Non-linear regression analysis of Molecular weight (MW) versus relative Rf value for Cy3- and Cy5-scanned Gels. The standard curve was generated using molecular weight markers detected via Cy3 and Cy5 channels, providing a reference for estimating molecular weights of unidentified protein bands. The close alignment of Rf values between Cy3 and Cy5 markers validates the Coomassie-based molecular weight estimation approach in cases where fluorescent Cy3 detection is limited.

Chapter 3: Spectrophotometer-based assay of ABHD6 activity in rat brain preparations

This chapter focuses on ABHD6, a transmembrane serine hydrolase that is highly expressed in both peripheral and central tissues. As a member of the α/β -hydrolase fold superfamily (Labar et al., 2010a), it is involved in the degradation of monoacylglycerol lipids, particularly 2-AG to generate glycerol and arachidonic acid (AA). Initial evidence suggesting that enzymes other than MAGL contribute to 2-AG hydrolysis emerged from studies conducted on the BV2 microglial cell line, which, despite lacking MAGL expression, still exhibited significant 2-AG hydrolytic activity (Muccioli et al., 2007). Further research employing ABPP with the FP-rhodamine probe in complex proteomes identified ABHD6 and ABHD12 as additional, relatively minor enzymes involved in the degradation of 2-AG (Blankman et al., 2007). Since its identification, there has been growing interest in the therapeutic potential of ABHD6. Inhibition of ABHD6 activity has been proposed as a promising target for therapeutic intervention in a variety of diseases. Therefore, developing reliable assays, substrates, and inhibitors to study ABHD6 is essential for understanding its physiological roles and therapeutic potential. To investigate ABHD6 activity in rat brain tissues, 4-MUH hydrolysis assay was selected. 4-MUH, a fluorescent substrate, has been widely used in lipase assays due to its resistance to hydrolysis by non-lipase esterases (Gilham et al., 2005). Upon hydrolysis, it produces 4-methylumbelliferone (4MU), a strongly fluorescent product that enables accurate detection of enzyme activity (Gilham et al., 2005). Notably, a study by Nada Mahmood (2018) demonstrated that ABHD6, but not MAGL or ABHD12, could hydrolyse 4-MUH in a recombinant system (Figure 2.2). This suggests that 4-MUH could be a suitable substrate for specifically measuring ABHD6 activity, even in a complex proteome, such as that of rat brain preparations.

3.1 Objective

To investigate the potential of 4-methylumbelliferyl-heptanoate (4-MUH) as a substrate for measuring ABHD6 activity in rat brain tissue

3.2 Results

In this chapter, the inhibitory effects of several compounds of different selectivity —namely JKKK048, KT203, WWL70, and MAFP— were investigated on 4-MUH hydrolysis in rat brain tissues. MAFP is a non-selective irreversible inhibitor of the serine hydrolase family

(Deutsch et al., 1997). JJKK048 is reported as a selective, ‘ultra-potent’ inhibitor of monoacylglycerol lipase (MAGL) (Aaltonen et al., 2013). WWL70 is a selective, early-generation carbamate-based inhibitor of ABHD6 (Li et al., 2007). KT203 is a next-generation carbamate-based ABHD6 inhibitor developed with an improved in vivo profile (Hsu et al., 2013). By assessing the inhibitory effects of these compounds, this study aimed to establish an assay for ABHD6 using 4-MUH hydrolysis in rat brain. Preliminary experiments indicated that a 200-fold dilution was suitable (Figure 3.1), and thus it was used in subsequent experiments. The 200-fold dilution was chosen for both the soluble (S1, S2) and particulate (P1, P2) fractions of the rat brain preparation as it ensured effective enzymatic activity without substrate saturation. Furthermore, this dilution allowed for reliable detection of enzymatic activity while maintaining consistency across experimental conditions. All experiments were carried out using a 4-MUH concentration of 50 μ M. This choice was guided by the results from Miralpeix et al. (2021), who demonstrated that ABHD6 activity remained stable up to 50 μ M of 4-MUH. At concentrations above 50 μ M, the formation of 4-MU reached a steady state, indicating that further increases in the substrate concentration do not enhance enzyme activity.

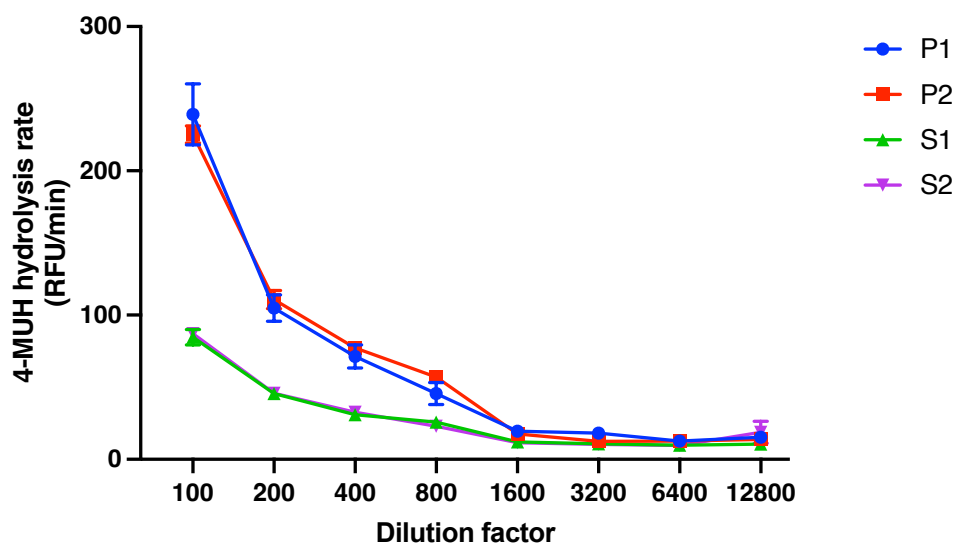


Figure 3.1 The hydrolysis rates of 4-MUH were measured for both soluble (S1, S2) and particulate (P1, P2) fractions of rat brain at various dilutions. Data represent mean \pm SEM of a single experiment performed in triplicate, representative of four separate preparations.

3.2.1 MAFP

The non-selective serine hydrolase inhibitor MAFP evoked a complex concentration-dependent inhibition of 4-MUH hydrolysis in both the soluble and particulate fractions of rat brain tissue (Figure 3.2). The soluble fraction appeared to be slightly less sensitive to MAFP compared to the particulate fraction. At the highest concentration of MAFP used (10 μ M), 75% or more of the 4-MUH hydrolysis activity was inhibited in both preparations.

As shown in Table 3.1, the R max% for the soluble fraction was 2 ± 6 , indicating that a small fraction of enzymatic activity (approximately 2%) remained after MAFP inhibition, reflecting near-complete inhibition. As shown in Table 3.2, the mean R max% for the particulate fraction was calculated as -4 ± 8 , with some individual experiments showing negative values, suggesting that enzymatic activity in these cases was reduced to undetectable levels.

However, not all R max% values for the particulate fraction were negative; some experiments showed slight residual activity. This variability reflects potential biological or experimental differences and will be further explored in the Discussion section. Nevertheless, these findings emphasize the potent inhibitory effects of MAFP, particularly in the particulate fraction, where most measurements indicated near-total inhibition of 4-MUH hydrolysis.

The analysis of the quantitative summary statistics revealed that the one site model for inhibition of the soluble fraction showed a slightly better coefficient of variation ($R^2 = 0.91$) compared to the two site (0.90), indicating a better overall fit. For the particulate fraction, both models showed similar R squared values (0.80), suggesting no significant improvement with the 2-site model. In terms of inhibitor potency, the soluble fraction exhibited a mean LogIC₅₀ of $-6.82 (\pm 0.25)$, while the particulate fraction had a mean LogIC₅₀ of $-7.30 (\pm 0.20)$. The slope of the concentration-response curve was also analysed, revealing a mean slope of $-0.34 (\pm 0.04)$ for the soluble fraction and $-0.42 (\pm 0.07)$ for the particulate fraction. The steeper slope in the particulate fraction suggests a more pronounced response to changes in inhibitor concentration compared to the soluble fraction.

Overall, the soluble fraction appeared to be slightly less sensitive to the inhibitor compared to the particulate fraction. The analysis did not provide strong evidence for a two-site fit model being superior, as the improvements in fit were not significant.

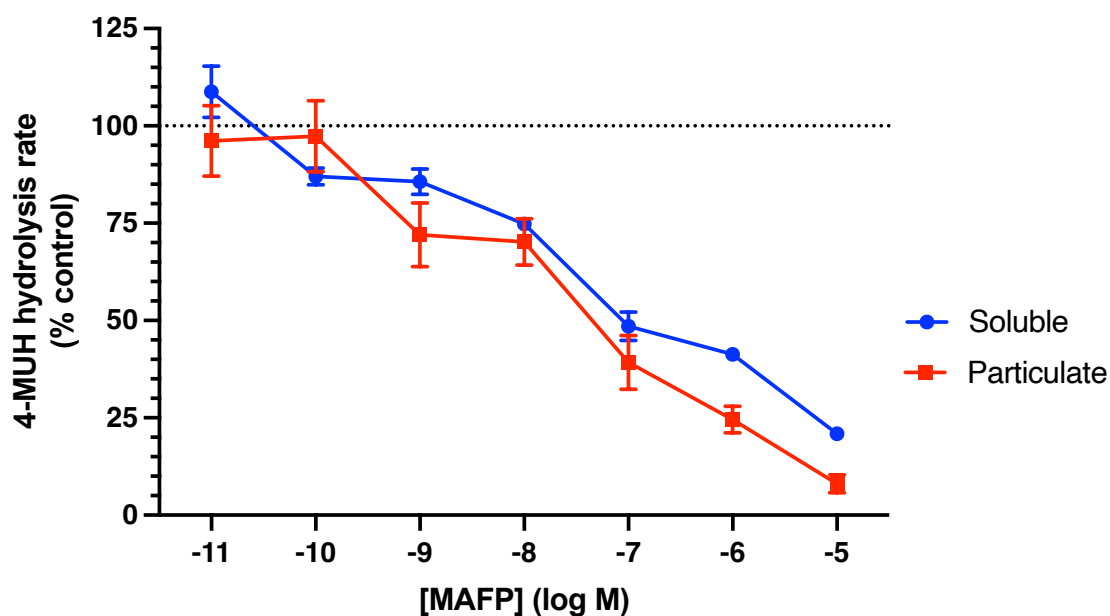


Figure 3.2 Concentration inhibition curves of MAFP for 4-MUH hydrolysis in soluble and particulate fractions of rat brain. The blue line represents the soluble fraction, while the red line corresponds to the particulate fraction, allowing for a comparative analysis of MAFP inhibition in each fraction. Data were analyzed using a nonlinear regression model, comparing both one-site (four-parameter logistic, 4PL) and two-site binding models to determine the best fit for inhibition dynamics. Data are means \pm SEM of five independent preparations, each conducted in triplicate.

Table 3.1 A comparison of one-site vs two-site models for MAFP inhibition of 4-MUH hydrolysis in rat brain soluble fractions.

	S1	S2	S3	S4	S5	Mean \pm SEM
P value			0.2410		0.5346	
log(agonist) vs. response -- Variable slope (four parameters)						
R max%	8.07	-11.57	15.77	-14.86	10.60	2 \pm 6
LogEC₅₀	-7.18	-6.33	-7.52	-6.20	-6.85	-6.82 \pm 0.25
HillSlope	-0.3225	-0.3324	-0.3437	-0.2463	-0.4730	-0.34 \pm 0.04
R squared	0.935	0.875	0.881	0.932	0.925	0.910 \pm 0.013
Two sites - Fit logIC₅₀						
R max%	~ -56.94	~ -2380	30.62	27.64	20.76	26 \pm 3
FractionHi	~ 0.3697	~ 0.02245	0.2686	0.3571	0.2979	0.31 \pm 0.03
LogIC₅₀HI	-8.15	-7.84	-10.27	-10.14	-8.85	-9.05 \pm 0.50
LogIC₅₀Lo	-4.41	~ -3.074	-7.46	-6.78	-6.54	-6.30 \pm 0.59
R squared	0.893	0.897	0.893	0.925	0.927	0.907 \pm 0.008

Table 3.2 A comparison of one-site vs. two-site models for MAFP inhibition of 4-MUH hydrolysis in rat brain particulate fractions.

	P1	P2	P3	P4	P5	Mean ± SEM
P value	0.5883		0.2413		0.5708	
log(agonist) vs. response -- Variable slope (four parameters)						
R max%	4.326	-33.59	9.688	-5.962	4.239	-4 ± 8
LogEC50	-7.41	-7.00	-7.19	-7.99	-6.78	-7.30 ± 0.20
HillSlope	-0.4640	-0.2226	-0.4486	-0.2974	-0.6492	-0.42 ± 0.07
R squared	0.909	0.937	0.723	0.632	0.786	0.797 ± 0.057
Two sites - Fit logIC₅₀						
R max%	18.00	5.946	20.59	10.08	6.736	12 ± 3
FractionHi	0.2215	0.4424	0.3208	0.4208	0.3634	0.35 ± 0.04
LogIC50HI	-9.92	-10.26	-9.47	-10.08	-7.93	-9.53 ± 0.40
LogIC50Lo	-7.33	-6.93	-6.88	-7.40	-6.26	-6.96 ± 0.20
R squared	0.910	0.934	0.745	0.630	0.790	0.802 ± 0.056

Best-fit values from the nonlinear regression of log(agonist) vs. response curves using a variable slope (four-parameter) model on baseline-corrected soluble fraction or particulate.

Data are from five soluble and five particulate preparations.

3.2.2 KT203

The inhibitory effects of the ABHD6-selective inhibitor KT203 on 4-MUH hydrolysis in rat brain tissue was evaluated (Figure 3.3). The concentration-inhibition analysis of ABHD6 activity by KT203 revealed that at low concentrations (<10 nM), KT203 produced minimal inhibition of 4-MUH hydrolysis in both the soluble and particulate fractions of the rat brain. However, at higher concentrations (>10 nM), the inhibition of 4-MUH hydrolysis by KT203 was more pronounced in the particulate fractions compared to the soluble phase. Even at the highest concentration tested (10 µM), over 50% of 4-MUH hydrolysis activity remained in both fractions, suggesting the involvement of a serine hydrolase enzyme(s) other than ABHD6 that contributes to 4-MUH hydrolysis in rat brain tissue fractions.

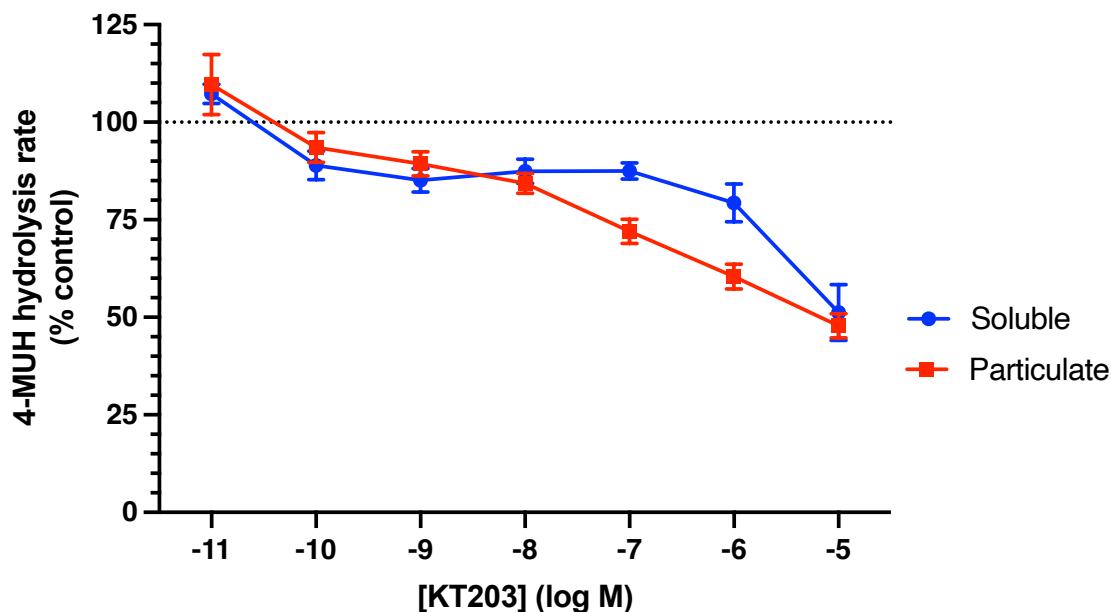


Figure 3.3 Concentration inhibition curves of KT203 for 4-MUH hydrolysis in soluble and particulate fractions of rat brain. The blue line represents the soluble fraction, while the red line corresponds to the particulate fraction, allowing for a comparative analysis of MAFP inhibition in each fraction. Data were analyzed using a nonlinear regression model, comparing both one-site (four-parameter logistic, 4PL) and two-site binding models to determine the best fit for inhibition dynamics. Data are means \pm SEM of five independent preparations, each conducted in triplicate.

The quantitative analysis comparing one-site and two-site curve fitting models for both soluble and particulate fractions of KT203 indicated different levels of fit depending on the fraction. For the five soluble fractions, the two-site model provided a better fit for the data in four of the five preparations, as indicated by higher R^2 values, though P-values were not provided for all comparisons (Table 3.3). In contrast, for the five particulate fractions, the one-site model provided a better fit for the data in four of the five preparations (Table 3.4). The mean LogIC_{50} values for the soluble fractions were -10.01 ± 0.27 ($\text{LogIC}_{50\text{HI}}$, representing the high-affinity binding site) and -5.13 ± 0.14 ($\text{LogIC}_{50\text{Lo}}$, representing the low-affinity binding site), consistent with the two-site model. The fraction of high-affinity sites ($\text{Fraction}_{\text{Hi}}$) was 0.18 ± 0.03 , indicating that approximately 18% of the total binding sites exhibited high-affinity interactions, with the remaining majority exhibiting low-affinity binding. This reflects the heterogeneity of binding interactions within the soluble fractions. In contrast, the mean LogIC_{50} value for the particulate fractions was -5.73 ± 0.80 , consistent

with the one-site model. Overall, these findings indicate that the two-site model better explains the inhibition observed in the soluble fractions, while the one-site model is more appropriate for the particulate fractions.

Table 3.3 A comparison of one-site vs two-site models for KT203 inhibition of 4-MUH hydrolysis in rat brain soluble fractions.

	S1	S2	S3	S4	S5	Mean ± SEM
log(agonist) vs. response -- Variable slope (four parameters)						
R max%	~ -80893	~ -56721	~ -55095	~ -38452	~ -3973	
LogEC₅₀	~ 8.686	~ 13.29	~ 9.840	~ 7.225	~ 1.267	
HillSlope	-0.2308	-0.1640	-0.2031	-0.2515	-0.3485	-0.24 ± 0.03
R squared	0.8072	0.7440	0.7026	0.5362	0.6372	0.685 ± 0.046
Two sites - Fit logIC₅₀						
R max%	5.244	26.06	-21.49	~ -7055	54.13	16 ± 16
FractionHi	0.1590	0.2644	0.1488	~ 0.001349	0.1327	0.18 ± 0.03
LogIC₅₀HI	-10.42	-10.50	-10.06	-10.08	-9.01	-10.01 ± 0.27
LogIC₅₀Lo	-5.12	-5.55	-4.81	~ -2.564	-5.04	-5.13 ± 0.14
R squared	0.9127	0.8693	0.8383	0.7020	0.6633	0.797 ± 0.049

Table 3.4 A comparison of one-site vs two-site models for KT203 inhibition of 4-MUH hydrolysis in rat brain particulate fractions.

	P1	P2	P3	P4	P5	Mean ± SEM
P value	0.1875	0.3670	0.6137	0.6213	0.0128	
log(agonist) vs. response -- Variable slope (four parameters)						
R max%	-3.900	40.76	-107.4	59.48	30.06	4 ± 30
LogEC₅₀	-5.80	-6.30	-2.73	-7.48	-6.33	-5.73 ± 0.80
HillSlope	-0.2230	-0.4732	-0.1889	-1.026	-0.2823	-0.44 ± 0.16
R squared	0.811	0.661	0.550	0.737	0.800	0.712 ± 0.048
Two sites - Fit logIC₅₀						
R max%	38.03	44.94	46.50	59.12	49.97	48 ± 3
FractionHi	0.3796	0.3468	0.2098	0.07272	0.3398	0.27 ± 0.06
LogIC₅₀HI	-10.18	-8.33	-11.94	-9.43	-9.84	-9.94 ± 0.59
LogIC₅₀Lo	-6.48	-5.71	-6.74	-7.39	-6.42	-6.55 ± 0.27
R squared	0.830	0.677	0.557	0.739	0.830	0.727 ± 0.051

Best-fit values from the nonlinear regression of log(agonist) vs. response curves using a variable slope (four-parameter) model on baseline-corrected soluble fraction or particulate.

Data are from five soluble and five particulate preparations.

3.2.3 WWL70

WWL70, a reported ABHD6-selective inhibitor, was tested across a range of concentrations to evaluate its inhibitory effects on both the soluble and particulate fractions (Figure 3.4). The $\log IC_{50}$ value was determined to be -8.16 for the soluble fraction and -8.01 for the particulate fraction, indicating that WWL70 is slightly more potent in the soluble fraction. The extent of inhibition also varied. In the soluble fraction, WWL70 achieved a maximum inhibition of only about 40%, meaning that half of the enzyme activity remained unaffected.

In the particulate fraction, the maximum inhibition was even lower, around 30%, suggesting that a substantial portion of the enzyme activity in the particulate fraction was resistant to WWL70.

The analysis comparing one-site versus two-site curve fitting models for both soluble and particulate fractions revealed distinct binding dynamics. In the soluble fractions, the two-site model adequately described the data in three out of five preparations (S3, S4, and S5), supported by significant P-values and higher R-squared values, indicating the presence of both high- and low-affinity binding sites. The mean FractionHi for these preparations was 0.49 (49%), indicating that high-affinity interactions accounted for nearly half of the total binding sites, while the majority exhibited low-affinity binding. In contrast, the one-site model better fit the remaining two preparations (S1 and S2) (Table 3.5). In the particulate fractions, the data for preparations P3 and P4 did not fit either the one-site or two-site model closely enough to allow a definitive conclusion, resulting in inconclusive analysis. In contrast, the data for the remaining preparations (P1, P2, and P5) fit the one-site model more closely (Table 3.6).

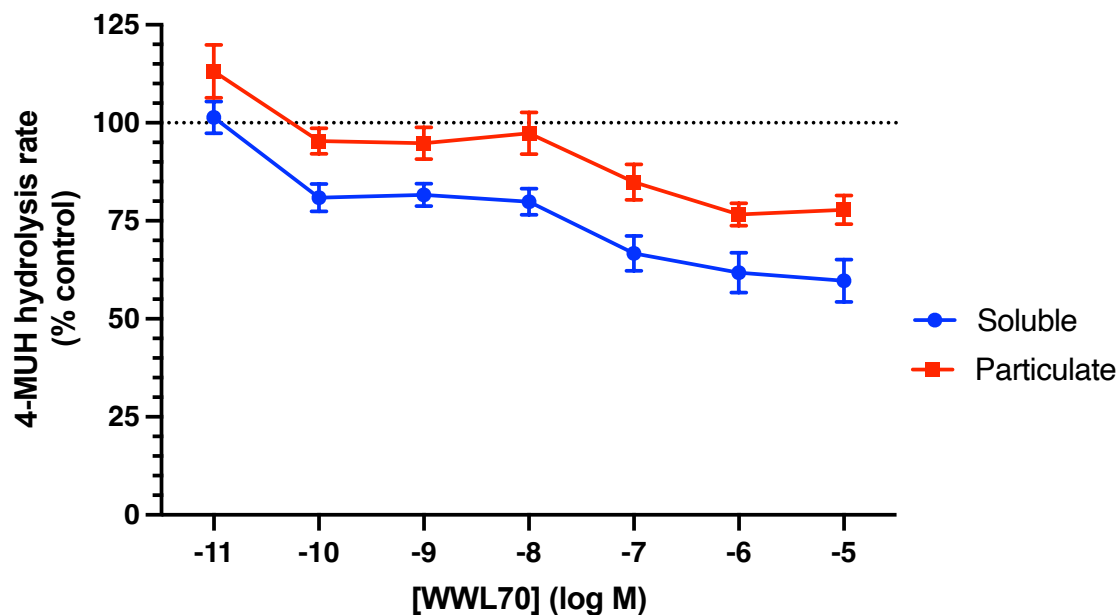


Figure 3.4 Concentration inhibition curves of WWL70 for 4-MUH hydrolysis in soluble and particulate fractions of rat brain. The blue line represents the soluble fraction, while the red line corresponds to the particulate fraction, allowing for a comparative analysis of MAFP inhibition in each fraction. Data were analyzed using a nonlinear regression model, comparing both one-site (four-parameter logistic, 4PL) and two-site binding models to determine the best fit for inhibition dynamics. Data are means \pm SEM of five independent preparations, each conducted in triplicate.

Table 3.5 A comparison of one-site vs two-site models for WWL70 inhibition of 4-MUH hydrolysis in rat brain soluble fractions.

	S1	S2	S3	S4	S5	Mean \pm SEM
P value	0.1240	0.0796	0.0324	0.0236	0.0492	
log(agonist) vs. response -- Variable slope (four parameters)						
R max%	42.20	64.73	20.33	62.31	70.51	52 \pm 9
LogEC₅₀	-7.57	-8.17	-7.80	-7.89	-9.37	-8.16 \pm 0.32
HillSlope	-0.2015	-0.3592	-0.1904	-0.4490	-0.4559	-0.44 \pm 0.16
R squared	0.791	0.686	0.714	0.792	0.751	0.712 \pm 0.048
Two sites - Fit logIC₅₀						
R max%	57.49	67.24	39.85	64.45	69.66	60 \pm 5
FractionHi	0.4895	0.4741	0.5022	0.3220	0.6551	0.49 \pm 0.05
LogIC₅₀HI	-10.69	-10.20	-10.84	-10.17	-10.24	-10.43 \pm 0.14
LogIC₅₀Lo	-7.15	-7.06	-7.17	-7.31	-7.18	-7.17 \pm 0.04
R squared	0.819	0.739	0.783	0.847	0.803	0.798 \pm 0.018

Table 3.6 A comparison of one-site vs. two-site models for WWL70 inhibition of 4-MUH hydrolysis in rat brain particulate fractions.

	P1	P2	P3	P4	P5	Mean ± SEM
P value	0.7462				0.3021	
log(agonist) vs. response -- Variable slope (four parameters)						
R max%	73.50	86.61	77.15	76.21	69.39	77 ± 3
LogEC₅₀	-7.02	-7.48	~ -7.171	~ -6.908	-9.51	-8.01 ± 0.59
HillSlope	-0.5543	-0.9603	~ -9.449	~ -11.40	-0.4268	-0.65 ± 0.16
R squared	0.469	0.512	0.382	0.615	0.560	0.508 ± 0.040
Two sites - Fit logIC₅₀						
R max%	76.12	86.41	75.00	74.65	68.74	76 ± 3
FractionHi	0.2267	0.2369	~ 0.008366	0.003715	0.6661	0.28 ± 0.14
LogIC₅₀HI	-9.22	~ -10505	~ -7.224	~ -6.548	-10.29	-9.75 ± 0.37
LogIC₅₀Lo	-6.89	-7.16	~ -7.22	~ -6.55	-7.23	-7.09 ± 0.08
R squared	0.472	0.651	0.354	0.561	0.596	0.527 ± 0.052

Best-fit values from the nonlinear regression of log(agonist) vs. response curves using a variable slope (four-parameter) model on baseline-corrected soluble fraction or particulate.

Data are from five soluble and five particulate preparations.

3.2.4 JJKK048

At the highest concentration of 10 µM, JJKK048 inhibited 4-MUH hydrolysis in both soluble and particulate fractions (Figure 3.5). However, a substantial portion of enzymatic activity remained unaffected, indicating that even at this higher concentration, JJKK048 did not achieve complete inhibition.

In the soluble fraction, the R max% was 48 ± 3, indicating that approximately 48% of enzymatic activity remained after JJKK048 inhibition, reflecting incomplete inhibition of were best described by the two-site model, while the remaining three samples (S1, S2, S3) were best fit by the MAGL. Conversely, in the particulate fraction, the R max% was 29.04, suggesting that approximately 29% of enzymatic activity persisted, indicating more effective inhibition compared to the soluble fraction. In the soluble fractions, two out of five samples (S4, S5) one-site model (Table 3.7).

In the particulate fractions, four out of five samples (P1, P3, P4, P5) were best described by the two-site model, indicating heterogeneity in binding dynamics. These samples showed both high-affinity (LogIC₅₀HI -9.65) and low-affinity (LogIC₅₀Lo -5.61) binding sites (Table 3.8). The high-affinity sites likely correspond to MAGL inhibition, while the low-affinity sites may represent potential off-target activity on ABHD6. The potential off-target activity of JJKK048 on ABHD6 may contribute to the observed heterogeneity in the particulate fraction.

ABHD6 is primarily localized to membranes, and its inhibition by JJKK048 could explain the presence of low-affinity binding sites in the particulate fraction. In the soluble fraction, the inability to distinguish multiple sites suggests minimal off-target interactions, likely due to the absence of membrane-associated ABHD6.

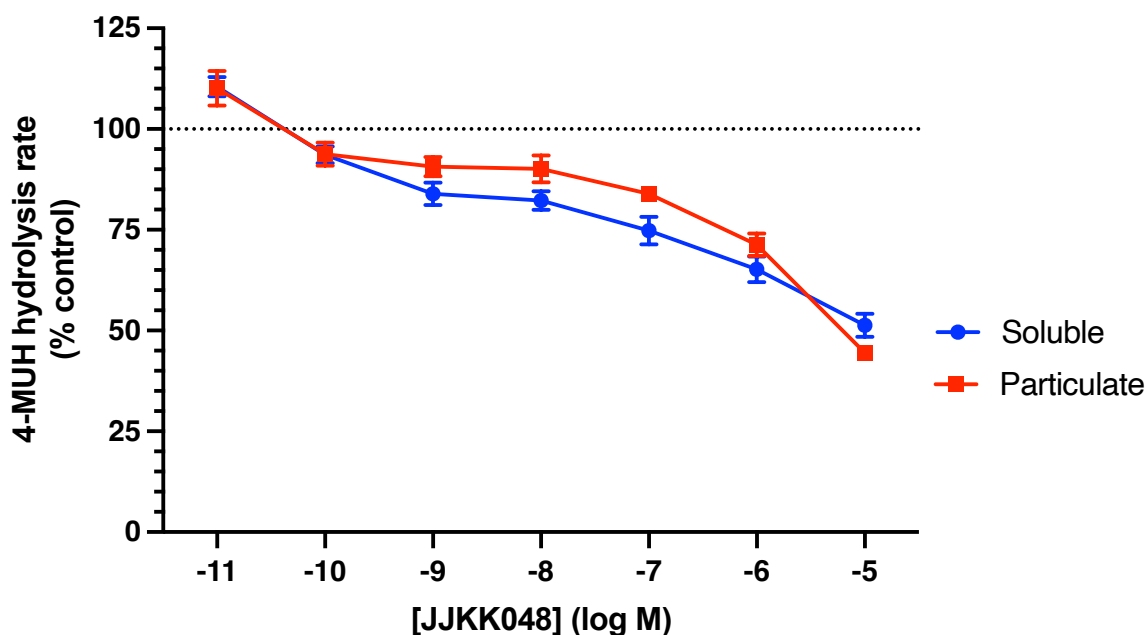


Figure 3.5 illustrates the concentration-dependent inhibition of 4-MUH hydrolysis by JJKK048 in the soluble and particulate fractions of rat brain tissue. The blue line represents the soluble fraction, while the red line corresponds to the particulate fraction, allowing for a comparative analysis of MAFP inhibition in each fraction. Data were analyzed using a nonlinear regression model, comparing both one-site (four-parameter logistic, 4PL) and two-site binding models to determine the best fit for inhibition dynamics. Data are means \pm SEM of five different preparations, each conducted in triplicate.

Table 3.7 A comparison of one-site vs two-site models for JJKK048 inhibition of 4-MUH hydrolysis in rat brain soluble fractions.

	S1	S2	S3	S4	S5	Mean ± SEM
P value		0.0812	0.2443			
log(agonist) vs. response -- Variable slope (four parameters)						
R max%	35.14	16.15	27.63	~ -34140	~ -3833	26 ± 6
LogEC₅₀	-6.45	-4.79	-6.63	~ 17.79	~ 4.874	-5.96 ± 0.45
HillSlope	-0.2901	-0.2775	-0.2103	-0.1221	-0.1928	-0.22 ± 0.03
R squared	0.968	0.826	0.940	0.946	0.879	0.912 ± 0.026
Two sites - Fit logIC₅₀						
R max%	52.65	56.86	51.02	38.05	43.69	48 ± 3
FractionHi	0.3691	0.3044	0.4787	0.4337	0.2859	0.37 ± 0.04
LogIC₅₀HI	-9.37	-9.18	-9.85	-9.80	-9.82	-9.61 ± 0.14
LogIC₅₀Lo	-6.40	-5.86	-6.63	-5.83	-5.68	-6.08 ± 0.18
R squared	0.966	0.859	0.946	0.972	0.921	0.933 ± 0.020

Table 3.8 A comparison of one-site vs. two-site models for JJKK048 inhibition of 4-MUH hydrolysis in rat brain particulate fractions.

	P1	P2	P3	P4	P5	Mean ± SEM
P value		0.6377				
log(agonist) vs. response -- Variable slope (four parameters)						
R max%	~ -25964	39.29	~ -5197	~ -191988	~ -11531	
LogEC₅₀	~ 5.44	-6.22	~ 2.65	~ 15.78	~ 2.44	
HillSlope	-0.2540	-0.7556	-0.2599	-0.1706	-0.3187	-0.35 ± 0.10
R squared	0.707	0.754	0.844	0.836	0.751	0.778 ± 0.027
Two sites - Fit logIC₅₀						
R max%	27.92	42.95	35.21	23.25	29.77	32 ± 3
FractionHi	0.1742	0.06211	0.2281	0.2495	0.1411	0.17 ± 0.03
LogIC₅₀HI	-9.91	-9.73	-8.66	-10.32	-9.61	-9.65 ± 0.27
LogIC₅₀Lo	-5.58	-6.22	-5.58	-5.36	-5.31	-5.61 ± 0.16
R squared	0.723	0.758	0.854	0.937	0.769	0.808 ± 0.039

Best-fit values from the nonlinear regression of log(agonist) vs. response curves using a variable slope (four-parameter) model on baseline-corrected soluble fraction or particulate.

Data are from five soluble and five particulate preparations.

3.2.5 Combining KT203 and JJKK048

As JJKK048 and KT203 were anticipated to inhibit MAGL and ABHD6 activities preferentially, the effects on 4-MUH hydrolysis of combining the two inhibitors was investigated. JJKK048 was used at a final concentration of 100 nM in the presence and absence of serial dilutions of KT203. (Figure 3.6).

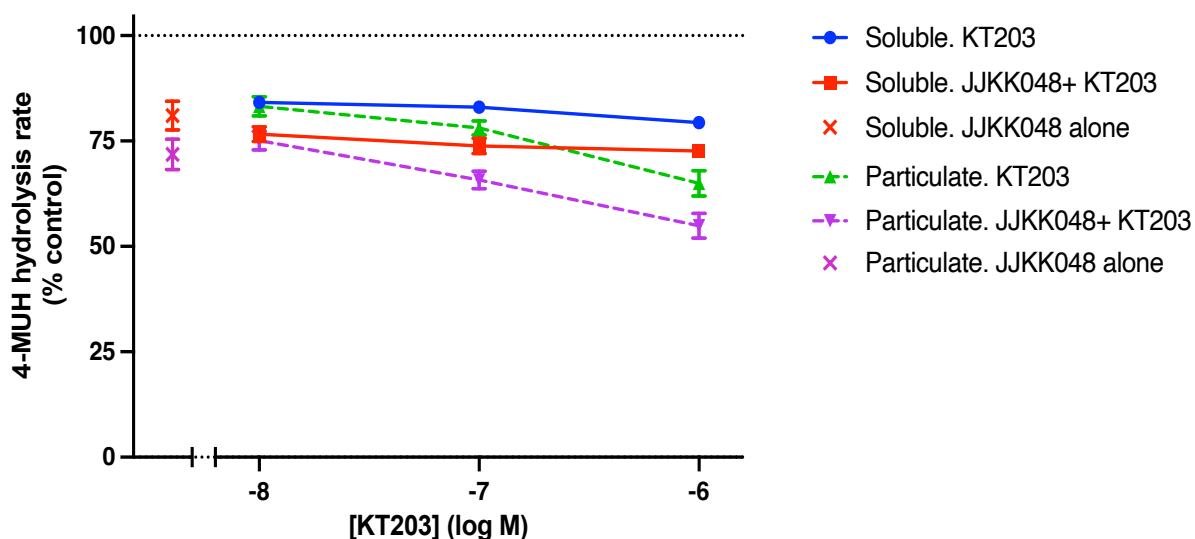


Figure 3.6 4-MUH hydrolysis in soluble and particulate fractions of rat brain in the presence of serial dilutions of KT203 and a single concentration (100 nM) of JJKK048. The figure compares the inhibitory effects of KT203 alone, JJKK048 alone, and their combination. Data represent mean \pm SEM from six independent preparations, each conducted in triplicate. A one-way ANOVA followed by Šídák's multiple comparisons test was performed to assess inhibition in both fractions.

A one-way ANOVA, followed by Šídák's multiple comparisons test, was conducted to evaluate the effects of JJKK048 alone and in combination with KT203 in both soluble and particulate fractions. In the soluble fraction, the comparison between JJKK048 at 100 nM and JJKK048 at 100 nM in combination with KT203 at 1 μ M revealed no significant difference (Mean Difference = 6.078, 95% CI = -5.904 to 18.06, Adjusted P Value = 0.4671), indicating that KT203 did not significantly alter the inhibitory effect of JJKK048 on 4-MUH hydrolysis in the soluble fraction. Conversely, in the particulate fraction, the combination of KT203 with JJKK048 at 100 nM still evoked a significant inhibitory effect on 4-MUH hydrolysis (Mean Difference = 25.36, 95% CI = 0.2717 to 50.45, Adjusted P Value = 0.0478).

3.3 Discussion

The effects of various inhibitors with different selectivity on 4-MUH hydrolysis were investigated in rat brain tissues to assess the enzymatic contributions and determine whether 4-MUH serves as a specific substrate for ABHD6. MAFP resulted in near-complete inhibition, confirming the involvement of multiple serine hydrolases. KT203 and WWL70, both selective for ABHD6, caused significant but incomplete inhibition, particularly in the particulate fraction, suggesting ABHD6's role and the presence of other hydrolases. JJKK048, a selective MAGL inhibitor with some effects on ABHD6 at higher concentrations, also led to an incomplete inhibition, highlighting the complexity of enzymatic contributions to 4-MUH hydrolysis. These results indicate the involvement of ABHD6 and other serine hydrolases in the 4-MUH breakdown in these preparations.

3.3.1 MAFP

MAFP caused significant inhibition in both fractions, suggesting a predominant role for serine hydrolases in 4-MUH hydrolysis. The soluble fraction, however, was slightly less sensitive to MAFP compared to the particulate fraction, suggesting that the particulate fraction may contain a higher proportion of serine hydrolases that are more sensitive to MAFP inhibition. MAFP is reported to inhibit ABHD6 as well as multiple other serine hydrolases (Manterola et al., 2018; Blankman et al., 2007) which explains the broad inhibitory effect observed. Due to MAFP's broad inhibitory profile, a more precise definition of the specific hydrolases involved could not be made. This indicates that while serine hydrolases are significant contributors to the hydrolysis process, MAFP's non-selectivity makes it challenging to isolate the activity of individual enzymes. The inhibition pattern of MAFP in this study is consistent with previous findings. Nada Mahmood (2018) reported that MAFP caused significant inhibition of MUH hydrolysis in rat brain tissues, achieving over 75% inhibition, similar to the effects observed in both the soluble and particulate fractions in this study. This suggests that MAFP-sensitive serine hydrolases contribute to 4-MUH hydrolysis in rat brain tissue. Moreover, the broad inhibitory profile of MAFP has been documented in various studies. For instance, in mouse brain membranes, FP-rhodamine-tagged activity described as ABHD6 was inhibited in the presence of 10 μ M MAFP (Manterola et al., 2018; Blankman et al., 2007).

Investigating the total enzyme activity for one- or two-site fits provided critical insights into the binding and inhibition dynamics of MAFP in both soluble and particulate fractions. This

dual-model approach allowed us to evaluate whether the observed inhibition was best described by a single dominant binding site (one-site model) or by the presence of distinct populations of binding sites with varying affinities (two-site model). The analysis revealed that the one-site model provided a better overall fit for both fractions, since the R^2 values for the two-site model did not show significant improvement, suggesting that multiple distinct binding sites could not be reliably differentiated.

The one-site model assumes a single homogeneous population of binding sites or enzymes contributing to the observed activity. This simpler model is appropriate when there is no evidence of heterogeneity in binding interactions. Biologically, this suggests that the inhibition dynamics in both fractions are dominated by a single enzyme or a population of enzymes with highly similar kinetic properties.

In contrast, the two-site model assumes the presence of two distinct populations of binding sites: one with high affinity (LogIC50_HI) and another with low affinity (LogIC50_Lo). This model also includes Fraction_HI, which represents the proportion of total binding contributed by high-affinity sites.

This model is particularly relevant in biological systems with heterogeneous enzyme or receptor populations, such as those involving multiple isoforms or subtypes with varying sensitivities to an inhibitor. For MAFP, previous studies (e.g., Blankman et al., 2007; Manterola et al., 2018) have highlighted its broad inhibitory profile across several serine hydrolases, each potentially exhibiting different affinities for the inhibitor. Given its non-selective nature, MAFP would theoretically be best described by a two-site model, as it targets multiple serine hydrolases with differing binding affinities.

From a biological perspective, evaluating the total enzyme activity using both one- and two-site models provided a comprehensive analysis of inhibition dynamics. However, in this study, statistical comparisons in GraphPad Prism did not show significant improvement when applying the two-site model, suggesting that distinct binding contributions could not be statistically resolved within the dataset. This could be due to overlapping affinities among the targeted enzymes, resulting in a pattern that appears more homogeneous than it truly is.

Although the one-site model was statistically the best fit, the broad reactivity of MAFP across multiple serine hydrolases suggests an underlying enzymatic heterogeneity that the current analysis could not fully resolve.

The variability observed in MAFP inhibition may indicate differences in the enzymatic activity of serine hydrolases across tissue samples. Nonlinear fitting in Prism revealed high variability in enzyme responses among the five animal tissues tested, indicating substantial

inter-individual variability. This variation could reflect biological differences in the expression or activity of enzymes such as ABHD6 and MAGL. Importantly, differences in how these enzymes respond to MAFP may lead to variations in inhibition patterns, including inconsistent $R_{max\%}$ values and IC_{50} estimates. Another factor contributing to variability during MAFP inhibition could be protein modifications due to prolonged storage of tissue samples. Although the archived brain tissues were carefully stored at $-80\text{ }^{\circ}\text{C}$, potential oxidation or protein degradation over time may have altered the activity of serine hydrolases, including their susceptibility to MAFP inhibition. Structural changes in the enzymes caused by storage conditions could affect their substrate affinity or binding dynamics with MAFP, contributing to variability in hydrolysis rates and $R_{max\%}$ values. It is possible that enzymes in some tissue samples were more affected than others, resulting in discrepancies in the extent of MAFP-induced inhibition. We had initially planned to use fresh samples; however, unforeseen restrictions in the school's animal unit prevented access to fresh rat brain tissues throughout the study period. This necessitated the use of archived brain preparations, which, despite optimal storage conditions, may have undergone some degree of protein modification over time. To directly assess whether storage duration correlates with enzymatic function, future studies should compare hydrolysis rates and inhibition profiles in freshly isolated tissues versus archived samples. Such a comparison would clarify whether fresh tissues provide more consistent and reliable data for evaluating serine hydrolase activity and inhibitor sensitivity. Despite the variability, the overall trend of near-complete inhibition of 4-MUH hydrolysis by MAFP was consistent across samples, reaffirming its potent inhibitory effect on serine hydrolases.

3.3.2 KT203

The more pronounced inhibition in the particulate fraction at higher KT203 concentrations ($>10\text{ nM}$) suggests a higher expression or activity of ABHD6 in membrane-associated components. This observation is consistent with previous findings that ABHD6 predominantly localizes to membrane structures (Blankman et al., 2007; Marrs et al., 2010; Poursharifi et al., 2017; Savinainen et al., 2012). However, KT203 also inhibited 4-MUH hydrolysis in the soluble fraction, and as a selective ABHD6 inhibitor, this inhibition is likely at least partially due to ABHD6 activity in this fraction.

When assessing the total enzyme activity for one- or two-site fits, the data for the particulate fraction were best described by a single-site model, indicating that multiple binding sites

could not be distinguished. However, for the soluble fraction, the two-site model provided a better fit for most preparations. This suggests the presence of distinct binding populations within the soluble fraction, including a high-affinity site likely corresponding to ABHD6 and a low-affinity site, potentially representing off-target interactions with other serine hydrolases that also contribute to 4-MUH hydrolysis. FractionHi values indicate that high-affinity binding accounts for only a small portion (18%) of the total binding population.

Although ABHD6 is predominantly membrane-localized, there is limited evidence supporting its presence and activity in the soluble fraction. The Human Protein Atlas reports nuclear, membranous, and cytoplasmic expression of ABHD6 in most tissues, suggesting the possibility of a soluble or cytosolic form. Additionally, fluorescence from an ABHD6-GFP fusion protein has been observed in the cytoplasm of transfected AD293 cells, indicating that under certain conditions, a portion of ABHD6 can localize to the cytoplasm (Li et al., 2009). Furthermore, ABHD6 activity has been detected in the soluble fraction of INS832/13 cells (rat pancreatic β -cells), where its activity was inhibited by approximately 60% with 10 μ M WWL70, another selective ABHD6 inhibitor (Zhao et al., 2014). A possible explanation for its presence in the soluble fraction is proteolytic cleavage, whereby proteases release a soluble form of the enzyme from membranes. Another possible explanation for the inhibition observed in the soluble fraction is that KT203 may also inhibit other enzymes capable of hydrolyzing 4-MUH. Although KT203 exhibits high selectivity for ABHD6, its potential off-target interactions with other serine hydrolases cannot be completely excluded in a complex proteomic environment like the soluble fraction of rat brain tissue. Overall, while ABHD6's activity is predominantly membrane-associated, the observed inhibition of 4-MUH hydrolysis in the soluble fraction may indicate a minor contribution from soluble ABHD6 or potential off-target interactions with other hydrolases.

Complete inhibition in the particulate fraction was not achieved even at these higher concentrations, implying that other serine hydrolases contribute to 4-MUH hydrolysis in this compartment. Therefore, while KT203 appeared to effectively inhibit ABHD6, the residual hydrolysis activity within the particulate fraction points to the involvement of additional enzymes not inhibited by KT203.

Hsu et al. (2013) identified KT203 as a potent and specific ABHD6 inhibitor both *in vitro* and *in vivo* models. They demonstrated that KT203 inhibited over 90% of ABHD6 activity in Neuroblastoma 2A cells using the ABBP-SILAC (Stable Isotope Labelling by Amino acids in Cell culture) mass spectrometry technique. In the present experiments, we assessed the inhibitory potency of KT203 using rat brain preparations with 4-MUH as the substrate,

yielding a log IC_{50} of -5.7, corresponding to an IC_{50} of approximately 2 μ M. This contrasts with Hsu et al.'s reported IC_{50} of 3.9 nM, obtained using recombinant ABHD6 expressed in HEK293T cells with 2-AG as the substrate.

The notable difference in IC_{50} values suggests that KT203 exhibits a higher inhibitory potency in recombinant ABHD6-expressing HEK293T cells with 2-AG as the substrate compared to the rat brain preparations with 4-MUH. Several factors likely contribute to this variation. The most apparent difference lies in the experimental models. Hsu et al. used a purified enzyme in a controlled cellular environment. In contrast, our experiment used rat brain fractions, which contain a complex mix of enzymes, membrane components, and possible endogenous inhibitors. This complexity likely impacts how KT203 interacts with its targets and affects its inhibitory action.

In vivo, KT203 almost completely inhibited ABHD6 in the murine liver at a relatively high dose of 1 mg/kg and showed minimal interaction with carboxylesterases (CESs), which are more frequently reported off-targets for inhibitors targeting serine hydrolases (Bachovchin et al., 2010; Hsu et al., 2012). At lower doses, KT203 still achieved approximately 80% inhibition of liver ABHD6. Notably, it exhibited minimal inhibition of ABHD6 in the brain in vivo, likely due to its limited ability to cross the blood-brain barrier because of its carboxylic acid group.

3.3.3 WWL70

The log IC_{50} values indicate that WWL70 is slightly more potent in the soluble fraction than in the particulate fraction. However, complete inhibition in both fractions was not achieved even at higher concentrations, implying that other serine hydrolases contribute to MUH hydrolysis. Similarly, KT203 also did not completely inhibit 4-MUH breakdown in these preparations. These results suggest that while WWL70 and KT203 effectively target ABHD6, additional enzymes are involved in the hydrolysis of 4-MUH. WWL70 exhibited a similar pattern to KT203, where the data were best described by different models in the soluble and particulate fractions. In the particulate fraction, the single-site model provided the best fit in most preparations, indicating a failure to distinguish multiple binding sites. Conversely, for the soluble fraction, the two-site model better described the data in three out of five preparations, reflecting heterogeneity in binding interactions. FractionHi values for WWL70 suggest that high-affinity binding sites contributed nearly 49% of the total binding population, which is higher than the proportion observed for KT203 in the soluble fraction.

This suggests that WWL70 targets a larger proportion of high-affinity binding sites in the soluble fraction.

The inhibition observed in the soluble fraction by WWL70 could be attributed to two factors. First, while ABHD6 is predominantly membrane-associated, some evidence suggests it may contribute to inhibition in the soluble fraction, as discussed earlier (see Section 3.2.2).

Second, although WWL70 is selective for ABHD6, it may also interact with other enzymes capable of hydrolyzing 4-MUH. The complex proteomic environment of the soluble fraction may facilitate such off-target interactions, which cannot be entirely ruled out. These results are consistent with those reported in Nada Mahmood's thesis (2018), where WWL70 was similarly tested using 4-MUH as a substrate in ABHD6-HEK293 membrane preparations and rat hippocampal particulate preparations. In the ABHD6-HEK293 membrane preparation, WWL70 exhibited a pIC_{50} value of 7.3 ± 0.05 , with residual activity of $6 \pm 1\%$ control. In the rat hippocampal particulate preparation, a pIC_{50} value was 7.4, with a maximal inhibition of only about 30%, aligning closely with the inhibition observed in the particulate fraction of the current study. Both studies employed the same assay, reinforcing the conclusion that while WWL70 is potent, it does not fully inhibit the hydrolytic activity in complex tissue environments, likely due to the involvement of other serine hydrolases beyond ABHD6. Similarly, Miralpeix et al. (2021) measured the activity of ABHD6 in HEK-293T cells overexpressing ABHD6 and brain tissue homogenates using 4-MUH as a substrate. They found that inhibition of ABHD6 activity in brain tissue was 25–30% less than in the overexpressing cells. The lack of specificity of 4-MUH for ABHD6 could be the result of other lipase enzymes also being able to hydrolyse it. In brain tissue homogenates, multiple enzymes are involved in the breakdown of 4-MUH, which may explain why the inhibitory effect of WWL70 is less pronounced in these samples. In contrast, in HEK-293T cells overexpressing ABHD6, the enzyme is the primary driver of 4-MUH hydrolysis, as shown by the minimal activity observed in cells transfected with an empty vector. This discrepancy is likely due to the contribution of other active lipases in more complex tissues, such as the brain. These observations are consistent with earlier studies that reported lower ABHD6 activity in neural tissue compared to other serine hydrolases (Cao et al., 2019).

3.3.4 JJKK048

The inhibition of 4-MUH hydrolysis by JJKK048 suggests that MAGL contributes alongside ABHD6 to 4-MUH hydrolysis in these tissues. Since JJKK048 is known as a selective

MAGL inhibitor, its ability to reduce 4-MUH hydrolysis indicates that a substantial portion of this activity is mediated by MAGL. However, a substantial portion of enzymatic activity remained unaffected, indicating that even at this higher concentration, JJKK048 did not achieve complete inhibition.

MAGL is known to be a soluble enzyme that can also associate with membranes, as demonstrated in multiple studies (Blankman et al., 2007; McKinney & Cravatt, 2005). In agreement with these findings, immunoblotting has identified MAGL in both cytosolic and membrane-bound fractions of the mouse brain, further supporting its dual subcellular localization (Marrs et al., 2010). Its presence has also been consistently observed in both fractions across various tissues and cell types (Savinainen et al., 2012). This dual localization of MAGL likely explains its contribution to enzymatic activity in both the soluble and particulate fractions in this study. Although JJKK048 is a potent and selective MAGL inhibitor, its off-target activity on ABHD6 has been well-documented. ABPP analysis using mouse brain membranes have shown that JJKK048 inhibits both ABHD6 and FAAH at 1 μ M (Aaltonen et al., 2013). Consistent with this, JJKK048 has demonstrated activity against ABHD6 in ABHD6-HEK293 membrane preparations, where it exhibited a pIC_{50} value of 7.1 ± 0.06 and achieved complete inhibition of ABHD6 activity. However, in rat hippocampal particulate preparations using 4-MUH as a substrate, JJKK048 produced significant inhibition, with $69 \pm 10\%$ residual enzymatic activity remaining. This indicates that JJKK048 reduced enzymatic activity by approximately 31% but failed to achieve complete inhibition, consistent with the findings of this study, where incomplete inhibition was observed in both soluble and particulate fractions, even at a higher concentration of 10 μ M.

The broader inhibitory profile observed at higher concentrations of JJKK048 likely reflects its reduced selectivity, where it may target ABHD6 alongside MAGL. ABHD6 is primarily a membrane-bound enzyme, with its activity closely associated with membrane compartments (Blankman et al., 2007; Savinainen et al., 2012). The two-site binding model observed in the particulate fraction, which is characterized by distinct high-affinity and low-affinity binding sites, may reflect interactions between JJKK048 and both MAGL and ABHD6. The high-affinity binding sites are consistent with MAGL inhibition, since MAGL is the primary target of JJKK048. In contrast, the low-affinity sites may correspond to off-target activity on ABHD6. This potential interaction with ABHD6 might explain the heterogeneity in binding dynamics observed in the particulate fraction.

3.3.5 Combining JJKK048 and KT203

In the soluble fraction, no significant difference was observed between JJKK048 alone and JJKK048 combined with KT203. This suggests that the enzymatic activity in the soluble fraction is primarily due to MAGL. Since KT203 selectively inhibits ABHD6, the lack of effect in this fraction indicates that ABHD6 is not significantly present or active in the soluble fraction.

In the particulate fraction, the combination of KT203 with JJKK048 at 100 nM led to a significant additional inhibition of 4- MUH hydrolysis. This indicates presence of both MAGL and ABHD6 in the particulate fraction contributes to the 4-MUH hydrolysis. The fact that JJKK048 alone already reduces hydrolysis but further inhibition is seen with KT203 suggests a cooperative or overlapping role of MAGL and ABHD6 in this fraction.

This study highlights the significant role of serine hydrolases in 4-MUH hydrolysis, as demonstrated by the near-complete inhibition observed with MAFP in both soluble and particulate fractions. These findings confirm that serine hydrolases play a predominant role in 4-MUH hydrolysis in rat brain tissues. However, despite their selectivity for ABHD6, the inhibitors KT203 and WWL70 did not achieve complete inhibition in either fraction. This suggests that 4-MUH is not a highly specific substrate for ABHD6 and that other hydrolases contribute to its hydrolysis. Data from Nada Mahmood's thesis (2018) (Figure 2.2) indicated that 4-MUH was not effectively hydrolyzed by ABHD12 in human recombinant systems. Based on these findings, DO064, a selective ABHD12 inhibitor, was excluded from this study, as ABHD12 was not expected to significantly contribute to 4-MUH hydrolysis in rat brain preparations. However, the possibility that rat ABHD12 exhibits different substrate preferences and may hydrolyze 4-MUH more efficiently than its human counterpart cannot be ruled out. To address this, future studies should evaluate DO064 in rat brain homogenates using 4-MUH as a substrate, which would help determine whether ABHD12 contributes to 4-MUH hydrolysis in complex proteomes.

Nonlinear fitting in Prism revealed substantial variability among the animal tissues tested, particularly in R max%, LogIC₅₀, and model fitting outcomes for MAFP, KT203, WWL70, and JJKK048. This substantial inter-individual variation may arise from differences in enzyme expression or activity between samples. Additionally, as discussed with MAFP, potential protein modifications due to prolonged storage could further contribute to inconsistencies in R max% values and LogIC₅₀ estimates across inhibitors, complicating the interpretation of inhibition profiles.

Finally, the inhibition observed in the soluble fraction with KT203 and WWL70 raises questions about whether ABHD6 is present and active in this compartment or if the observed effects are due to off-target interactions with other enzymes capable of hydrolyzing 4-MUH. To address these uncertainties, future studies could utilize tissue from genetically modified mice lacking ABHD6 and MAGL to determine if these inhibitors act specifically through these enzymes in the 4-MUH assay. Additionally, ABPP in rat brain tissues could provide a more comprehensive evaluation of the selectivity and potency of these inhibitors. While genetic disruption studies remain a future direction, the next chapter (Chapter 4) will focus on ABPP as a method to further investigate the selectivity of the inhibitors in rat brain preparations.

Chapter 4: Activity-Based Protein Profiling

Activity-Based Protein Profiling (ABPP) is a chemoproteomic technique used in drug discovery and development. It enables the measurement of enzyme activities within complex biological systems in a single experiment, without the need for natural substrates. ABPP overcomes the limitations of conventional substrate-based assays by utilizing chemical probes that covalently bind to the active site of target enzymes. The probes are designed with a reporter tag for detecting enzymatic activity (Liu et al., 1999). This method has been particularly effective in characterizing the roles of ABHD6 and ABHD12 in the hydrolysis of 2-AG (Blankman et al., 2007) and is suitable for simultaneously screening several enzymes from the same protein family. However, due to their broad design, ABPP probes often lack specificity, making them less suitable for distinguishing individual enzyme activities in distinct tissues.

4.1 Objective

To utilize ABPP in rat brain tissues to evaluate the selectivity and potency of inhibitors targeting ABHD6 and ABHD12.

4.2 Results

4.2.1 Enzyme activities in rat brain fractions measured using FP-rhodamine

As anticipated, FP-rhodamine was able to label more active enzymes than MB064 in both the soluble and particulate fractions of rat brain preparations (Figure 4.1).

The gels in Figure 4.1 reveal distinct enzyme activity patterns in the particulate and soluble fractions of rat brain tissue. The labelling shows multiple protein bands at varying molecular weights, with differences in band intensity between the two fractions. The distribution of high-intensity bands differed between the fractions, with bands 13 and 14 showing the highest activity in the particulate fraction, while bands 5, 19, and 20 dominated in the soluble fraction.

In the particulate fraction, a total of 21 bands were identified. Bands 13 and 14 exhibited the highest intensity, reflecting strong enzyme activity. KT203 at concentrations of 10 and 100 μM blocked the labelling of bands 6, 7, and 15. However, at a lower concentration of 1 μM , only band 15 was blocked. In contrast, DO264 and NAGly at all tested concentrations

showed no observable changes compared to the control lane, indicating that none of the bands were inhibited.

In the soluble fraction, 20 bands were observed. The most intense bands, bands 5, 19, and 20, indicated the highest enzyme activity in this fraction. While most of the test compounds did not cause significant changes relative to the control lane, KT203 at 10 μM blocked the labelling of band 5. At a higher concentration of 100 μM , KT203 induced more pronounced effects, blocking over five bands, including bands 3, 4, 5, 13, 16, and 18.

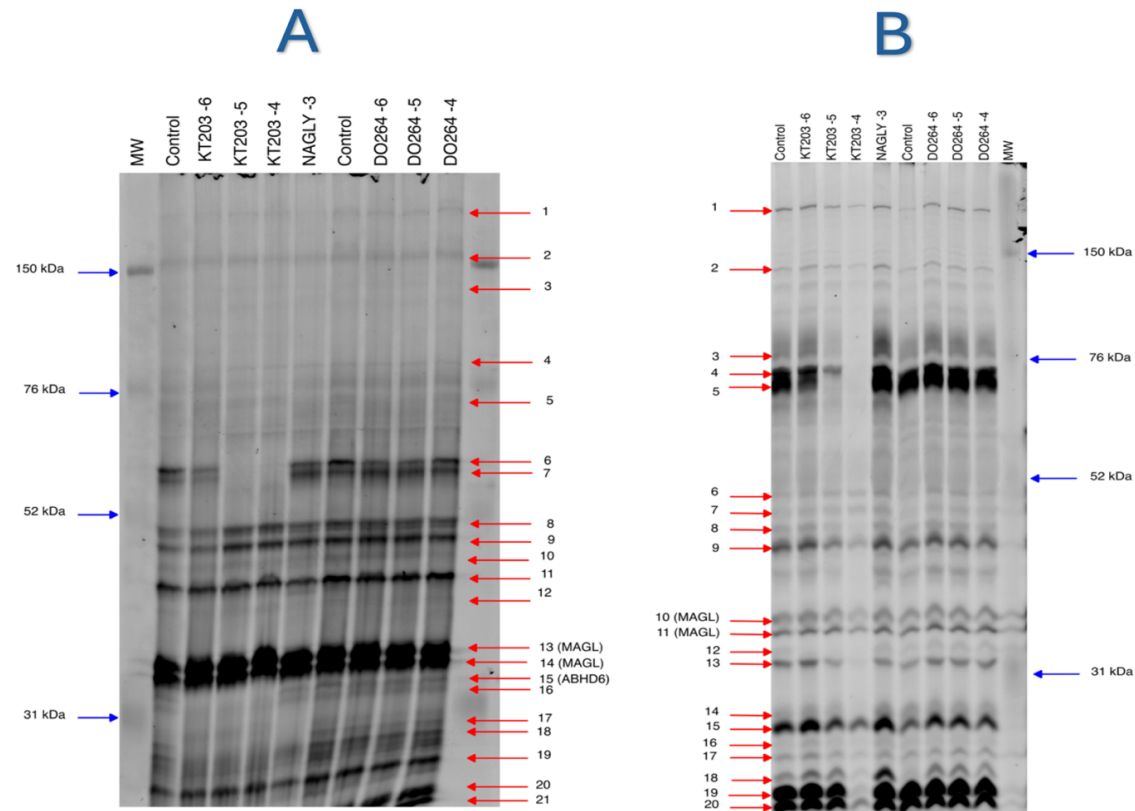


Figure 4.1 Representative gel scans of a rat brain particulate (A) and soluble (B) fraction measured using the activity-based probe FP-Rhodamine (500 nM) in the absence and presence of various inhibitors. Samples were pre-incubated with KT203 (100 μ M, 10 μ M, and 1 μ M), DO264 (100 μ M, 10 μ M, and 1 μ M), and NAGly (1000 μ M) to evaluate their effects on target enzyme activity. The left-hand lane in the particulate fraction (A) displays molecular weight markers corresponding to the particulate fraction, while the right-hand lane in the soluble fraction (B) contains molecular weight markers for the soluble fraction. Protein bands detected and quantified are indicated numerically (red arrows), with notable bands MAGL and ABHD6 labelled for reference. The gel contained samples from a single animal; tissues from five other animals were processed in an identical manner.

The enzyme activity profiles of the particulate and soluble fractions of rat brain tissue, tagged with FP-rhodamine, were compared to investigate differences in protein distribution between the two fractions. The data were expressed as a percentage of band 13 for the particulate fraction and band 10 for the soluble fraction, both of which are likely to represent MAGL. This identification is based on findings from Aldossari's PhD thesis (Aldossari, 2023), which used ABPP with FP-rhodamine labeling in the soluble and particulate fractions of rat brain tissue. MAGL was observed to migrate as a doublet at 33 and 34 kDa. Its identification was confirmed by significant inhibition by 2-AG and JJKK048, a potent and selective inhibitor of MAGL. Higher expression was detected in the particulate fraction compared to the soluble fraction, confirming MAGL's differential distribution in rat brain tissue. This observation aligns with earlier findings that MAGL is expressed in both soluble and membrane fractions of rat brain (Ghafouri et al., 2004).

Figure 4.2 provides two complementary visualizations of enzyme activity across the fractions. The top panels (A, B) present enzyme activity as adjusted volume (%) relative to band 13 (particulate fraction) and band 10 (soluble fraction). The bottom panels (A, B) represent the same data but plotted against band migration (Rf values) rather than band numbers. This visualization suggests that bands 10 and 13 exhibit identical Rf values, providing supporting evidence that they likely correspond to the same enzyme across both fractions.

The analysis, as shown in Figure 4.2, revealed two distinct patterns of enzyme activity between the two fractions. In the particulate fraction, band 14 showed the highest activity, while in the soluble fraction, other bands, such as band 5, exhibited higher activity than band 10. This initial visual observation confirms the different enzyme activity distributions in both fractions from Figure 4.4. The size of the error bars in the analysis in Figure 4.5 suggests that the differences between the six donor animals are small particularly for the particulate, but also the soluble fraction.

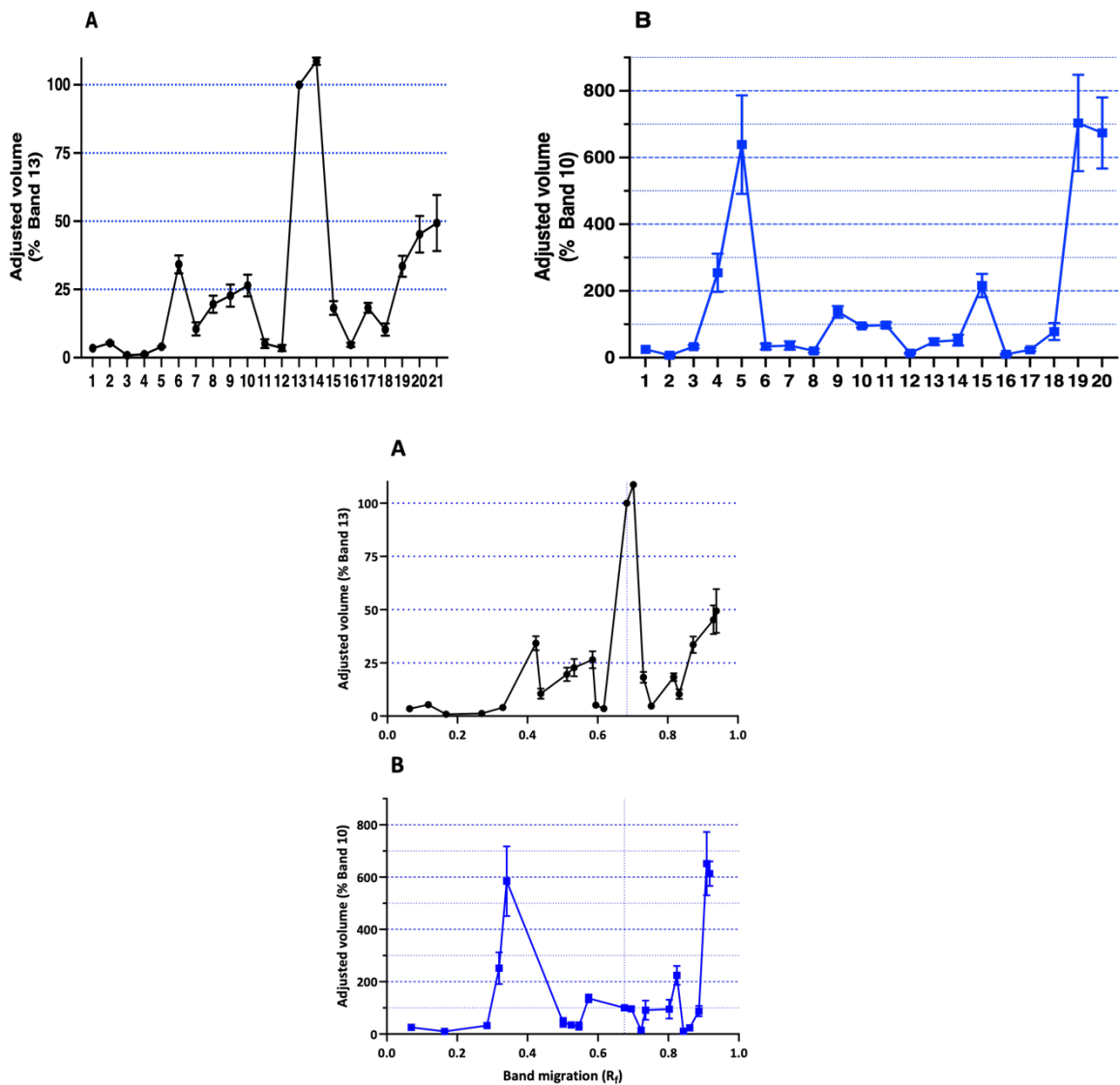


Figure 4.2 Comparison of enzyme activity in the particulate (A) and soluble (B) fractions of rat brain using ABPP with FP-rhodamine. Data are presented as mean \pm SEM of adjusted volumes, expressed as a percentage of band 13 (MAGL) for the particulate fraction (A) and band 10 (MAGL) for the soluble fraction (B). Data were obtained from six independent preparations. The vertical dashed line marks the higher molecular weight (MW) band of MAGL in both fractions, providing a reference for migration patterns and relative enzyme activity across the fractions.

The pharmacological effects of the inhibitors KT203, DO264, along with the endogenous metabolite NAGly, were assessed to determine their impact on enzyme activity in both the particulate and soluble fractions of rat brain tissue. Figure 4.6 illustrates the inhibition patterns of these inhibitors, while Table 4.1 (particulate fraction) and Table 4.2 (soluble fraction) provide a quantitative analysis of enzyme activity across different concentrations of the inhibitors and the estimated molecular sizes of the bands identified in each fraction. In the particulate fraction, 21 major bands were detected, ranging in molecular weight from 22 kDa to 188 kDa (Table 4.1).

KT203 caused significant inhibition across several bands. Band 6 (58.8 kDa) was inhibited at all concentrations tested. Similarly, Band 15 (33.4 kDa), corresponding to ABHD6, was significantly inhibited at all concentrations of KT203. Additionally, Band 20 (23.9 kDa) and Band 21 (22.2 kDa) were only inhibited at the highest concentration of KT203. In contrast, neither 1000 μ M NAGly nor any concentration of DO264 caused significant inhibition of any bands in the particulate fraction (Figure 4.3).

In the soluble fraction, 20 major bands were detected using FP-rhodamine, with molecular weights ranging from 25 kDa to 136.4 kDa (Table 4.2). At 100 μ M KT203 (the highest concentration), four bands were significantly inhibited: Band 4 (73.3 kDa), Band 5 (70 kDa), Band 19 (25 kDa), and Band 20 (25 kDa). At a lower concentration of 10 μ M KT203, only Band 5 (70 kDa) showed significant inhibition. However, in the presence of DO264 at any concentration or 1 mM NAGly, no significant inhibition of enzyme activity was observed for any of these bands in the soluble fraction (Figure 4.3).

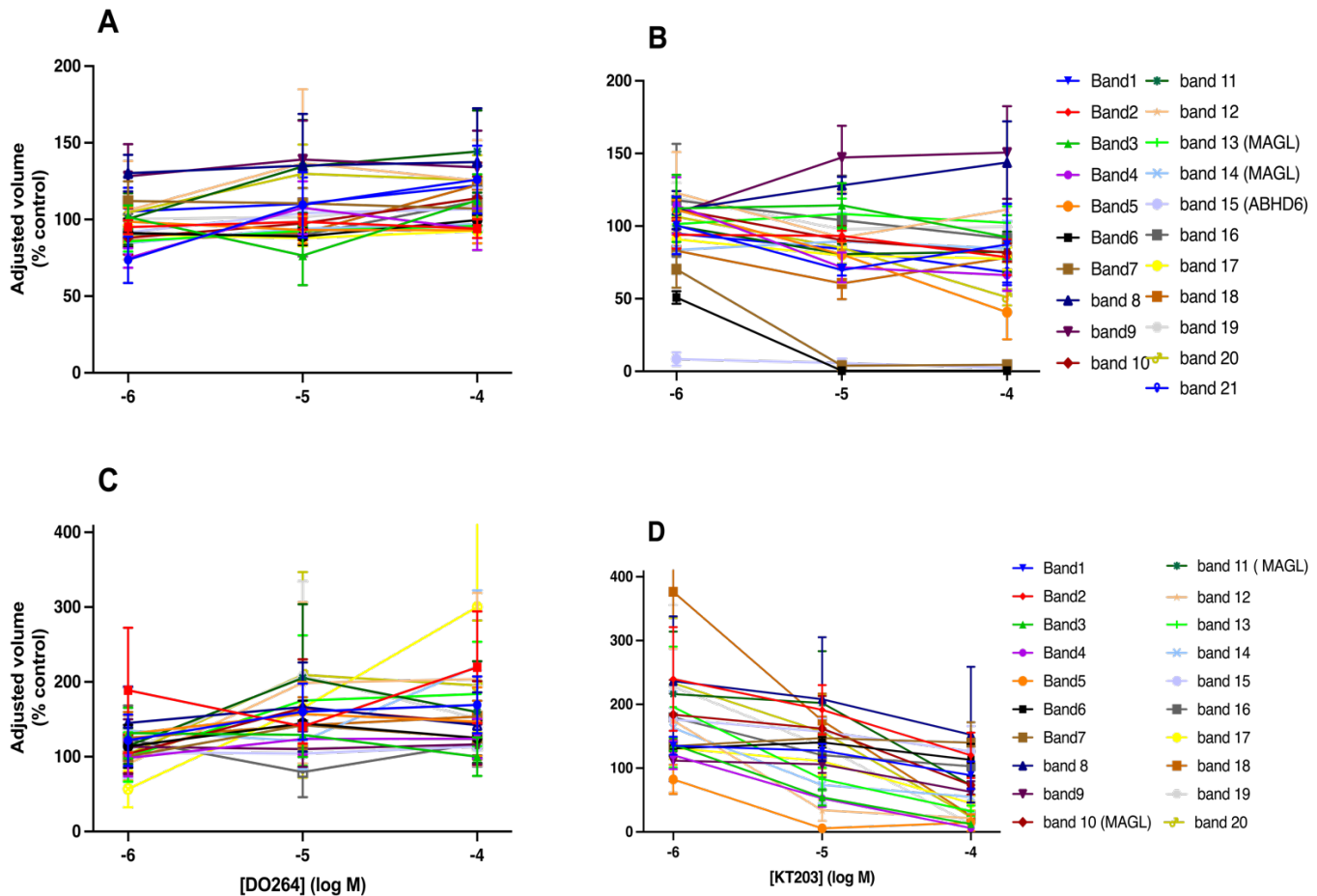


Figure 4.3 The effects of selective inhibitors on band densities from ABPP gel scans of rat brain preparations. Samples were pre-incubated with KT203 (100 μ M, 10 μ M, and 1 μ M) or DO264 (100 μ M, 10 μ M, and 1 μ M). Activity was measured using FP-Rhodamine (500 nM). Data are presented as means \pm SEM from six independent samples of the particulate (A and B) or soluble (C and D) fractions. * P <0.05 versus the control, 2-way repeated measures ANOVA with Dunnett's multiple comparisons.

Table 4.1 The effects of selected inhibitors on enzyme activity in rat brain particulate fractions labelled with FP-rhodamine.

Band No.	Estimated MW (kDa)	KT-6	KT -5	KT -4	NAGLY-3	DO -6	DO -5	DO -4	Potential identification	SH-selective inhibitors
1	>210	101±17	70±3	87±24	90±26	74±12	109±19	126±19		
2	150-188	94±8	93±3	79±11	96±7	95±4	99±4	94±5		
3	128-140	112±21	114±14	92±13	98±14	101±7	77±17	113±15		
4	85-87.6	114±18	71±9	66±10	109±12	75±6	108±16	94±12	HSL/LIPE?	
5	71.3-75.6	111±6	81±8	41±17	95±6	98±8	93±8	93±8	DAGL-β?	THL?
6	58.8-61.5	51±4*	1±0*	1±0*	98±6	91±8	89±5	100±3	FAAH?	URB597?
7	57.2-59.7	70±12	7±3	5±2	112±7	112±11	111±9	107±5	BAT5/ABHD16A?	
8	49.6-51.8	111±12	128±5	144±26	151±24	130±11	135±31	138±32	PLA2G7/NCEH1?	JW480?
9	47.8-49.6	109±10	147±20	151±29	164±36	128±19	139±23	134±22	NCEH1?	JW480?
10	43.4-44.7	111±6	90±9	82±6	102±7	88±10	98±10	114±13		
11	42.7-44	100±18	80±6	83±13	102±15	100±15	134±28	144±25		
12	41-42.2	123±26	92±28	111±27	112±23	106±29	137±44	125±24	ABHD4?	
13	36.4-36.7	100±5	106±10	104±10	92±6	85±6	93±4	96±4	MAGL	JZL184/JJKB048
14	35.2-35.8	101±4	107±9	101±9	94±4	85±6	94±4	97±2	MAGL	JZL184/JJKB048
15	33.4-33.9	4±1*	3±1*	2±0*	66±17	91±21	104±15	107±13	ABHD6	
16	32.1-33.0	102±39	89±33	74±28	108±22	90±11	90±12	112±9		
17	28.7	95±8	83±4	81±6	106±4	90±6	88±5	93±2		
18	28.1	75±8	56±8	75±8	115±11	86±8	91±7	123±13		
19	26.2	120±8	97±6	95±4	97±8	100±12	101±6	110±6		
20	22.9	106±10	85±5	51±5*	92±8	104±7	130±17	126±15	APT2?	ML349?
21	22.2	95±10	84±5	68±6*	93±10	105±13	110±16	122±12	APT1?	ML348?

Data are mean ± SEM of adjusted volumes expressed as a percentage of the controls from the matching tissue sample. Data are taken from six independent preparations. *P<0.05 versus the control, 2-way repeated measures ANOVA with Dunnett's multiple comparisons.

Table 4.2 The effects of selected inhibitors on enzyme activity in rat brain soluble labelled with FP-rhodamine.

Band No.	Estimated MW (kDa)	KT -6	KT -5	KT -4	NAGly -3	DO -6	DO -5	DO -4	Potential identification
1	>210	135±13	127±10	89±20	121±55	122±32	160±34	169±35	
2	135.1-136.4	240±74	191±36	120±33	244±84	189±76	140±21	220±68	
3	82.4-85.2	137±9	54±12	12±3	145±37	132±30	129±26	100±23	
4	73.3-77.8	120±20	53±13	6±2*	92±25	98±23	124±19	124±24	?
5	70.-73.2	82±21	6±3*	15±12*	80±23	131±23	157±39	147±42	?
6	50.1-53	131±10	140±8	113±23	102±29	114±26	145±28	125±22	
7	48.-50	135±8	147±7	140±29	117±34	100±24	142±29	125±27	
8	46-48	236±93	208±89	152±97	127±51	145±45	167±54	142±40	
9	43.6-46	112±30	106±12	63±15	63±20	113±34	110±22	116±24	
10	36-39	184±50	162±47	74±13	91±18	104±23	165±59	145±51	MAGL?
11	34.7-37.8	216±89	202±74	73±13	85±18	114±22	205±90	160±62	MAGL?
12	32.9-36	204±99	54±20	23±5	76±26	90±15	199±99	204±105	
13	32.1-35.2	196±87	83±17	33±8	73±16	99±30	175±80	184±64	
14	31.2	163±53	74±26	55±22	97±16	135±52	121±34	221±93	
15	29.9	176±16	157±19	126±36	99±35	106±32	104±18	113±24	
16	28.7	180±33	120±31	103±31	149±38	123±41	79±30	118±28	
17	27.7	131±15	111±19	45±10	65±17	66±26	117±43	134±27	
18	26.3	377±174	175±38	26±7	218±83	125±31	142±34	154±19	
19	25.1	228±115	135±55	12±5*	82±8	108±25	208±113	151±39	APT2?
20	25.1	233±88	157±50	24±4*	107±11	103±30	209±119	195±75	APT1?

Data are mean ± SEM of adjusted volumes expressed as a percentage of the controls from the matching tissue sample. Data are taken from six independent preparations. *P<0.05 versus the control, 2-way repeated measures ANOVA with Dunnett's multiple comparisons test. Band 1 fell outside the range of the MW standards.

4.2.2 Enzyme activities in rat brain fractions measured using MB064

After measuring enzyme activity with FP-rhodamine, we used the more selective probe MB064 in the next phase of the experiment. MB064 was chosen for its selectivity towards ABHD6 and ABHD12, allowing us to specifically investigate the activity of these enzymes in both the soluble and particulate fractions of rat brain tissue.

The gels in Figure 4.4 reveal distinct enzyme activity patterns in the particulate and soluble fractions of rat brain tissue, labelled using MB064. Compared to FP-rhodamine, MB064 labelled fewer active enzymes, with obvious visual differences in band intensity between the two fractions.

In the particulate fraction, seven distinct bands were detected using MB064. The most intense bands were band 3 and band 6, at a molecular size consistent with ABHD6, which was inhibited by KT203 at all concentrations (100 μ M, 10 μ M, and 1 μ M). Band 7 was inhibited only at the highest concentration of KT203 (100 μ M). DO264 selectively inhibited Band 4 (45.6 kDa), associated with ABHD12, at all concentrations. However, NAGly had no observable effect on any of the bands in the particulate fraction. In the soluble fraction, six bands were detected, with the most prominent being Band 1 and Band 2. These findings, observed from the gel images, highlight the differential enzyme activity and inhibitor selectivity between the soluble and particulate fractions when labelled with the more selective MB064 probe.

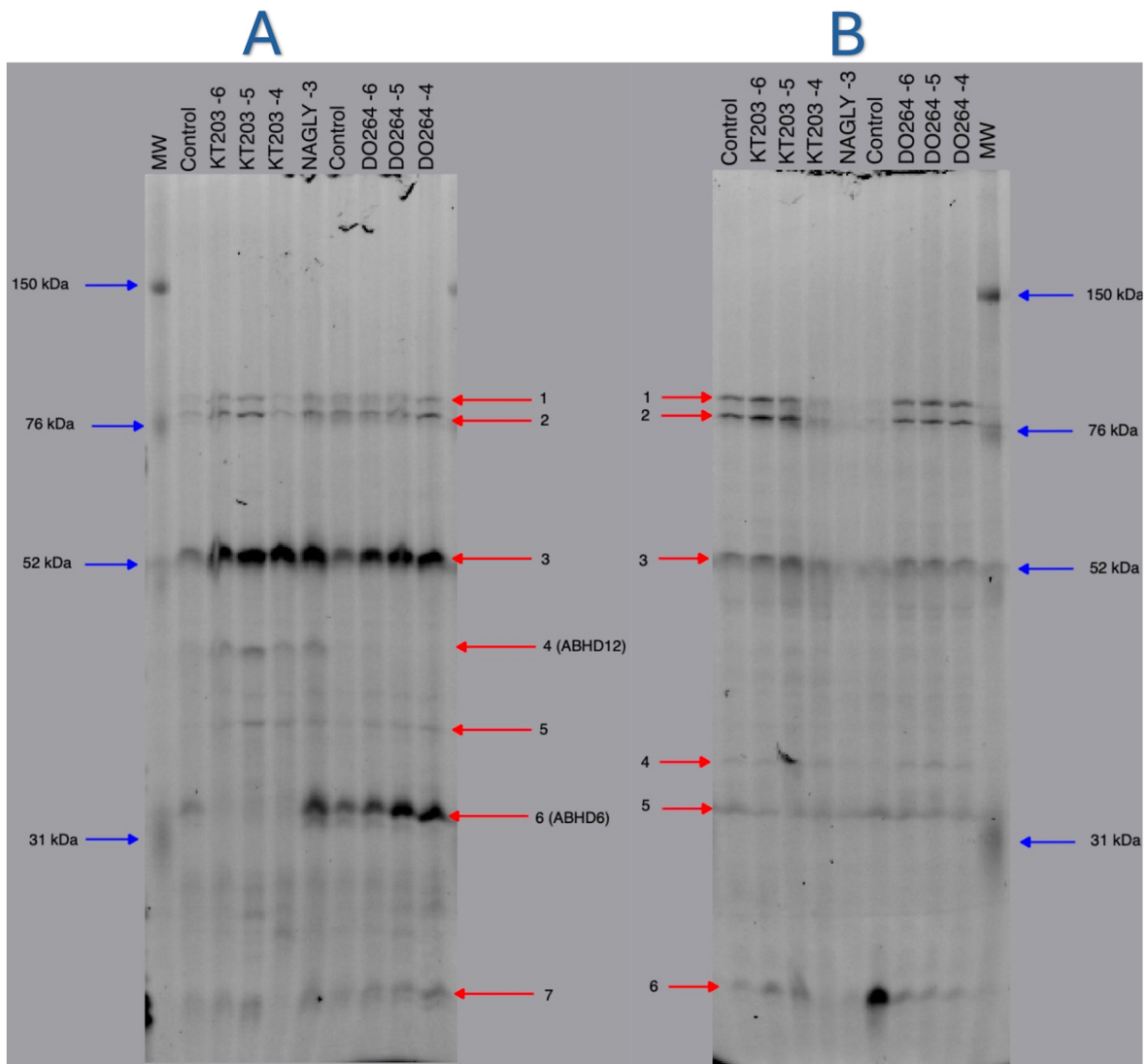


Figure 4.4 Representative gel scans of the particulate (A) and soluble (B) fractions of rat brains measured using the activity-based probe MB064 (500 nM) in the absence and presence of various inhibitors. Samples were pre-incubated with KT203 (100 μ M, 10 μ M, and 1 μ M), DO264 (100 μ M, 10 μ M, and 1 μ M), and NAGly (1000 μ M) to evaluate their effects on target enzyme activity. The left-hand lane in the particulate fraction (A) displays molecular weight markers corresponding to the particulate fraction, while the right-hand lane in the soluble fraction (B) contains molecular weight markers for the soluble fraction. Protein bands detected and quantified are indicated numerically (red arrows), with notable bands ABHD12 and ABHD6 labeled for reference. The gel contained samples from a single animal; tissues from five other animals were processed in an identical manner.

The pharmacological effects of KT203, DO264, along with the endogenous metabolite NAGly, were evaluated to determine their impact on enzyme activity in both the particulate and soluble fractions of rat brain tissue. Figure 4.5 shows the inhibition patterns of these inhibitors, while Table 4.3 (particulate fraction) and Table 4.4 (soluble fraction) provide a quantitative analysis of enzyme activity across different inhibitor concentrations and the estimated molecular weights of the bands in each fraction.

For the particulate fraction, seven major bands were detected using MB064, ranging in apparent molecular weight from 23.9 kDa to 88.8 kDa. The activity of Band 6 (33.1 kDa) was inhibited by all three concentrations of the ABHD6-selective inhibitor KT203. KT203 failed to alter the density of any other band in rat brain particulate fractions. The activity of Band 4 (45.6 kDa) was inhibited by all three concentrations of the ABHD12-selective inhibitor DO264 (Figure 4.5). DO264 failed to alter the density of any other band in the rat brain particulate fractions.

For the soluble fraction, six major bands were detected using MB064, ranging in apparent molecular weight from 25.8 kDa to 89.9 kDa. In the presence of any concentration of KT203, DO264, and NAGly, no significant inhibition of enzyme activity was observed for any of these bands in the soluble fraction. In both the soluble and particulate fractions, 1 mM NAGly did not cause significant inhibition of enzyme activity.

The statistical analysis, using a two-way repeated measures ANOVA with Dunnett's multiple comparisons test, confirmed the differential inhibition patterns observed in Figure 4.4. KT203 significantly inhibited ABHD6 (Band 6) across all tested concentrations, while DO264 significantly inhibited ABHD12 (Band 4) at each concentration in the particulate fraction (Figure 4.5, Table 4.3). NAGly showed no statistically significant inhibition in either fraction.

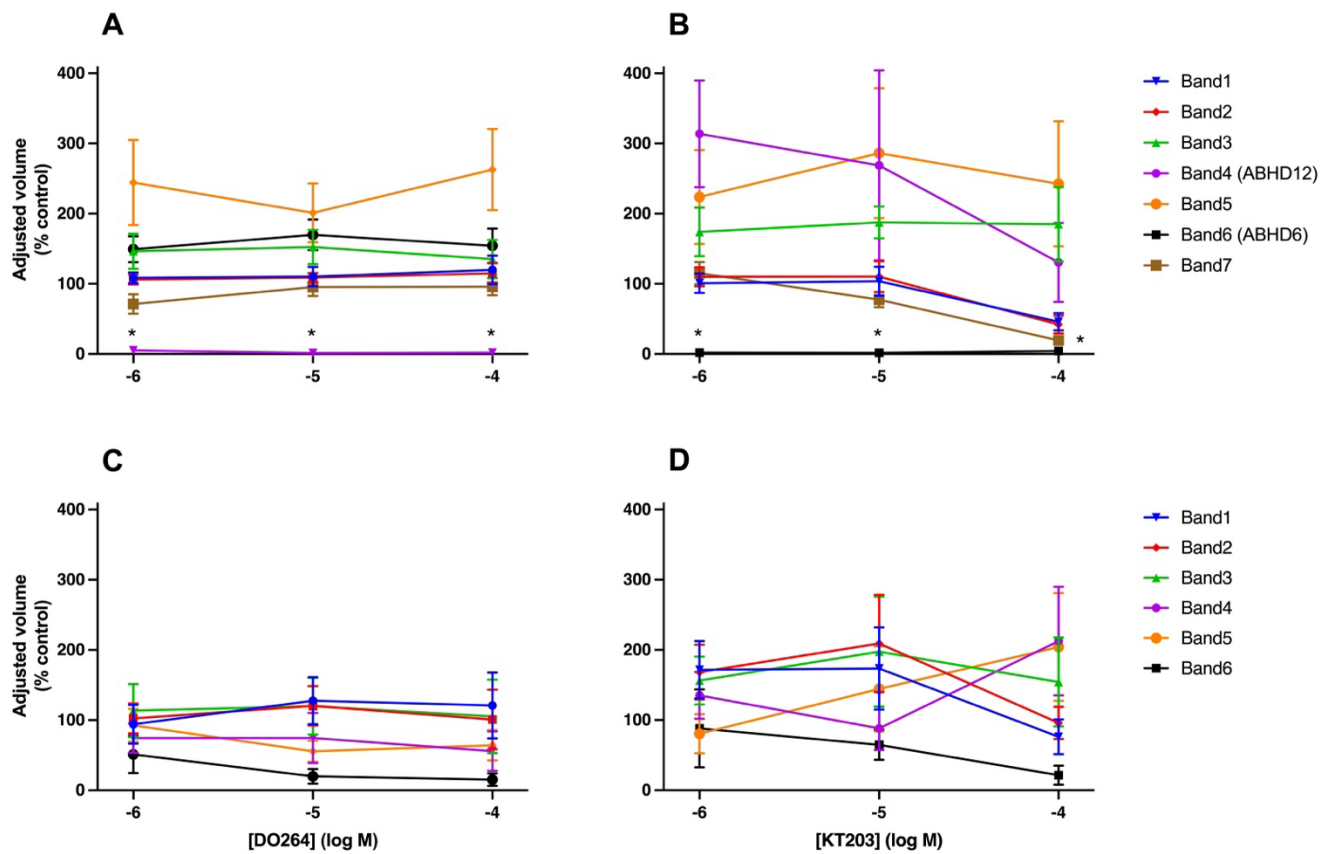


Figure 4.5 The effects of selective inhibitors on band densities from ABPP gel scans of rat brain preparations. Samples were pre-incubated with KT203 (100 μ M, 10 μ M, and 1 μ M) or DO264 (100 μ M, 10 μ M, and 1 μ M). Activity was measured using MB064 (500 nM). Data are presented as means \pm SEM from six independent samples of the particulate (A and B) or soluble (C and D) fractions. * P <0.05 versus the control, 2-way repeated measures ANOVA with Dunnett's multiple comparis

Table 4.3 The effects of selected inhibitors on enzyme activity in rat brain particulate fraction labelled with MB064.

Band No.	Estimated MW (kDa)	KT -6	KT -5	KT -4	NAGLY-3	DO -6	DO -5	DO -4	Potential identification
1	88.8-91	101 ± 13	104 ± 19	46 ± 11*	93 ± 14	108 ± 7	110 ± 13	120 ± 19	DDHD2?
2	82.1-86	110 ± 13	110 ± 20	42 ± 12	114 ± 12	106 ± 6	109 ± 6	115 ± 13	DDHD2?
3	55.7-58.6	174 ± 31	188 ± 21	185 ± 49	197 ± 26	146 ± 23	153 ± 22	135 ± 25	ABHD16a?
4	45.6-48.1	314 ± 69	269 ± 124	131 ± 52	256 ± 84	5 ± 2*	1 ± 0*	2 ± 1*	ABHD12
5	39.1-41.4	224 ± 58	286 ± 80	242 ± 77	153 ± 16	244 ± 53	201 ± 36	263 ± 50	
6	33.1-35.2	2 ± 0*	2 ± 0*	4 ± 1*	199 ± 16	149 ± 21	170 ± 20	154 ± 22	ABHD6
7	23.9	115 ± 14	77 ± 10	19 ± 4*	104 ± 14	71 ± 13	96 ± 12	96 ± 11	

Data are mean ± SEM of adjusted volumes expressed as a percentage of the controls from the matching tissue sample. Data are taken from six independent preparations. *P<0.05 versus the control, 2-way repeated measures ANOVA with Dunnett's multiple comparisons test.

Table 4.4 The effects of selected inhibitors on enzyme activity in rat brain soluble fraction labelled with MB064.

Band No.	Estimated MW (kDa)	KT-6	KT-5	KT-4	NAGly-3	DO-6	DO-5	DO-4	Potential identification
1	86.5-89.9	172 ± 37	173 ± 53	76 ± 23	130 ± 49	94 ± 25	128 ± 31	121 ± 42	DDHD2?
2	81.3-82.5	168 ± 36	209 ± 63	96 ± 21	130 ± 45	102 ± 20	121 ± 26	101 ± 38	DDHD2?
3	55.7	156 ± 31	197 ± 72	154 ± 58	164 ± 67	114 ± 34	120 ± 37	105 ± 47	
4	37.8-38.1	135 ± 30	88 ± 28	349 ± 138	127 ± 61	75 ± 19	75 ± 33	56 ± 25	
5	34.7-35.1	81 ± 25	144 ± 55	204 ± 70	135 ± 50	93 ± 21	56 ± 14	64 ± 19	
6	25.8	88 ± 50	65 ± 19	22 ± 12	219 ± 109	51 ± 24	10 ± 3	15 ± 8	

Data are mean ± SEM of adjusted volumes expressed as a percentage of the controls from the matching tissue sample. Data are taken from six independent preparations. *P<0.05 versus the control, 2-way repeated measures ANOVA with Dunnett's multiple comparisons test.

4.3 Discussion

This is the first study to investigate ABHD6 and ABHD12 in the rat brain using two distinct probes, FP-rhodamine and MB064, and to evaluate the selectivity and potency of KT203 and DO264 on these enzymes, respectively. Additionally, it examines the effects of the endogenous metabolite NAGly in the rat brain.

Previous studies have predominantly used mice for these assessments, but the use of rats offers several advantages. Rats are known to exhibit more complex behaviors and provide better models for behavioral studies (Ellenbroek & Youn, 2016), which could be particularly important for future investigations into the physiological roles of ABHD6 and ABHD12 in cognition, emotion, and reward systems. However, there is limited information on their biochemical properties, enzymatic activity, and pharmacological regulation in rat brain tissues. While ABHD6 and ABHD12 are known to play roles in lipid metabolism and signaling, their biochemical and pharmacological profiles in the rat brain have not been well characterized. Most existing studies have focused on mouse models, and it remains unclear to what extent findings from these studies translate to rats. Investigating these enzymes in the rat brain will provide valuable comparative data and may offer insights into potential species differences in enzyme function, inhibitor sensitivity, and broader physiological roles.

Because there are well-established methods for gene disruption and amplification in mice and not rats, 60% of animals used for experimental procedures in 2023 in the UK were mice ([Annual statistics of scientific procedures on living animals, Great Britain 2023 - GOV.UK \(www.gov.uk\)](https://www.gov.uk/government/uploads/system/uploads/attachment_data/file/115442/annual-statistics-of-scientific-procedures-on-living-animals-great-britain-2023.pdf)). However, both mice and rats are well-established models in cannabinoid research. For example, studies have used rats to investigate inflammatory pain behaviour and the modulation of the endocannabinoid system. In two distinct pain models using rats, FAAH and MAGL were shown to influence pain-induced behaviours and spinal processing (Okine et al. (2012), Woodhams et al., 2012). In another study, Rahman et al. (2015) used rats to evaluate the role of Ca_v2.2 voltage-gated calcium channels in mediating pain in a rat model of osteoarthritis (OA), demonstrating the utility of rats in both behavioural and electrophysiological studies. Because of the larger size of the rat brain in comparison to mice, Sarmad et al. (2011) used rat brain slices to show the selective influence of FAAH inhibition on AEA, but not 2AG, levels. So, while much of the information from ABPP studies is focussed on mouse preparations, it is important to report data from rats for comparison with behavioural and functional studies in these animals.

4.3.1 Detection of ABHD6 and ABHD12 in Rat Brain Fractions

4.3.1.1 ABHD6 detection in the Particulate Fraction

Based on previously published literature using mouse brain, we expected both ABHD6 and ABHD12 to be detectable in the particulate fraction of rat brain tissue.

ABHD6 was anticipated to migrate with a molecular weight of 33-35 kDa, as observed in studies using FP-rhodamine (Blankman et al., 2007; Manterola et al., 2018) or MB064 (Baggelaar et al., 2015; Baggelaar et al., 2017). Given that ABHD6 is membrane-associated (Blankman et al., 2007), we predicted it would be present in the particulate fraction.

Furthermore, KT203, a selective ABHD6 inhibitor, has been shown to inhibit ABHD6 at concentrations below 1 μM (Hsu et al., 2013). Therefore, we anticipated detecting ABHD6 with both probes, with inhibition expected at the tested concentrations of KT203.

Comparing gels from mouse brain labelled with FP-rhodamine (Figure 4.6) (Blankman et al., 2007) with Figure 4.1, there are similarities and differences. Notably, MAGL and ABHD6 appear as three bands, with the ABHD6 band migrating faster than the MAGL doublet. While this pattern is also apparent in the current study (Figure 4.4), the lowest band, consistent with ABHD6, is less prominent in the rat brain compared to the published study using mouse brain. Using FP-rhodamine, we observed ABHD6 (Band 15) with a molecular weight of 33.4 kDa (Table 4.1), consistent with the reported molecular weight of 33-35 kDa for ABHD6 in previous studies using FP-rhodamine in mouse brain tissue (Blankman et al., 2007; Manterola et al., 2018). KT203 significantly inhibited this band across all tested concentrations, conforming it corresponds to ABHD6. Hsu et al. (2013) demonstrated that KT203 at concentrations of 1 μM and 10 μM significantly inhibited ABHD6 in mouse brain proteomes using the FP-rhodamine probe. Additionally, Manterola et al. (2018) reported complete inhibition of ABHD6 in brain proteomes from EAE mice following KT203 treatment using the same probe.

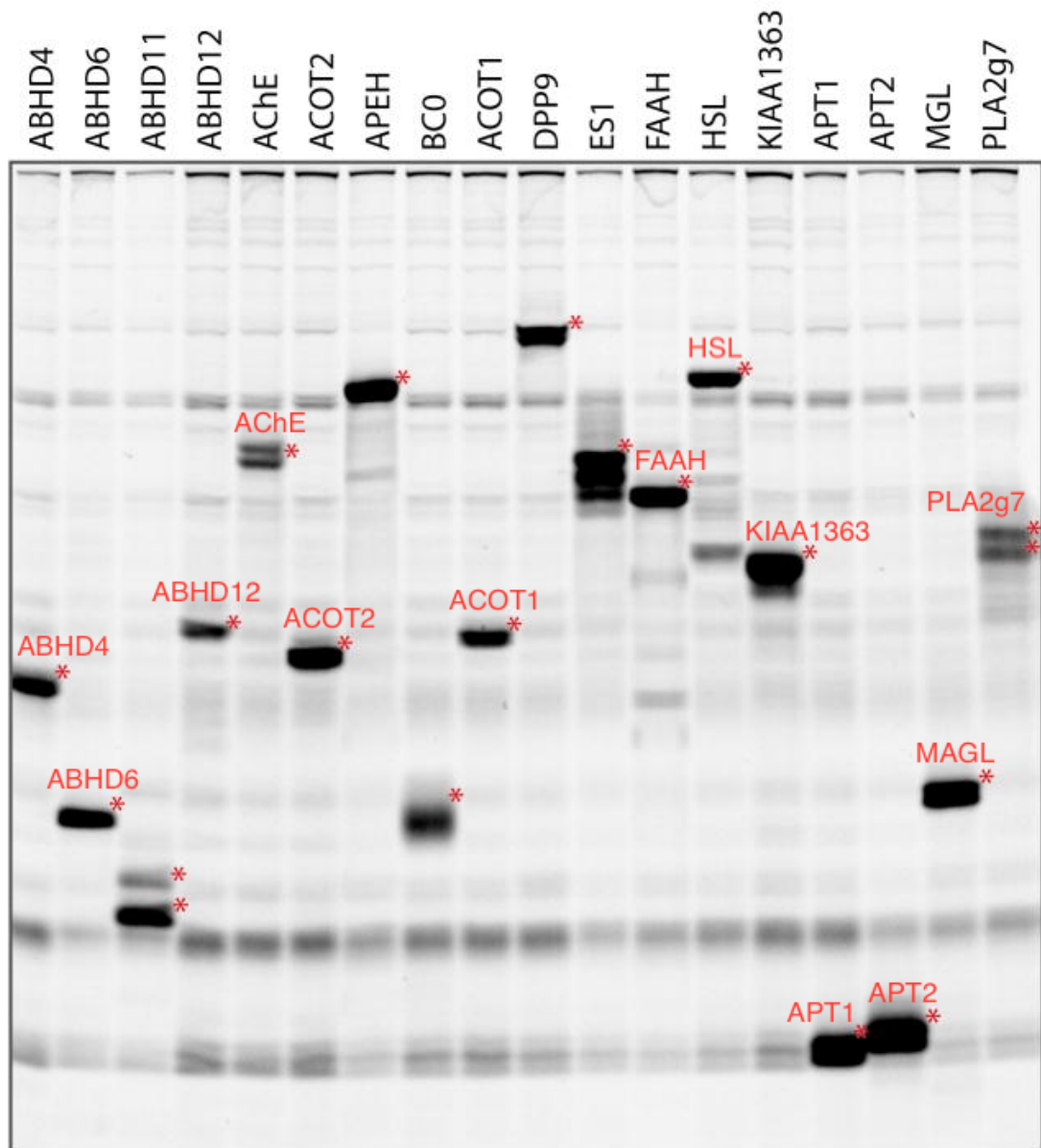


Figure 4.6 The expression of recombinant mouse brain serine hydrolases was analyzed in COS-7 cells transiently transfected with cDNAs encoding these enzymes. Following transfection, cells were incubated with FP-rhodamine (2 μ M) for 1 hour. Proteins were then separated via SDS-PAGE and analyzed using in-gel fluorescence scanning for visualization, confirmation of enzyme expression, and quantification of band intensities corresponding to active enzymes. For clarity, enzyme names have been labeled in red next to their corresponding bands to enhance readability and facilitate identification. Adapted from Blankman et al. (2007).

Using MB064, we also observed ABHD6 (Band 6) with an estimated molecular weight of 33.1 kDa (Table 4.3), consistent with the molecular weight range of 33-35 kDa for ABHD6 as reported in previous studies using MB064 in mouse brain proteome (Baggelaar et al., 2015; Baggelaar et al., 2017). KT203 significantly inhibited this band across all tested concentrations, confirming it corresponds to ABHD6. The fact that both FP-rhodamine and MB064 identified ABHD6, and that both bands were inhibited by KT203, confirms the presence of ABHD6 in the particulate fraction of rat brain tissue.

It is possible that ABPs, FP-rhodamine and MB064, may influence protein migration in SDS-PAGE due to their covalent binding and steric effects. The attachment of these probes can add molecular mass or alter the protein's charge distribution, potentially leading to minor shifts in electrophoretic mobility. However, the impact of probe binding on migration is generally minimal compared to other factors that more significantly influence protein migration, such as phosphorylation, glycosylation, or proteolysis (Baggelaar et al., 2017), which can substantially alter the molecular weight and charge of protein.

4.3.1.2 ABHD12 Detection in the Particulate Fraction

Similarly, ABHD12 was expected to migrate at an approximate molecular weight of 45 kDa, as seen in studies using FP-rhodamine (Blankman et al., 2007; Ogasawara et al., 2018) or MB064 (Baggelaar et al., 2015; Baggelaar et al., 2017). As with ABHD6, ABHD12 is also predicted to be membrane-associated (Blankman et al., 2007), suggesting its presence in the particulate fraction. DO264 has been shown to inhibit ABHD12 at concentrations below 1 μ M (Ogasawara et al., 2018), so we anticipated detecting ABHD12 with both probes and observing inhibition in response to DO264 at the tested concentrations.

ABHD12 was detected in the particulate fraction using MB064 at a molecular weight of 45 kDa (Band 4), aligning with the results of Baggelaar et al. (2015), where ABHD12 was detected in mouse brain proteomes at a similar molecular weight using MB064. However, ABHD12 was not detected using FP-rhodamine (Figure 4.4). This contrasts with a study using mouse brain (Blankman et al., 2007), where FP-rhodamine labelled a band that was relatively less prominent than the ABHD6 activity. It appears that both ABHD6 and ABHD12 are expressed at lower activity levels in rat brain compared to mouse brain. Additionally, the broad-spectrum nature of FP-rhodamine, which reacts with numerous enzymes in brain tissue, likely contributed to the lack of detection. The high abundance of co-migrating serine hydrolases may have masked ABHD12's signal, particularly since ABHD12

is known to produce a relatively thin band. These higher-intensity bands likely overshadowed ABHD12, preventing its detection with FP-rhodamine.

4.3.2 Selectivity of ABHD6 and ABHD12 Inhibitor

4.3.2.1 Selectivity of KT203

KT203 demonstrated significant inhibition of several bands in the rat brain particulate fraction when analyzed with FP-rhodamine, revealing both its selective and off-target effects. The most prominent inhibition was observed on Band 15 (33.4 kDa), corresponding to ABHD6, in the particulate fraction with FP-rhodamine. This band was significantly inhibited across all tested concentrations of KT203. This finding aligns with KT203's known selectivity as an ABHD6 inhibitor, consistent with previous findings in mouse brain studies (Hsu et al., 2013; Manterola et al., 2018).

Using the MB064 probe, the activity of Band 6 (33.1 kDa), corresponding to ABHD6, was also inhibited by all three concentrations of KT203, further supporting its selective inhibitory effect on ABHD6. In addition, Band 6 (58.8 kDa) in the particulate with FP-rhodamine was inhibited at all concentrations of KT203, suggesting off-target activity. The molecular weight of this band is consistent with FAAH, which has a reported molecular weight of approximately 63 kDa in rat, according to UniProt. FAAH was also detected using FP-rhodamine ABPP in mouse brain membranes with a molecular weight around 60 kDa (Manterola et al., 2018; Blankman et al., 2007). Although Hsu et al. (2013) reported cross-reactivity of KT203 with FAAH in vivo when administered via oral gavage, our findings suggest that this cross-reactivity also occurs in vitro. To confirm this off-target inhibition, selective FAAH inhibitors such as URB597 (Piomelli et al., 2006) or proteomic approaches could be used.

KT203 also inhibited Band 20 (23.9 kDa) and Band 21 (22.2 kDa) in the rat brain particulate fraction, but only at the highest concentration tested. These bands likely correspond to APT2 and APT1, respectively, based on their molecular weights and previous studies (Blankman et al., 2007; Hsu et al., 2013), which detected APT2 and APT1 in mouse brain proteomes using FP-rhodamine. To conclusively verify these enzymes, selective inhibitors, such as ML348 for APT1 and ML349 for APT2 (Hulce et al., 2010) could be used in future experiments.

As expected, KT203 did not inhibit any bands around the estimated molecular weight of ABHD6 in the soluble fraction, consistent with the fact that ABHD6 is an integral membrane

enzyme (Blankman et al., 2007) and would not be expected in the soluble fraction. However, at the highest concentration of 100 μ M, KT203 significantly inhibited four bands: Band 4 (73.3 kDa), Band 5 (70 kDa), Band 19 (25 kDa), and Band 20 (25 kDa).

Band 5 (70 kDa) was significantly inhibited at 100 μ M and 10 μ M, but not at 1 μ M, suggesting that this enzyme is sensitive to higher concentrations of KT203. However, the precise identity of the enzyme remains unidentified. Further investigation using non-selective inhibitors or proteomic approaches would be needed to verify the enzyme corresponding to Band 5.

When using the MB064 probe, no significant inhibition of enzyme activity was observed for any of the bands in the soluble fraction, even at the highest concentration of KT203.

At 100 μ M KT203, Bands 4 (73.5 kDa), 19 (25 kDa), and 20 (25 kDa) were also inhibited.

Based on molecular weight similarities and findings in both fractions, Band 19 in the soluble fraction likely corresponds to Band 20 in the particulate fraction, while Band 20 in the soluble fraction may correspond to Band 21 in the particulate fraction. Both bands, around 25 kDa, may represent APT2 and APT1, which are expressed in both fractions, as indicated by Blankman et al. (2007), where APT2 and APT1 were detected in a recombinant mouse brain system, and Hsu et al. (2013), who identified these enzymes in native mouse brain proteomes using FP-Rhodamine. To confirm this, selective inhibitors such as ML348 for APT1 and ML349 for APT2 (Adibekian et al., 2014) or proteomic techniques could be used.

4.3.2.2 Selectivity of DO264

DO264 demonstrated a better selectivity profile compared to KT203, as it selectively inhibited ABHD12 (Band 4) at a molecular weight of 45 kDa in the particulate fraction when using MB064. Even at the highest concentration of 100 μ M, DO264 did not inhibit any other bands, suggesting a high degree of selectivity for ABHD12.

This observation is consistent with previous findings in mouse brain studies. Ogasawara et al. (2018) reported that DO264 exhibited excellent selectivity for ABHD12 in comparison to other serine hydrolases in the mouse brain membrane proteome using the FP-rhodamine probe. This high degree of selectivity, even at higher concentrations, positions DO264 as a strong candidate for further in vivo investigation of ABHD12.

4.3.2.3 NAGly as a substrate/inhibitor of rat brain serine hydrolases

Based on a screening study in rat brain at a concentration of 100 μM , NAGly was initially indicated to interact with multiple enzymes, with ABHD6 being a potential target (Aldossari, 2023). However, the current results showed no statistically significant inhibition in either the particulate or soluble fractions when using FP-rhodamine and MB064 as probes. This suggests that NAGly may not interact with ABHD6 as initially anticipated from the screening study.

4.3.3 Additional Enzyme Activities Detected with FPR and MB064 in Rat Brain Fractions

In this study, we observed multiple serine hydrolase activities in rat brain fractions labelled with both FP-rhodamine and MB064. To identify the detected bands that were not affected by the selective inhibitors KT203 or DO264, we compared these results with gel patterns from previous studies that used similar probes in mouse brain samples.

Blankman et al. (2007) performed ABPP profiling on recombinant serine hydrolases in mouse brain using FP-rhodamine. Their gel (Figure 4.6) serves as a reference for identifying serine hydrolases in rat brain samples (Figure 4.1). By comparing molecular weights and subcellular distributions, several bands in the FP-rhodamine-labeled rat brain gels likely correspond to those reported in Blankman's mouse brain study. For example, bands at comparable molecular weights suggest similar serine hydrolase activities between the two species. However, these identifications are preliminary, and further validation is necessary to confirm the identity of these bands in the rat brain.

Similarly, Baggelaar et al. (2015) used ABPP with MB064 in mouse brain membrane proteomes (Figure 4.7). Comparing their gels with those from Figure 4.4, we identified bands at molecular weights similar to those detected in mouse brain. However, as with FP-rhodamine, these comparisons provide only preliminary identifications.

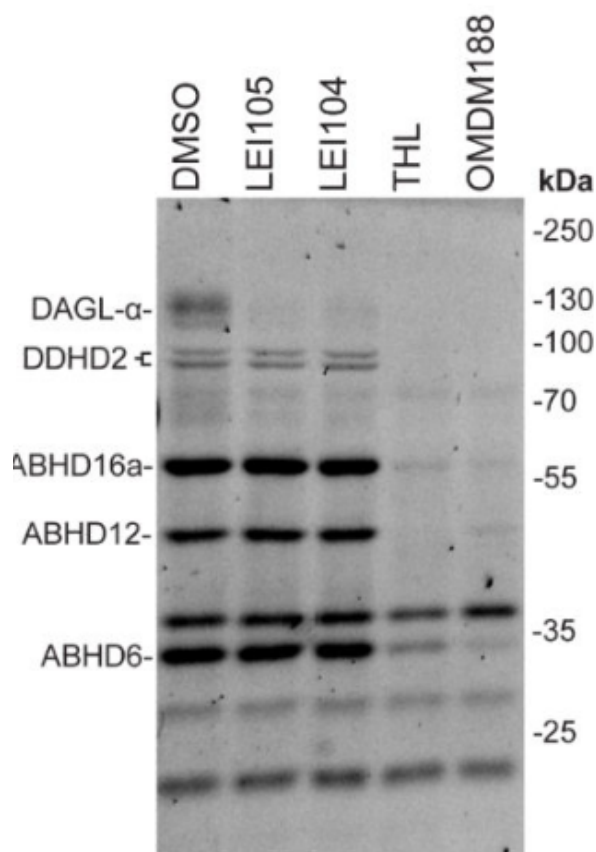


Figure 4.7 Mouse Brain Membrane Proteome Labeled with MB064 Probe performed using LEI104 (10 μ M) (a selective inhibitor of DAGL- α), LEI105 (10 μ M) (a reversible dual DAGL- α /DAGL- β inhibitor), OMDM188 (1 μ M) (a DAGL inhibitor), and THL (10 μ M) as inhibitors. Proteins were labeled with MB064 (250 nM) and subsequently separated via SDS-PAGE, followed by in-gel fluorescence scanning to assess the inhibition of target enzymes.

The detected protein bands correspond to active serine hydrolases, including DAGL- α , DDHD2, ABHD16a, ABHD12, and ABHD6, which were differentially inhibited by the tested compounds. The resulting fluorescent gel image is displayed in grayscale. Adapted from (Baggelaar et al.,2015)

4.3.3.1 ABHD16a (63 kDa in rat, UniProt)

The molecular size of Band 7 in the particulate fraction, detected with FP-rhodamine, is estimated at approximately 57 kDa, which is consistent with ABHD16a (formerly known as BAT5). ABHD16a has previously been identified in mouse brain membranes using FP-rhodamine ABPP, with a reported molecular weight of around 59 kDa (Hoover et al., 2008;

Blankman et al., 2007). In both studies, ABHD16a appeared just below the FAAH band, displaying a distribution pattern similar to that observed in the current study. Given the close match in molecular weight and migration patterns, Band 7 in the rat brain gel likely corresponds to ABHD16a.

Additionally, Band 3 in the particulate fraction, labeled with MB064, has a molecular weight of 55.7 kDa and may also represent ABHD16a. A band of similar molecular weight (~55 kDa) was previously identified using ABPP with MB064 in mouse brain membrane proteomes (Baggelaar et al., 2015). The detection of nearly identical molecular weights by both FP-rhodamine and MB064 probes in this study suggests that both probes effectively label ABHD16a. To confirm these bands as ABHD16a, non-selective inhibitors like THL or MAFP could be used, as these inhibitors have been shown to block ABHD16a activity in HEK293 cell lysates (Hoover et al., 2008). Proteomic approaches could further validate this identification.

4.3.3.2 PLA2G7/ NCEH1 (49.4/45.8 kDa in rat, UniProt)

The molecular weight of Band 8, approximately 49 kDa, has been detected at a similar size in mouse brain membranes using FP-rhodamine ABPP (Blankman et al., 2007). However, both Band 8 (49 kDa) and Band 9 (47 kDa) are also consistent with neutral cholesterol ester hydrolase 1 (NCEH1), which has been reported to migrate as a doublet in mouse brain membranes (Hoover et al., 2008; Hsu et al., 2013), suggesting that NCEH1 may also migrate as a doublet in rat brain. To distinguish between PLA2G7 and NCEH1, selective inhibitors, proteomic analysis, and FP-biotin labelling could be used. Given that a selective inhibitor for NCEH1 (JW480) is available (Chang et al., 2011), it could be used to confirm the identity of Band 8 as NCEH1.

4.3.3.3 MAGL (33.5 kDa in rat, UniProt)

Bands 13 (matching Band 10 in the soluble fraction) and Band 14 (matching Band 11 in the soluble fraction) align with the profile of MAGL. These bands appeared as a doublet of 36 and 35 kDa in both fractions, with higher expression in the particulate fraction. Previous studies have shown MAGL migrates as a doublet in mouse brain membranes (Patel et al., 2015), suggesting that it might migrate similarly in rat brain samples. Moreover, similar results were observed in Qulayl Aldossari's PhD thesis 2023, where MAGL migrated as a doublet of 34 and 33 kDa in rat brain with higher expression in the particulate fraction.

Therefore, based on the molecular weight, migration patterns, and higher expression in the particulate fraction, it is likely that Band 13 and Band 14 correspond to MAGL. Further identification could be achieved using selective inhibitors such as JZL184 or JJKK048 (Aaltonen et al., 2013).

4.3.3.4 DDHD2 (79.5 kDa in rat, UniProt)

Band 1 (86 kDa) and Band 2 (82 kDa) in both the soluble and particulate fractions could correspond to DDHD2. DDHD2 has been detected as a double band, with a molecular weight around 85 kDa, using ABPP with MB064 in mouse brain membrane proteomes (Baggelaar et al., 2015). A similar pattern to that observed in mouse brain was found in this study, where DDHD2 appeared to migrate as a double band in the rat brain preparations. Further identification could be achieved using KLH45, a DDHD2 selective inhibitor (Inloes et al 2014).

Chapter 5: General Discussion

Endocannabinoids (ECBs) are involved in multiple physiological, psychological, and pathological processes, with ongoing research exploring ways to enhance endogenous ECB levels for therapeutic benefits. One approach involves the pharmacological or genetic inhibition of ECB-metabolizing enzymes, such as ABHD6 and ABHD12, to regulate 2-AG metabolism. A comprehensive understanding of their subcellular distribution and expression across different cellular and tissue contexts is essential for determining their roles in disease and evaluating their therapeutic potential. Targeting ABHD6 has demonstrated therapeutic potential in several disease models, as its inhibition has been associated with seizure suppression via modulation of GABAergic transmission, reducing the severity of epileptic seizures (Naydenov et al., 2014; Westenbroek et al., 2023).

Additionally, ABHD6 inhibition has been linked to reduced neuroinflammation and pain by reducing pro-inflammatory cytokine production and PGE2 levels, contributing to its potential application in multiple sclerosis and chronic pain disorders (Li et al., 2007; Wen et al., 2018). Furthermore, ABHD6 inhibition has shown promise in metabolic regulation by improving glucose tolerance, enhancing insulin secretion, and protecting against obesity-related metabolic dysfunction (Zhao et al., 2014; Thomas et al., 2013). Emerging evidence also suggests a role in autoimmune conditions, where its inhibition may mitigate inflammatory responses in diseases such as SLE (Poursharifi et al., 2017; Oparina et al., 2015). Due to its role in multiple signaling pathways, ABHD6 inhibition is a promising therapeutic target for neurological, inflammatory, metabolic, and autoimmune disorders. Similarly, ABHD12 inhibition has demonstrated therapeutic relevance in neurodegenerative disorders, particularly in PHARC. Studies in ABHD12 knockout mice revealed that loss of ABHD12 function leads to abnormal Lyso-PS accumulation, triggering chronic neuroinflammation and progressive neurodegeneration (Blankman et al., 2013). These findings suggest that targeting ABHD12 could modulate neuroinflammatory pathways, potentially offering therapeutic benefits in PHARC and related neurodegenerative disorders.

Additionally, ABHD12 inhibition has been implicated in cancer therapy. Elevated ABHD12 expression has been identified in colorectal cancer (CRC), breast cancer, and hepatocellular carcinoma (LIHC), where it facilitates tumor progression, metastasis, and therapy resistance (Yoshida et al., 2010; Jun et al., 2020; Cai et al., 2023). Pharmacological inhibition or genetic knockdown of ABHD12 in breast and liver cancer models has been shown to suppress tumor proliferation, invasion, and migration, highlighting its potential as

an oncogenic target (Jun et al., 2020; Cai et al., 2023). Furthermore, in LIHC, ABHD12 has been shown to induce sorafenib resistance, contributing to reduced treatment efficacy (Cai et al., 2023). The use of ABHD12 inhibitors, such as DO264, increased the sensitivity of hepatocellular carcinoma (HCC) cells to sorafenib-induced ferroptotic cell death, indicating that targeting ABHD12 may potentiate the therapeutic efficacy of sorafenib in LIHC patients. Given the significance of ABHD6 and ABHD12 in endocannabinoid signaling and disease, precise measurement of their enzymatic activity is essential for understanding their function and identifying selective inhibitors. This study employed two methodologies to assess ABHD6 activity: the 4-MUH-based spectrophotometric assay and ABPP. In contrast, ABPP was the sole method used to evaluate ABHD12 activity, as discussed previously, since ABHD12 did not efficiently hydrolyze 4-MUH in human recombinant systems. Each approach had distinct advantages and limitations in evaluating enzyme activity.

The 4-MUH assay, though effective in recombinant systems, presented challenges in accurately capturing ABHD6 activity within complex tissue samples. In contrast, ABPP proved to be a more versatile tool, allowing for the simultaneous profiling of multiple enzymes, including ABHD6 and ABHD12, without the need for natural substrates.

In Chapter 3, the effectiveness of the 4-MUH assay for measuring ABHD6 activity was evaluated. While the selective ABHD6 inhibitor KT203 induced only modest inhibition in the particulate fraction, this contrasted with findings from Nada Mahmood (2018), where ABHD6 efficiently hydrolyzed 4-MUH in a recombinant system, whereas MAGL and ABHD12 exhibited poor hydrolytic activity toward this substrate.

However, in rat brain tissues, inhibition of 4-MUH hydrolysis by JJKK048, suggests that MAGL contributes to 4-MUH hydrolysis in native tissue, unlike in the recombinant system. Additionally, when MAGL and ABHD6 inhibitors were used together, they still failed to fully inhibit 4-MUH hydrolysis, indicating that other hydrolases present in the rat brain contribute to this activity. These findings suggest that while 4-MUH is a reliable substrate for ABHD6 in recombinant systems, its specificity is reduced in native tissue preparations, likely due to species differences and the presence of multiple enzymes capable of hydrolyzing it, limiting its reliability for measuring ABHD6 activity in more complex tissue samples, such as those from the rat brain. To address this, it would be beneficial to investigate 4-MUH hydrolysis in recombinant rat ABHD6, allowing for a direct comparison between human and rat enzymes. Conducting serial inhibition curves with rat recombinant ABHD6 could help determine whether the reduced inhibition observed in rat brain tissue is due to intrinsic species-specific differences or the influence of additional enzymatic contributors in tissue

homogenates. Furthermore, utilizing genetically modified mice lacking ABHD6 and MAGL could provide valuable insights into the contribution of these enzymes to 4-MUH hydrolysis in tissue-based assays. These findings indicate that, without further characterization, 4-MUH may not be a reliable substrate for screening ABHD6 activity in a complex proteome.

In contrast, the results from Chapter 4 demonstrate that using ABPP allowed for the effective measurement of ABHD6 activity with both the MB064 and FP-rhodamine probes. Through this method, we were also able to confirm the selectivity and potency of KT203 for ABHD6 at the appropriate concentrations. Unlike the substrate-dependent approach used in the 4-MUH assay, ABPP uses an irreversible tag to measure enzyme activity, making it a more versatile and effective tool for enzyme profiling. Additionally, the use of ABPP with the MB064 probe enabled the simultaneous measurement of ABHD12 activity, and we were able to confirm the selectivity of DO264 for ABHD12.

Using conventional methods, such as the 4-MUH-based spectrophotometric assay, provides certain advantages, particularly in high-throughput settings. With this approach, enzyme activity can be measured in mixed populations, allowing for the screening of thousands of potential novel inhibitors or substrates. They are also scalable to robotic systems and can be highly automated (Inglese et al., 2007). If the assay is well-optimized and includes a good non-selective inhibitor (one that can inhibit all enzymes except ABHD6, for example) or an effective substrate, this method becomes highly efficient for large-scale screening. In contrast, while the ABPP technique offers precision in identifying multiple enzyme activities simultaneously, ABPP requires the design and synthesis of chemical probes, which may be expensive and time-consuming. Additionally, the lack of specificity in probes can make it difficult to target a single enzyme (Liu et al., 1999). Moreover, the ABPP technique is constrained by limited resolution and sensitivity, which can hinder precise enzyme activity detection. The identity of the proteins measured may also remain ambiguous, and the technique is not easily automated, reducing its feasibility for high-throughput applications (Patricelli et al., 2001). Preparing the gel components for ABPP can be time-consuming, with the risk of failure after extensive preparation. Additionally, interpreting ABPP data can be complex and less straightforward than spectrophotometric methods.

This study investigated the activity of ABHD6 in rat brain tissue using a 4-MUH-based spectrophotometric assay and validated the selectivity and potency of inhibitors for ABHD6 and ABHD12 through ABPP. While effective in recombinant systems, the 4-MUH assay showed reduced specificity in complex tissue samples due to contributions from additional

hydrolases. In contrast, ABPP provided a more reliable method for profiling multiple enzymes and confirming the selectivity of KT203 for ABHD6 and DO264 for ABHD12.

5.1 Future perspectives

This research has shown that KT203 inhibited ABHD6 as well as other bands in both the particulate and soluble fractions, particularly at higher concentrations. The most prominent of these inhibited bands include Band 6 (58.8 kDa) in the particulate fraction, which likely corresponds to FAAH, and Bands 20 (23.9 kDa) and 21 (22.2 kDa), found in both particulate and soluble fractions, which may correspond to APT2 and APT1, respectively. However, these identifications are tentative and require further investigation to be confirmed.

Additionally, some bands, such as Band 4 (73.3 kDa) and Band 5 (70 kDa) in the soluble fraction, remain uncharacterized which require Further investigation to conclusively identify these bands. Given KT203's inhibition profile against these other enzymes, the urea-based inhibitor chemical series (see Section 1.2.3.3) could be explored further. Specifically, analogues that are less potent against ABHD6 might exhibit greater potency against the KT203-sensitive serine hydrolases.

It would be of interest to use selective pharmacological tools to confirm the proposed identities of these other bands. For example, the FAAH-selective inhibitor URB597 could be used to confirm the identity of Band 6 as FAAH, while selective inhibitors ML348 and ML349 could confirm the identities of APT1 and APT2, respectively (Adibekian et al., 2014). As a further extension of this work, FP-biotin could be incorporated in future experiments using mass spectrometry proteomics for triangulation of the active serine hydrolases in this tissue. FP-biotin, an activity-based probe for serine hydrolases, irreversibly binds to reactive SH enzymes. The biotin tag enables detection and purification of the labelled enzyme (Liu et al., 1999) using avidin chromatography and liquid chromatography-mass spectrometry (LC-MS) to selectively isolate and identify labelled enzymes, offering a comprehensive profile of active serine hydrolases in the sample (Cravat et al., 2008). This approach would focus on unidentified bands of high activity, such as Band 4 and Band 5 in the soluble fraction, and could help identify KT203's off-target effects.

To further enhance confidence in protein identification, integrating Western blotting alongside MS would be valuable, as MS provides high-throughput proteomic data but is susceptible to false positives due to database-dependent peptide matching (Noor et al., 2021). Western blotting, utilizing specific antibodies against ABHD6 and other hydrolases, could serve as an independent validation tool to confirm protein identification. This approach

would be particularly useful for verifying the identities of enzymes suspected of hydrolyzing 4-MUH in rat brain preparations, ensuring a more reliable characterization of enzymatic activity.

MAFP caused significant inhibition of 4-MUH hydrolysis in rat brain fractions, suggesting that multiple serine hydrolases are involved in this enzymatic process. In contrast, selective ABHD6 inhibitors, such as KT203 and WWL70, exhibited only partial inhibition, even at higher concentrations. This suggests that while ABHD6 contributes to 4-MUH hydrolysis, other serine hydrolases likely contribute to the remaining enzymatic activity in rat brain. To identify the other hydrolases involved in 4-MUH hydrolysis, future experiments could utilize 4-MUH in combination with the ABPP probes, FP-rhodamine or MB064, in the spectrophotometer assay. This approach would identify whether the 4-MUH-hydrolysing enzymes might be detected with the ABPP technique. Similarly, 4-MUH could be used in the ABPP assay with FP-rhodamine and MB064 as probes to identify which enzymes, other than ABHD6, are also sensitive to 4-MUH. Projecting forward, synaptosomes could be a useful tool for ABPP and proteomic analysis to allow a focus on the enzymes involved in synaptic neurotransmission. Given the suggested differential locations of ABHD6 and MAGL around the synapse (see the Introduction), this approach could provide additional biochemical evidence.

Due to DO264's high selectivity for ABHD12 over other serine hydrolases, as demonstrated in both this study and previous mouse brain research (Ogasawara et al., 2018), future studies could explore the use of DO264 to investigate the functional role of ABHD12 in complex systems, such as rat brain slices, particularly in the context of electrophysiological assessments or pain-related functions in the rat spinal cord. Although mutations in ABHD12 have been repeatedly associated with sensory disturbances, the function of ABHD12 is still underexamined.

List of References

- Aaltonen, N., Savinainen, J.R., Ribas, C.R., Rönkkö, J., Kuusisto, A., Korhonen, J., Navia-Paldanius, D., Häyrinen, J., Takabe, P., Käsnänen, H. and Pantsar, T., 2013. Piperazine and piperidine triazole ureas as ultrapotent and highly selective inhibitors of monoacylglycerol lipase. *Chemistry & Biology*, 20(3), pp.379-390.
- Adibekian, A., Martin, B.R., Chang, J.W., Hsu, K.L., Tsuboi, K., Bachovchin, D.A., Speers, A.E., Brown, S.J., Spicer, T., Fernandez-Vega, V. and Ferguson, J., 2014. Characterization of a selective, reversible inhibitor of lysophospholipase 2 (LYPLA2). *Probe Reports from the NIH Molecular Libraries Program [Internet]*.
- Ahn, K., McKinney, M.K. and Cravatt, B.F., 2008. Enzymatic pathways that regulate endocannabinoid signaling in the nervous system. *Chemical Reviews*, 108(5), pp.1687-1707.
- Aldossari, Q.F.M., 2023. *The CNS endocannabinoid system: Synthetic cannabinoids and metabolic enzymes*. Ph.D. Thesis, University of Nottingham.
- Bachovchin, D.A., Ji, T., Li, W., Simon, G.M., Blankman, J.L., Adibekian, A., Hoover, H., Niessen, S. and Cravatt, B.F., 2010. Superfamily-wide portrait of serine hydrolase inhibition achieved by library-versus-library screening. *Proceedings of the National Academy of Sciences*, 107(49), pp.20941-20946.
- Baggelaar, M.P., Chameau, P.J., Kantae, V., Hummel, J., Hsu, K.L., Janssen, F., van der Wel, T., Soethoudt, M., Deng, H., den Dulk, H. and Allarà, M., 2015. Highly selective, reversible inhibitor identified by comparative chemoproteomics modulates diacylglycerol lipase activity in neurons. *Journal of the American Chemical Society*, 137(27), pp.8851-8857.
- Baggelaar, M.P., van Esbroeck, A.C., van Rooden, E.J., Florea, B.I., Overkleeft, H.S., Marsicano, G., Chaouloff, F. and van der Stelt, M., 2017. Chemical proteomics maps brain region specific activity of endocannabinoid hydrolases. *ACS Chemical Biology*, 12(3), pp.852-861.
- Benabdelaziz, I., Gómez-Ruiz, S., Benkhaled, M. et al., 2018. New cycloartane-type ester triterpenes from *Euphorbia pterococca* and biological evaluation. *Fitoterapia*, 127, pp.271–278. Available at: <https://doi.org/10.1016/j.fitote.2018.02.027>.
- Bisogno, T., Howell, F., Williams, G., Minassi, A., Cascio, M.G., Ligresti, A., Matias, I., Schiano-Moriello, A., Paul, P., Williams, E.J. and Gangadharan, U., 2003. Cloning of the first sn1-DAG lipases points to the spatial and temporal regulation of endocannabinoid signaling in the brain. *The Journal of Cell Biology*, 163(3), pp.463-468.

Bisogno, T., Ligresti, A. and Di Marzo, V., 2005. The endocannabinoid signalling system: biochemical aspects. *Pharmacology Biochemistry and Behavior*, *81*(2), pp.224-238.

Blankman, J.L., Long, J.Z., Trauger, S.A., Siuzdak, G. and Cravatt, B.F., 2013. ABHD12 controls brain lysophosphatidylserine pathways that are deregulated in a murine model of the neurodegenerative disease PHARC. *Proceedings of the National Academy of Sciences of the United States of America*, **110**, pp.1500–1505.

Blankman, J.L., Simon, G.M. and Cravatt, B.F., 2007. A comprehensive profile of brain enzymes that hydrolyze the endocannabinoid 2-arachidonoylglycerol. *Chemistry & Biology*, *14*(12), pp.1347-1356.

Bottemanne, P., Paquot, A., Amaraoui, H., Alhouayek, M. and Muccioli, G.G., 2019. The α/β -hydrolase domain 6 inhibitor WWL70 decreases endotoxin-induced lung inflammation in mice, potential contribution of 2-arachidonoylglycerol, and lysoglycerophospholipids. *The FASEB Journal*, *33*(6), pp.7635-7646.

Burstein, S.H., McQuain, C.A., Ross, A.H., Salmonsén, R.A. and Zurier, R.E., 2011. Resolution of inflammation by N-arachidonoylglycine. *Journal of Cellular Biochemistry*, **112**(11), pp.3227–3233. Available at: <https://doi.org/10.1002/jcb.23245>.

Cabral, G.A., Raborn, E.S., Griffin, L., Dennis, J. and Marciano-Cabral, F., 2008. CB2 receptors in the brain: role in central immune function. *British Journal of Pharmacology*, *153*(2), pp.240-251.

Cai, M., Luo, J., Yang, C. et al., 2023. ABHD12 contributes to tumorigenesis and sorafenib resistance by preventing ferroptosis in hepatocellular carcinoma. *iScience*, **26**(12), p.108340. Available at: <https://doi.org/10.1016/j.isci.2023.108340>.

Cao, J.K., Kaplan, J. and Stella, N., 2019. ABHD6: its place in endocannabinoid signaling and beyond. *Trends in pharmacological sciences*, *40*(4), pp.267-277.

Chang, J.W., Nomura, D.K. and Cravatt, B.F., 2011. A potent and selective inhibitor of KIAA1363/AADACL1 that impairs prostate cancer pathogenesis. *Chemistry & Biology*, *18*(4), pp.476-484.

Chen, X., Li, J., Kang, R., Klionsky, D.J. and Tang, D., 2021. Ferroptosis: machinery and regulation. *Autophagy*, **17**(9), pp.2054–2081. Available at: <https://doi.org/10.1080/15548627.2020.1810918>.

Cognetta, A.B., Niphakis, M.J., Lee, H.C., Martini, M.L., Hulce, J.J. and Cravatt, B.F., 2015. Selective N-hydroxyhydantoin carbamate inhibitors of mammalian serine hydrolases. *Chemistry & Biology*, *22*(7), pp.928-937.

Cravatt, B.F., Wright, A.T. and Kozarich, J.W., 2008. Activity-based protein profiling: from enzyme chemistry to proteomic chemistry. *Annu. Rev. Biochem.*, 77(1), pp.383-414.

Deng, H. and Li, W., 2020. Therapeutic potential of targeting α/β -Hydrolase domain-containing 6 (ABHD6). *European Journal of Medicinal Chemistry*, 198, p.112353. doi:10.1016/j.ejmech.2020.112353

Deng, H., van der Wel, T., van den Berg, R.J., van den Nieuwendijk, A.M., Janssen, F.J., Baggelaar, M.P., Overkleeft, H.S. and van der Stelt, M., 2017. Chiral disubstituted piperidiny ureas: a class of dual diacylglycerol lipase- α and ABHD6 inhibitors. *MedChemComm*, 8(5), pp.982-988.

Deutsch, D.G. and Chin, S.A., 1993. Enzymatic synthesis and degradation of anandamide, a cannabinoid receptor agonist. *Biochemical pharmacology*, 46(5), pp.791-796.

Deutsch, D.G., Omeir, R., Arreaza, G., Salehani, D., Prestwich, G.D., Huang, Z. and Howlett, A., 1997. Methyl arachidonyl fluorophosphonate: a potent irreversible inhibitor of anandamide amidase. *Biochemical Pharmacology*, 53(3), pp.255-260.

Devane, W.A., Hanuš, L., Breuer, A., Pertwee, R.G., Stevenson, L.A., Griffin, G., Gibson, D., Mandelbaum, A., Etinger, A. and Mechoulam, R., 1992. Isolation and structure of a brain constituent that binds to the cannabinoid receptor. *Science*, 258(5090), pp.1946-1949.

Dixon, S.J., Lemberg, K.M., Lamprecht, M.R. et al., 2012. Ferroptosis: an iron-dependent form of nonapoptotic cell death. *Cell*, 149(5), pp.1060–1072. Available at: <https://doi.org/10.1016/j.cell.2012.03.042>.

Ellenbroek, B. and Youn, J., 2016. Rodent models in neuroscience research: is it a rat race?. *Disease Models & Mechanisms*, 9(10), pp.1079-1087.

Fiskerstrand, T., H'Mida-Ben Brahim, D., Johansson, S., M'Zahem, A., Haukanes, B.I., Drouot, N., Zimmermann, J., Cole, A.J., Vedeler, C., Bredrup, C., Assoum, M. et al., 2010. Mutations in ABHD12 cause the neurodegenerative disease PHARC: An inborn error of endocannabinoid metabolism. *American Journal of Human Genetics*, 87, pp.410–417.

Fowler, C.J., Doherty, P. and Alexander, S.P., 2017. Endocannabinoid turnover. *Advances in Pharmacology*, 80, pp.31-66.

Frasch, S.C., Fernandez-Boyanapalli, R.F., Berry, K.A., Murphy, R.C., Leslie, C.C., Nick, J.A., Henson, P.M. and Bratton, D.L., 2013. Neutrophils regulate tissue neutrophilia in inflammation via the oxidant-modified lipid lysophosphatidylserine. *Journal of Biological Chemistry*, 288, pp.4583–4593.

Ghafouri, N., Tiger, G., Razdan, R.K., Mahadevan, A., Pertwee, R.G., Martin, B.R. and Fowler, C.J., 2004. Inhibition of monoacylglycerol lipase and fatty acid amide hydrolase by analogues of 2-arachidonoylglycerol. *British Journal of Pharmacology*, 143(6), pp.774-784.

Gilham, D. and Lehner, R., 2005. Techniques to measure lipase and esterase activity in vitro. *Methods*, 36(2), pp.139-147.

Grabner, G.F., Fawzy, N., Pribasni, M.A., Trieb, M., Taschler, U., Holzer, M., Schweiger, M., Wolinski, H., Kolb, D., Horvath, A. and Breinbauer, R., 2019. Metabolic disease and ABHD6 alter the circulating bis (monoacylglycerol) phosphate profile in mice and humans. *Journal of Lipid Research*, 60(5), pp.1020-1031.

Grüner, B.M., Schulze, C.J., Yang, D., Ogasawara, D., Dix, M.M., Rogers, Z.N., Chuang, C.H., McFarland, C.D., Chiou, S.H., Brown, J.M. and Cravatt, B.F., 2016. An in vivo multiplexed small-molecule screening platform. *Nature methods*, 13(10), pp.883-889.

Guilbault, G.G. and Hieserman, J., 1969. Fluorometric substrate for sulfatase and lipase. *Analytical Chemistry*, 41(14), pp.2006-2009.

Gulyássi, P., Puska, G., Györffy, B.A., Todorov-Völgyi, K., Juhász, G., Drahos, L. and Kékesi, K.A., 2020. Proteomic comparison of different synaptosome preparation procedures. *Amino Acids*, 52, pp.1529-1543.

Hoover, H.S., Blankman, J.L., Niessen, S. and Cravatt, B.F., 2008. Selectivity of inhibitors of endocannabinoid biosynthesis evaluated by activity-based protein profiling. *Bioorganic & Medicinal Chemistry Letters*, 18(22), pp.5838-5841.

Hourani, W. and Alexander, S.P.H., 2018. Cannabinoid ligands, receptors and enzymes: Pharmacological tools and therapeutic potential. *Brain and Neuroscience Advances*, 2, p.2398212818783908. Published 2018 Jun 19. doi:10.1177/2398212818783908

Howlett, A.C., Barth, F., Bonner, T.I. et al., 2002. International Union of Pharmacology. XXVII. Classification of cannabinoid receptors. *Pharmacological Reviews*, 54(2), pp.161-202. Available at: <https://doi.org/10.1124/pr.54.2.161>.

Hsu, K.L., Tsuboi, K., Adibekian, A., Pugh, H., Masuda, K. and Cravatt, B.F., 2012. DAGL β inhibition perturbs a lipid network involved in macrophage inflammatory responses. *Nature Chemical Biology*, 8(12), pp.999-1007.

Hsu, K.L., Tsuboi, K., Chang, J.W., Whitby, L.R., Speers, A.E., Pugh, H. and Cravatt, B.F., 2013. Discovery and optimization of piperidyl-1, 2, 3-triazole ureas as potent, selective, and in vivo-active inhibitors of α/β -hydrolase domain containing 6 (ABHD6). *Journal of Medicinal Chemistry*, 56(21), pp.8270-8279.

Hua, T., Vemuri, K., Pu, M., et al., 2016. Crystal structure of the human cannabinoid receptor CB1. *Cell*, 167(3), pp.750–762.

Huang, S.M., Bisogno, T., Petros, T.J., Chang, S.Y., Zavitsanos, P.A., Zipkin, R.E., Sivakumar, R., Coop, A., Maeda, D.Y., De Petrocellis, L. et al., 2001. Identification of a new class of molecules, the arachidonyl amino acids, and characterization of one member that inhibits pain. *Journal of Biological Chemistry*, 276, pp.42639–42644. Available at: <https://doi.org/10.1074/jbc.M107351200>.

Inglese, J., Johnson, R.L., Simeonov, A., Xia, M., Zheng, W., Austin, C.P. and Auld, D.S., 2007. High-throughput screening assays for the identification of chemical probes. *Nature Chemical Biology*, 3(8), pp.466-479.

Inloes, J.M., Hsu, K.L., Dix, M.M., Viader, A., Masuda, K., Takei, T., Wood, M.R. and Cravatt, B.F., 2014. The hereditary spastic paraplegia-related enzyme DDHD2 is a principal brain triglyceride lipase. *Proceedings of the National Academy of Sciences*, 111(41), pp.14924-14929.

Iwashita, M., Makide, K., Nonomura, T., Misumi, Y., Otani, Y., Ishida, M., Taguchi, R., Tsujimoto, M., Aoki, J., Arai, H. and Ohwada, T., 2009. Synthesis and evaluation of lysophosphatidylserine analogues as inducers of mast cell degranulation. Potent activities of lysophosphatidylthreonine and its 2-deoxy derivative. *Journal of Medicinal Chemistry*, 52, pp.5837–5863.

Jacks, T.J. and Kircher, H.W., 1967. Fluorometric assay for the hydrolytic activity of lipase using fatty acyl esters of 4-methylumbelliferone. *Analytical Biochemistry*, 21(2), pp.279-285.

Janssen, F.J., Deng, H., Baggelaar, M.P., Allarà, M., van der Wel, T., den Dulk, H., Ligresti, A., van Esbroeck, A.C., McGuire, R., Di Marzo, V. and Overkleeft, H.S., 2014. Discovery of glycine sulfonamides as dual inhibitors of sn-1-diacylglycerol lipase α and α/β -hydrolase domain 6. *Journal of Medicinal Chemistry*, 57(15), pp.6610-6622.

Jun, S., Kim, S.W., Lim, J.Y. and Park, S.J., 2020. ABHD12 knockdown suppresses breast cancer cell proliferation, migration and invasion. *Anticancer Research*, 40(5), pp.2601–2611. Available at: <https://doi.org/10.21873/anticancer.14231>.

Kaczocha, M., Glaser, S.T., Chae, J., Brown, D.A. and Deutsch, D.G., 2010. Lipid droplets are novel sites of N-acyl ethanolamine inactivation by fatty acid amide hydrolase-2. *Journal of Biological Chemistry*, 285(4), pp.2796-2806.

Kathman, S.G., Boshart, J., Jing, H. and Cravatt, B.F., 2020. Blockade of the lysophosphatidylserine lipase ABHD12 potentiates ferroptosis in cancer cells. *ACS Chemical Biology*, 15(4), pp.871–877. Available at: <https://doi.org/10.1021/acscchembio.0c00086>.

- Kohno, M., Hasegawa, H., Inoue, A., Muraoka, M., Miyazaki, T., Oka, K. and Yasukawa, M., 2006. Identification of N-arachidonylglycine as the endogenous ligand for orphan G-protein-coupled receptor GPR18. *Biochemical and Biophysical Research Communications*, **347**, pp.827–832. Available at: <https://doi.org/10.1016/j.bbrc.2006.06.175>.
- Labar, G., Bauvois, C., Borel, F., Ferrer, J.L., Wouters, J. and Lambert, D.M., 2010. Crystal structure of the human monoacylglycerol lipase, a key factor in endocannabinoid signaling. *Chembiochem*, *11*(2), pp.218-227.
- Lau, D., Tobin, S., Pribiag, H., Nakajima, S., Fiset, A., Matthys, D., Franco Flores, A.K., Peyot, M.L., Murthy Madiraju, S.R., Prentki, M., Stellwagen, D., Alquier, T. and Fulton, S., 2024. ABHD6 loss-of-function in mesoaccumbens postsynaptic but not presynaptic neurons prevents diet-induced obesity in male mice. *Nature Communications*, **15**(1), p.10652. Available at: <https://doi.org/10.1038/s41467-024-54819-5>.
- Li, F., Fei, X., Xu, J. and Ji, C., 2009. An unannotated α/β hydrolase superfamily member, ABHD6 differentially expressed among cancer cell lines. *Molecular Biology Reports*, *36*, pp.691-696.
- Li, W., Blankman, J.L. and Cravatt, B.F., 2007. A functional proteomic strategy to discover inhibitors for uncharacterized hydrolases. *Journal of the American Chemical Society*, *129*(31), pp.9594-9595.
- Liktor-Busa, E., Levine, A.A., Palomino, S.M., Singh, S., Wahl, J., Vanderah, T.W., Stella, N. and Largent-Milnes, T.M., 2023. ABHD6 and MAGL control 2-AG levels in the PAG and allodynia in a CSD-induced periorbital model of headache. *Frontiers in Pain Research*, **4**, p.1171188. Available at: <https://doi.org/10.3389/fpain.2023.1171188>.
- Liu, J., Wang, L., Harvey-White, J., Osei-Hyiaman, D., Razdan, R., Gong, Q., Chan, A.C., Zhou, Z., Huang, B.X., Kim, H.Y. and Kunos, G., 2006. A biosynthetic pathway for anandamide. *Proceedings of the National Academy of Sciences*, *103*(36), pp.13345-13350.
- Lord, C.C., Thomas, G. and Brown, J.M., 2013. Mammalian alpha beta hydrolase domain (ABHD) proteins: Lipid metabolizing enzymes at the interface of cell signaling and energy metabolism. *Biochimica et Biophysica Acta (BBA)-Molecular and Cell Biology of Lipids*, *1831*(4), pp.792-802.
- Lowry, O.H., Rosebrough, N.J., Farr, A.L. and Randall, R.J., 1951. Protein measurement with the Folin phenol reagent. *J Biol Chem*, *193*(1), pp.265-275.
- Lu, Y., Chan, Y.T., Tan, H.Y. et al., 2022. Epigenetic regulation of ferroptosis via ETS1/miR-23a-3p/ACSL4 axis mediates sorafenib resistance in human hepatocellular

carcinoma. *Journal of Experimental & Clinical Cancer Research*, **41**(1), p.3. Available at: <https://doi.org/10.1186/s13046-021-02208-x>.

Mahmood, N. S. (2018). *Molecular and functional characterization of endocannabinoid hydrolases*. Ph.D. Thesis, University of Nottingham.

Maier, S., Staffler, G., Hartmann, A., Höck, J., Henning, K., Grabusic, K., Mailhammer, R., Hoffmann, R., Wilmanns, M., Lang, R. and Mages, J., 2006. Cellular target genes of Epstein-Barr virus nuclear antigen 2. *Journal of Virology*, **80**(19), pp.9761-9771.

Malamas, M.S., Lamani, M., Farah, S.I., Mohammad, K.A., Miyabe, C.Y., Rajarshi, G., Wu, S., Zvonok, N., Chandrashekhar, H., Wood, J. and Makriyannis, A., 2023. Design and synthesis of highly potent and specific ABHD6 inhibitors. *ChemMedChem*, **18**(21), p.e202100406. Available at: <https://doi.org/10.1002/cmdc.202100406>.

Manterola, A., Bernal-Chico, A., Cipriani, R., Ruiz, A., Perez-Samartin, A., Moreno-Rodríguez, M., Hsu, K.L., Cravatt, B.F., Brown, J.M., Rodríguez-Puertas, R. and Matute, C., 2018. Re-examining the potential of targeting ABHD6 in multiple sclerosis: Efficacy of systemic and peripherally restricted inhibitors in experimental autoimmune encephalomyelitis. *Neuropharmacology*, **141**, pp.181-191.

Marrs, W.R., Horne, E.A., Ortega-Gutierrez, S., Cisneros, J.A., Xu, C., Lin, Y.H., Muccioli, G.G., Lopez-Rodriguez, M.L. and Stella, N., 2011. Dual inhibition of α/β -hydrolase domain 6 and fatty acid amide hydrolase increases endocannabinoid levels in neurons. *Journal of Biological Chemistry*, **286**(33), pp.28723-28728.

Max, D., Hesse, M., Volkmer, I. and Staeger, M.S., 2009. High expression of the evolutionarily conserved α/β hydrolase domain containing 6 (ABHD6) in Ewing tumors. *Cancer Science*, **100**(12), pp.2383-2389.

McKinney, M.K. and Cravatt, B.F., 2005. Structure and function of fatty acid amide hydrolase. *Annu. Rev. Biochem.*, **74**(1), pp.411-432.

Mechoulam, R., Ben-Shabat, S., Hanus, L., Ligumsky, M., Kaminski, N.E., Schatz, A.R., Gopher, A., Almog, S., Martin, B.R., Compton, D.R. and Pertwee, R.G., 1995. Identification of an endogenous 2-monoglyceride, present in canine gut, that binds to cannabinoid receptors. *Biochemical Pharmacology*, **50**(1), pp.83-90.

Miralpeix, C., Reguera, A.C., Fosch, A., Casas, M., Lillo, J., Navarro, G., Franco, R., Casas, J., Alexander, S.P., Casals, N. and Rodríguez-Rodríguez, R., 2021. Carnitine palmitoyltransferase 1C negatively regulates the endocannabinoid hydrolase ABHD6 in mice, depending on nutritional status. *British Journal of Pharmacology*, **178**(7), pp.1507-1523.

Mounsey, R.B., Mustafa, S., Robinson, L., Ross, R.A., Riedel, G., Pertwee, R.G. and Teismann, P., 2015. Increasing levels of the endocannabinoid 2-AG is neuroprotective in the 1-methyl-4-phenyl-1,2,3,6-tetrahydropyridine mouse model of Parkinson's disease. *Experimental Neurology*, **273**, pp.36–44. Available at: <https://doi.org/10.1016/j.expneurol.2015.07.024>.

Muccioli, G.G., Xu, C., Odah, E., Cudaback, E., Cisneros, J.A., Lambert, D.M., Rodríguez, M.L.L., Bajjalieh, S. and Stella, N., 2007. Identification of a novel endocannabinoid-hydrolyzing enzyme expressed by microglial cells. *Journal of Neuroscience*, *27*(11), pp.2883-2889.

Navia-Paldanius, D., Savinainen, J.R. and Laitinen, J.T., 2012. Biochemical and pharmacological characterization of human α/β -hydrolase domain containing 6 (ABHD6) and 12 (ABHD12). *Journal of lipid research*, *53*(11), pp.2413-2424.

Naydenov, A.V., Horne, E.A., Cheah, C.S., Swinney, K., Hsu, K.L., Cao, J.K., Marrs, W.R., Blankman, J.L., Tu, S., Cherry, A.E. and Fung, S., 2014. ABHD6 blockade exerts antiepileptic activity in PTZ-induced seizures and in spontaneous seizures in R6/2 mice. *Neuron*, *83*(2), pp.361-371.

Niphakis, M.J. and Cravatt, B.F., 2014. Enzyme inhibitor discovery by activity-based protein profiling. *Annual Review of Biochemistry*, *83*(1), pp.341-377.

Noor, Z., Ahn, S.B., Baker, M.S., Ranganathan, S. and Mohamedali, A., 2021. Mass spectrometry-based protein identification in proteomics—a review. *Briefings in Bioinformatics*, *22*(2), pp.1620–1638. <https://doi.org/10.1093/bib/bbz163>

Ogasawara, D., Ichu, T.A., Vartabedian, V.F., Benthuysen, J., Jing, H., Reed, A., Ulanovskaya, O.A., Hulce, J.J., Roberts, A., Brown, S. and Rosen, H., 2018. Selective blockade of the lyso-PS lipase ABHD12 stimulates immune responses in vivo. *Nature Chemical Biology*, *14*(12), pp.1099-1108.

Okine, B.N., Norris, L.M., Woodhams, S., Burston, J., Patel, A., Alexander, S.P., Barrett, D.A., Kendall, D.A., Bennett, A.J. and Chapman, V., 2012. Lack of effect of chronic pre-treatment with the FAAH inhibitor URB597 on inflammatory pain behaviour: evidence for plastic changes in the endocannabinoid system. *British Journal of Pharmacology*, *167*(3), pp.627-640.

Oparina, N.Y., Delgado-Vega, A.M., Martinez-Bueno, M., Magro-Checa, C., Fernández, C., Castro, R.O., Pons-Estel, B.A., D'Alfonso, S., Sebastiani, G.D., Witte, T. and Lauwerys, B.R., 2015. PXX locus in systemic lupus erythematosus: fine mapping and functional

analysis reveals novel susceptibility gene ABHD6. *Annals of The Rheumatic Diseases*, 74(3), pp.e14-e14.

Parkkari, T., Haavikko, R., Laitinen, T. et al., 2014. Discovery of triterpenoids as reversible inhibitors of α/β -hydrolase domain containing 12 (ABHD12). *PLOS ONE*, 9(5), p.e98286. Available at: <https://doi.org/10.1371/journal.pone.0098286>.

Parmar, N. and Ho, W.S.V., 2010. N-arachidonoyl glycine, an endogenous lipid that acts as a vasorelaxant via nitric oxide and large conductance calcium-activated potassium channels. *British Journal of Pharmacology*, 160, pp.594–603. Available at: <https://doi.org/10.1111/j.1476-5381.2009.00622.x>.

Parolaro, D., Massi, P., Rubino, T. and Monti, E., 2002. Endocannabinoids in the immune system and cancer. *Prostaglandins, Leukotrienes and Essential Fatty Acids (PLEFA)*, 66(2-3), pp.319-332.

Patel, J.Z., van Bruchem, J., Laitinen, T., Kaczor, A.A., Navia-Paldanius, D., Parkkari, T., Savinainen, J.R., Laitinen, J.T. and Nevalainen, T.J., 2015. Revisiting 1, 3, 4-oxadiazol-2-ones: utilization in the development of ABHD6 inhibitors. *Bioorganic & Medicinal Chemistry*, 23(19), pp.6335-6345.

Patricelli, M.P., Giang, D.K., Stamp, L.M. and Burbaum, J.J., 2001. Direct visualization of serine hydrolase activities in complex proteomes using fluorescent active site-directed probes. *PROTEOMICS: International Edition*, 1(9), pp.1067-1071.

Pertwee, R.G., Howlett, A.C., Abood, M.E., Alexander, S.P.H., Di Marzo, V., Elphick, M.R., Greasley, P.J., Hansen, H.S., Kunos, G., Mackie, K. and Mechoulam, R., 2010. International Union of Basic and Clinical Pharmacology. LXXIX. Cannabinoid receptors and their ligands: beyond CB1 and CB2. *Pharmacological Reviews*, 62(4), pp.588-631.

Petrocellis, L.D., Cascio, M.G. and Marzo, V.D., 2004. The endocannabinoid system: a general view and latest additions. *British Journal of Pharmacology*, 141(5), pp.765-774.

Piomelli, D., Tarzia, G., Duranti, A., Tontini, A., Mor, M., Compton, T.R., Dasse, O., Monaghan, E.P., Parrott, J.A. and Putman, D., 2006. Pharmacological profile of the selective FAAH inhibitor KDS-4103 (URB597). *CNS Drug Reviews*, 12(1), pp.21-38.

Poursharifi, P., Madiraju, S.R.M. and Prentki, M., 2017. Monoacylglycerol signalling and ABHD6 in health and disease. *Diabetes, Obesity and Metabolism*, 19, pp.76-89.

Poursharifi, P., Schmitt, C., Chenier, I., Leung, Y.H., Oppong, A.K., Bai, Y., Klein, L.L., Al-Mass, A., Lussier, R., Abu-Farha, M., Abubaker, J., Al-Mulla, F., Peyot, M.L., Madiraju, S.R.M. and Prentki, M., 2023. ABHD6 suppression promotes anti-inflammatory polarization of adipose tissue macrophages via 2-monoacylglycerol/PPAR signaling in obese mice.

Molecular Metabolism, **78**, p.101822. Available at:

<https://doi.org/10.1016/j.molmet.2023.101822>.

Pribasnig, M.A., Mrak, I., Grabner, G.F., Taschler, U., Knittelfelder, O., Scherz, B., Eichmann, T.O., Heier, C., Grumet, L., Kowaliuk, J. and Romauch, M., 2015. α/β Hydrolase domain-containing 6 (ABHD6) degrades the late endosomal/lysosomal lipid bis (monoacylglycero) phosphate. *Journal of Biological Chemistry*, *290*(50), pp.29869-29881.

Pusch, L.M., Riegler-Berket, L., Oberer, M., Zimmermann, R. and Taschler, U., 2022. α/β -Hydrolase Domain-Containing 6 (ABHD6)—A Multifunctional Lipid Hydrolase. *Metabolites*, *12*(8), p.761.

Rahman, W., Patel, R. and Dickenson, A.H., 2015. Electrophysiological evidence for voltage-gated calcium channel 2 (Cav2) modulation of mechano-and thermosensitive spinal neuronal responses in a rat model of osteoarthritis. *Neuroscience*, *305*, pp.76-85.

Rivera, P., Vargas, A., Pastor, A., Boronat, A., López-Gambero, A.J., Sánchez-Marín, L., Medina-Vera, D., Serrano, A., Pavón, F.J., de la Torre, R., Agirregoitia, E., Lucena, M.I., Rodríguez de Fonseca, F., Decara, J. and Suárez, J., 2020. Differential hepatoprotective role of the cannabinoid CB1 and CB2 receptors in paracetamol-induced liver injury. *British Journal of Pharmacology*, *177*(14), pp.3309–3326. Available at:

<https://doi.org/10.1111/bph.15051>.

Sarmad, S., Alexander, S.P., Barrett, D.A., Marsden, C.A. and Kendall, D.A., 2011. Depolarizing and calcium-mobilizing stimuli fail to enhance synthesis and release of endocannabinoids from rat brain cerebral cortex slices. *Journal of neurochemistry*, *117*(4), pp.665-677.

Savinainen, J.R., Navia-Paldanius, D. and Laitinen, J.T., 2016. A sensitive and versatile fluorescent activity assay for ABHD6. *Endocannabinoid Signaling: Methods and Protocols*, pp.169-178.

Savinainen, J.R., Saario, S.M. and Laitinen, J.T., 2012. The serine hydrolases MAGL, ABHD6 and ABHD12 as guardians of 2-arachidonoylglycerol signalling through cannabinoid receptors. *Acta Physiologica*, *204*(2), pp.267–276. doi:10.1111/j.1748-1716.2011.02280.x

Schlosburg, J.E., Blankman, J.L., Long, J.Z., Nomura, D.K., Pan, B., Kinsey, S.G., Nguyen, P.T., Ramesh, D., Booker, L., Burston, J.J. and Thomas, E.A., 2010. Chronic monoacylglycerol lipase blockade causes functional antagonism of the endocannabinoid system. *Nature Neuroscience*, *13*(9), pp.1113-1119.

- Schmid, P.C., Zuzarte-Augustin, M.L. and Schmid, H.H., 1985. Properties of rat liver N-acylethanolamine amidohydrolase. *Journal of Biological Chemistry*, 260(26), pp.14145-14149.
- Shao, Z., Yin, J., Chapman, K., et al., 2016. High-resolution crystal structure of the human CB1 cannabinoid receptor. *Nature*, 540, pp.602–606.
- Spector, A.A. and Fletcher, J.E., 1977. Fatty acid binding by serum albumin. In *Albumin: structure, biosynthesis, function* (pp. 51-60). Oxford: Pergamon Press.
- Succar, R., Mitchell, V.A. and Vaughan, C.W., 2007. Actions of N-arachidonoyl-glycine in a rat inflammatory pain model. *Molecular Pain*, 3, p.24. Available at: <https://doi.org/10.1186/1744-8069-3-24>.
- Sugiura, T., Kondo, S., Sukagawa, A., Nakane, S., Shinoda, A., Itoh, K., Yamashita, A. and Waku, K., 1995. 2-Arachidonoylglycerol: a possible endogenous cannabinoid receptor ligand in brain. *Biochemical and Biophysical Research Communications*, 215(1), pp.89-97.
- Thomas, G., Betters, J.L., Lord, C.C., Brown, A.L., Marshall, S., Ferguson, D., Sawyer, J., Davis, M.A., Melchior, J.T., Blume, L.C. and Howlett, A.C., 2013. The serine hydrolase ABHD6 Is a critical regulator of the metabolic syndrome. *Cell reports*, 5(2), pp.508-520.
- Turcotte, C., Chouinard, F., Lefebvre, J.S. and Flamand, N., 2015. Regulation of inflammation by cannabinoids, the endocannabinoids 2-arachidonoyl-glycerol and arachidonoyl-ethanolamide, and their metabolites. *Journal of Leukocyte Biology*, 97(6), pp.1049–1070. Available at: <https://doi.org/10.1189/jlb.3RU0115-021R>.
- Van Esbroeck, A.C., Kantae, V., Di, X., Van der Wel, T., Den Dulk, H., Stevens, A.F., Singh, S., Bakker, A.T., Florea, B.I., Stella, N. and Overkleeft, H.S., 2019. Identification of α , β -hydrolase domain containing protein 6 as a diacylglycerol lipase in neuro-2a cells. *Frontiers in Molecular Neuroscience*, 12, p.286.
- Wei, M., Zhang, J., Jia, M., Yang, C., Pan, Y., Li, S., Luo, Y., Zheng, J., Ji, J., Chen, J., Hu, X., Xiong, J., Shi, Y. and Zhang, C., 2016. α/β -Hydrolase domain-containing 6 (ABHD6) negatively regulates the surface delivery and synaptic function of AMPA receptors. *Proceedings of the National Academy of Sciences of the United States of America*, 113(19), pp.E2695–E2704. Available at: <https://doi.org/10.1073/pnas.1524589113>.
- Wen, J., Jones, M., Tanaka, M., Selvaraj, P., Symes, A.J., Cox, B. and Zhang, Y., 2018. WWL70 protects against chronic constriction injury-induced neuropathic pain in mice by cannabinoid receptor-independent mechanisms. *Journal of Neuroinflammation*, 15, pp.1-16.

- Wen, J., Ribeiro, R., Tanaka, M. and Zhang, Y., 2015. Activation of CB2 receptor is required for the therapeutic effect of ABHD6 inhibition in experimental autoimmune encephalomyelitis. *Neuropharmacology*, *99*, pp.196-209.
- Westenbroek, R., Kaplan, J., Viray, K. and Stella, N., 2023. The serine hydrolase ABHD6 controls survival and thermally induced seizures in a mouse model of Dravet syndrome. *Neurobiology of Disease*, *180*, p.106099. Available at: <https://doi.org/10.1016/j.nbd.2023.106099>.
- Woodhams, S.G., Wong, A., Barrett, D.A., Bennett, A.J., Chapman, V. and Alexander, S.P.H., 2012. Spinal administration of the monoacylglycerol lipase inhibitor JZL 184 produces robust inhibitory effects on nociceptive processing and the development of central sensitization in the rat. *British Journal of Pharmacology*, *167*(8), pp.1609-1619.
- Wootten, D., Christopoulos, A., Marti-Solano, M., Babu, M.M. and Sexton, P.M., 2018. Mechanisms of signalling and biased agonism in G protein-coupled receptors. *Nature Reviews Molecular Cell Biology*, *19*(10), pp.638-653. Available at: <https://doi.org/10.1038/s41580-018-0049-3>.
- Yea, K., Kim, J., Lim, S., Kwon, T., Park, H.S., Park, K.S., Suh, P.G. and Ryu, S.H., 2009. Lysophosphatidylserine regulates blood glucose by enhancing glucose transport in myotubes and adipocytes. *Biochemical and Biophysical Research Communications*, *378*, pp.783–788.
- Yoshida, T., Kobayashi, T., Itoda, M., Muto, T., Miyaguchi, K., Mogushi, K., Shoji, S., Shimokawa, K., Iida, S., Uetake, H., Ishikawa, T., Sugihara, K., Mizushima, H. and Tanaka, H., 2010. Clinical omics analysis of colorectal cancer incorporating copy number aberrations and gene expression data. *Cancer Informatics*, *9*, pp.147–161. Available at: <https://doi.org/10.4137/cin.s3851>.
- Yu, C.B., Zhu, L.Y., Wang, Y.G., Li, F., Zhang, X.Y. and Dai, W.J., 2016. Systemic transcriptome analysis of hepatocellular carcinoma. *Tumor Biology*, *37*, pp.13323-13331.
- Yu, X.H., Cao, C.Q., Martino, G., Puma, C., Morinville, A., St-Onge, S., Lessard, É., Perkins, M.N. and Laird, J.M.A., 2010. A peripherally restricted cannabinoid receptor agonist produces robust anti-nociceptive effects in rodent models of inflammatory and neuropathic pain. *Pain*, *151*(2), pp.337–344. Available at: <https://doi.org/10.1016/j.pain.2010.07.019>.
- Zhang, H., Lipinski, A.A., Liktor-Busa, E., Smith, A.F., Moutal, A., Khanna, R., Langlais, P.R., Largent-Milnes, T.M. and Vanderah, T.W., 2021. The effects of repeated morphine treatment on the endogenous cannabinoid system in the ventral tegmental area. *Frontiers in Pharmacology*, *12*, p.632757. Available at: <https://doi.org/10.3389/fphar.2021.632757>.

Zhao, S., Mugabo, Y., Ballentine, G., Attane, C., Iglesias, J., Poursharifi, P., Zhang, D., Nguyen, T.A., Erb, H., Prentki, R. and Peyot, M.L., 2016. α/β -Hydrolase domain 6 deletion induces adipose browning and prevents obesity and type 2 diabetes. *Cell Reports*, 14(12), pp.2872-2888.

Zhao, S., Mugabo, Y., Iglesias, J., Xie, L., Delghingaro-Augusto, V., Lussier, R., Peyot, M.L., Joly, E., Taïb, B., Davis, M.A. and Brown, J.M., 2014. α/β -Hydrolase domain-6-accessible monoacylglycerol controls glucose-stimulated insulin secretion. *Cell Metabolism*, 19(6), pp.993-1007.

Zhao, S., Poursharifi, P., Mugabo, Y., Levens, E.J., Vivot, K., Attane, C., Iglesias, J., Peyot, M.L., Joly, E., Madiraju, S.M. and Prentki, M., 2015. α/β -Hydrolase domain-6 and saturated long chain monoacylglycerol regulate insulin secretion promoted by both fuel and non-fuel stimuli. *Molecular Metabolism*, 4(12), pp.940-950.